AD-A173 100 DROPLET SIZING RESEARCH PROGRAM(U) SPECTRON DEVELOPMENT 1/2
LABS INC COSTA MESA CA C F HESS 10 MAR 86
SDL-86-2286-15F AFOSR-TR-86-0875 F49620-83-C-0060
UNCLASSIFIED F/G 4/1 NL

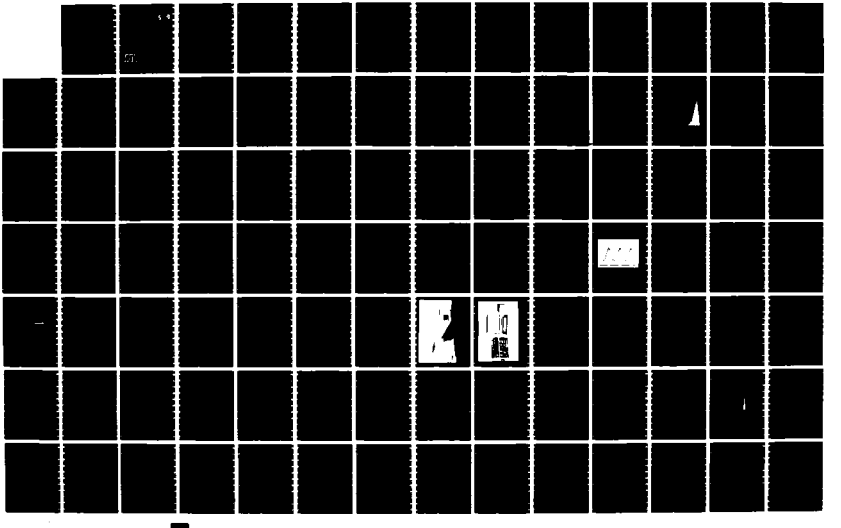

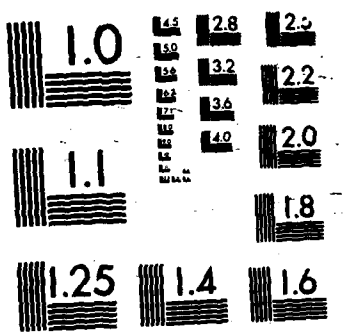
1.0
1.1
1.25
1.4
1.6
1.8
2.0
2.2
2.8
3.2
3.6
4.0

AFOSR-TR- 86-0875

AD-A173 100

DTIC ELECTE OCT 0 8 1986 S D

DROPLET SIZING RESEARCH PROGRAM

FINAL REPORT

10 March 1986

SDL No. 86-2286-15F

Approved for public release; distribution unlimited.

Prepared For:

AIR FORCE OFFICE OF SCIENTIFIC RESEARCH
Attn: Dr. Julian Tishkoff, AFOSR/NA
Directorate of Aerospace Sciences
Building 410
Bolling AFB, DC 20332

Under Contract No.
F49620-83-C-0060

DTIC FILE COPY

SDL
SPECTRON DEVELOPMENT LABORATORIES, INC.
3303 HARBOR BLVD., SUITE G-3, COSTA MESA, CA 92626 • (714) 549-8477

86 10 8 075

UNCLASSIFIED

SECURITY CLASSIFICATION OF THIS PAGE

AD-A173 105

REPORT DOCUMENTATION PAGE

1a. REPORT SECURITY CLASSIFICATION: UNCLASSIFIED	1b. RESTRICTIVE MARKINGS
2a. SECURITY CLASSIFICATION AUTHORITY	3. DISTRIBUTION/AVAILABILITY OF REPORT: Approved for public release, distribution unlimited
2b. DECLASSIFICATION/DOWNGRADING SCHEDULE	
4. PERFORMING ORGANIZATION REPORT NUMBER(S): 86-2286-15F	5. MONITORING ORGANIZATION REPORT NUMBER(S): AFOSR-TR- 86-0815
6a. NAME OF PERFORMING ORGANIZATION: SPECTRON DEVELOPMENT LABS; 6b. OFFICE SYMBOL (If applicable)	7a. NAME OF MONITORING ORGANIZATION: AFOSR
6c. ADDRESS (City, State and ZIP Code): 3303 Harbor Blvd., Ste. G-3, Costa Mesa, CA 92626	7b. ADDRESS (City, State and ZIP Code): Bolling AFB DC 20332-6448
8a. NAME OF FUNDING/SPONSORING ORGANIZATION: Air Force Office of Scientific Research; 8b. OFFICE SYMBOL (If applicable): NA	9. PROCUREMENT INSTRUMENT IDENTIFICATION NUMBER: F49620-83-C-0060
8c. ADDRESS (City, State and ZIP Code): Bldg. 410, Bolling Air Force, DC 20332-6448	10. SOURCE OF FUNDING NOS.

PROGRAM ELEMENT NO.	PROJECT NO.	TASK NO.	WORK UNIT NO.
61102F	2308	A3	

11. TITLE (Include Security Classification): DROPLET SIZING RESEARCH PROGRAM

12. PERSONAL AUTHOR(S): Dr. Cecil F. Hess

13a. TYPE OF REPORT	13b. TIME COVERED	14. DATE OF REPORT (Yr., Mo., Day)	15. PAGE COUNT
FINAL	FROM 1/15/83 TO 1/15/86	10 March 1986	138

16. SUPPLEMENTARY NOTATION

17. COSATI CODES			18. SUBJECT TERMS (Continue on reverse if necessary and identify by block number)
FIELD	GROUP	SUB. GR.	droplet sizing, particle velocity, mass flux, nonintrusive, advanced laser diagnostics.

19. ABSTRACT (Continue on reverse if necessary and identify by block number)

A three-year program in droplet sizing research has been completed. The major accomplishments include: (1) Establishing the errors and limitations associated with the Visibility technique; (2) Development of two new techniques utilizing absolute scattered light; (3) Extension of techniques to submicron particles; (4) Extension of techniques to nonspherical drops; (5) A solid spray diagnostic capability which has been synergistic with many programs from other agencies of the Air Force (AEDC, BMO, Wright-Patterson), the Government and Industry.

The new techniques have been applied to the measurement of sprays and solid particles with accuracies better than 10% and dynamic ranges between 10 and 30. Complex bimodal, trimodal and quadramodal distributions have been measured with an accuracy and resolution exceeding all available techniques. Keywords:

Finally, as a result of this research effort, existing instruments developed. These instruments will constitute an important part of ongoing Air Force programs.

20. DISTRIBUTION/AVAILABILITY OF ABSTRACT	21. ABSTRACT SECURITY CLASSIFICATION
UNCLASSIFIED/UNLIMITED ☒ SAME AS RPT. ☐ DTIC USERS ☐	Unclassified

22a. NAME OF RESPONSIBLE INDIVIDUAL	22b. TELEPHONE NUMBER (Include Area Code)	22c. OFFICE SYMBOL
Julian M Tishkoff	202 767-4935	NA

DD FORM 1473, 83 APR EDITION OF 1 JAN 73 IS OBSOLETE. UNCLASSIFIED

DTIC 8 10 86

TABLE OF CONTENTS

TABLE OF CONTENTS (Cont)

TABLE OF CONTENTS (Cont)

1.0 INTRODUCTION

This, the Final Report of the "Droplet Sizing Research" program, summarizes in a concise manner all the progress and significant accomplishments achieved in the three-year period of 15 January 1983 to 15 January 1986.

To facilitate the reading of this report we have organized the technical section into subsections, each corresponding to a specific technique or application. These techniques are presented chronologically since there is a logical development as a function of time. Most of the significant technical accomplishments have already been reported to AFOSR and furthermore have been published in journals or presented in meetings. The organization of this report will consist largely of these publications since they utilize concise statements and waste no time with unnecessary details.

Finally, Spectron Development Laboratories would like to express that this has been its single most important program in particle characterization. It has provided a broad-based capability in spray diagnostics and it has also been the stepping stone to other programs benefiting the Air Force, other government agencies, and private industry.

2.0 OBJECTIVES AND MAJOR ACCOMPLISHMENTS

To understand the objectives of this program it is necessary to briefly review the state-of-the-art when the program began.

The "Visibility" technique proposed by Farmer, Robinson, Adrian, Orloff, Roberds and Bachalo had become the most widely recognized method for measuring the size and velocity of droplets in a spray. The Principal Investigator of this program, in light of massive experimental evidence gathered by himself as well as other users of the "Visibility" instruments, questioned the validity of this technique. This experimental evidence was included in a proposal to AFOSR, resulting in this program which not only provided a solution to the "Visibility" problem, but produced alternative techniques which have shown to be much more powerful. The objectives of the program were then aimed at advancing the State-of-the-Art by establishing the limitations of the "Visibility" technique as well as developing alternative techniques which would yield accurate methods for characterizing sprays.

As will be shown throughout this report, these objectives have been met and in many ways exceeded. The detailed statement of work can be found in the proposal as well as in the two annual reports. Instead of repeating it here, we would prefer to list the major accomplishments of this program.

Major Accomplishments

1. Established the limitations and sometimes uselessness of the visibility technique.

2. Incorporated the visibility/intensity technique which provided a solution used to retrofit many instruments based on visibility only. These instruments are now used in several centers: G. E., Exxon, Shell, NRC (Canada), Rocketdyne, UCI, etc.

3. Developed the IMAX and PIMAX techniques which are capable of measuring large dynamic ranges with improved accuracy.

4. Generated spray data base with above techniques. These data also point out the limitations, sensitivity and performance capability of the various techniques.

5. Built instruments based on the IMAX technique.

6. In the research process, the techniques have been modeled analytically, including such items as:

   a. Signal sensitivity and error analysis;
   b. Probe volume.

7. Conducted research with nonspherical drops.

   a. Experiments were conducted with monodisperse ellipsoids.
   b. Theoretical model has been partly developed to predict the light scattered by large ellipsoids.

8. The size and velocity of solid particles were accurately measured.

9. The AFOSR research has been the inspiration and stepping stone to other research:

   a. Measurement of submicron particles in LDV applications for AEDC;
   b. Rocket plume diagnostics with laser line velocimeter for BMO;
   c. Rain droplets diagnostics with Top Hat technique for NASA.

10. Four major publications have resulted from this work.

3.0 TECHNICAL DISCUSSION

In this section we provide a concise summary of all the major technical accomplishments achieved throughout the program. There are six subsections, each one dealing with a specific technique or application. The first discusses the Visibility/Intentsity technique; the second discusses the IMAX technique; the third describes the development of an instrument based on IMAX and provides spray data. It also introduces PIMAX; the fourth discusses PIMAX in detail and provides detailed spray measurements; the fifth shows that IMAX/PIMAX can be extended to accurately measure submicron particles; the sixth subsection describes the measurement of nonspherical drops.

3.1 The Visibility/Intensity Technique

In this subsection, we discuss a technique combining the visibility of a Doppler signal and the intensity of the scattered light to measure the size and velocity of particles. It is shown that using only the visibility technique can lead to large errors under many conditions such as dense sprays. It is also shown that this error is considerably reduced and very high resolution is obtained by combining the visibility with the intensity of the scattered light. An instrument was developed using this new concept and measurements were performed in sprays of known characteristics. The results of monodispersed, bimodal and trimodal sprays are reported.

Associated Research

The interferometric technique to measure the size and velocity of particles flowing in a fluid has been in existence for approximately one decade. Farmer[1] introduced the concept of using visibility for particle sizing in the forward scattering direction. Since then, many researchers have contributed to the development of the technique. Robinson and Chu[2], for instance, rederived Farmer's results using a more rigorous approach, and the definition of visibility through the first order Bessel function was confirmed experimentally in forward scatter. However, contrary to what was thought at the time, this visibility relationship could not be used at any angle other than the forward or zero degree. Adrian and Orloff[3] showed that the simple relationship valid in forward scattering

could not be used in backscattering. This finding was also confirmed by Roberds[4], who in addition showed that the configuration of the receiving optics would also affect the relationship between visibility and size.

The biggest known limitation of the visibility technique was its inability to measure particles in a dense field. The main reason being that the probe volume when observed in the forward direction is big and, therefore, the criterion of single particle measurment is not always met. In addition, the technique dictated that the largest measurable droplet was of the order of the fringe spacing. This imposes a limitation of about 200 μm to the largest measurable particle and also results in a large probe volume, since a minimum number of fringes is needed (typically 8) to accurately process a Doppler signal.

Bachalo[5] formulated a mathematical model based on classical optics where the Mie scattering is approximated with refraction, diffraction and reflection. That model was used to predict the visibility of spherical particles in off-axis directions. Experimental results using monodispersed droplets confirmed the validity of the model under many conditions. Pendleton[6] later confirmed these results using a sophisticated numerical model that utilizes the full Mie equations. Recent work conducted by the author shows that there are two major limitations on the existing models. First, all the theories developed thus far predict the Mie scattering from beams of uniform intensity. Second, the formation of the fringe pattern at the probe volume may be affected by secondary scattering of particles immersed in the laser beams before they cross. As a result of these limitations, the relationship between visibility and size is not straight forward and considerable errors can

be made. A model proposed by M. L. Yeoman et al[7] pursues the solutions of the above problems. It consists of two concentric interferometric patterns of two colors such that the small one establishes a region of the big one where the hyperbolic variation of the visibility is negligible. Also digital analysis of the signals helps establish some that are in error. The research reported here shows that using the intensity of the pedestal of the scattered light in addition to the visibility will eliminate many of these errors, significantly improving measurement accuracy.

Errors in the Visibility Measurements

The prediction of the droplet size based on the visibility of the light scattered by the droplet crossing an interferometric pattern of fringes depends on the pattern itself. For a perfect system the fringe visibility should be 100% and the light scattered should be primarily of one type (refraction, reflection or diffraction). There are, however, many causes in practical environments that contribute to alter the fringe pattern and, therefore, confuse the relationship between visibility and size. The result is that apparent sizes instead of true sizes are often measured. As an example, droplets interacting with the laser beams before they cross will randomly reduce (or even destroy) the fringe visibility. If a droplet is measured at such time, it will appear bigger than its true size. There are several factors that produce an error in the visibility measurement and they are listed below. They are divided into two groups: the ones that reduce the visibility and the ones that increase it.

A) Factors that Reduce the Visibility

1) Particles prior to crossover destroy fringe contrast. This is a function of the spray density.

2) Beam excursions due to turbulent hot media.

3) Hyperboloidal reduction of visibility.

4) Light scattered by reflection/ refraction can add destructively for large droplets immersed in a non-uniform (typically Gaussian) beam.

5) Multiple particles in probe volume.

6) Increase in signal background. Normally from many little drops present in the probe volume.

7) Loss of fringe contrast due to faulty components (beamsplitter, etc.)

B) Factors that Increase the Visibility

1) Out of focus drops "masked" by the pinhole.

2) High time rise on leading edge of signal.

The Visibility/Intensity (V/I) Technique

This technique makes use not only of the visibility of a Doppler signal but also the peak intensity of the pedestal. Both parameters are available in the signal and their cross-correlation can be used to eliminate faulty signals produced in many practical environments. This technique will especially prevent small particles (high visibility) from appearing as large. Figure 1 shows a Doppler trace where both the visibility and the peak intensity of the pedestal are indicated. There is a relationship between the size of the droplet and the amount of scattered light given by Mie theory. This relationship can be used to eliminate

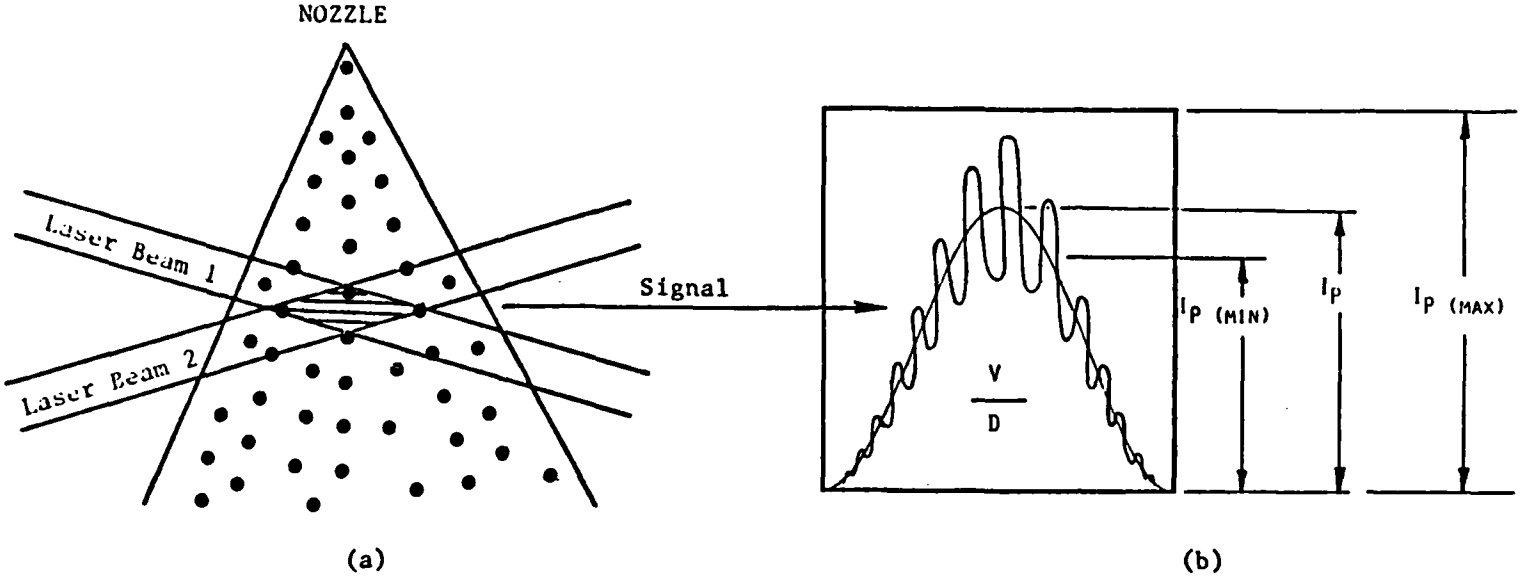

Figure 1. Schematic Representation of Doppler Burst Used in the Visibility/Intensity Technique.

signals with an apparently different size by using the following logic: droplets that produce a certain visibility are associated with a given size; hence, they should scatter light with a given intensity (characterized by I_p). Two exceptions are contemplated: first, droplets with the correct visibility will scatter different amounts of light due to the Gaussian nature of the probe volume's intensity; second, droplets with an erroneous visibility will not scatter light with an intensity corresponding to their apparent size.

The V/I method will then establish intensity limits for every measured visibility. This will produce a well established probe volume as a function of size and will reject droplets measured with an erroneous visibility. For instance, assume that the size corresponding to a visibility V_1 is d_1. Then the light scattered will have a pedestal with maximum intensity $I_{p_1}(max)$. Since this intensity would only be detected from droplets crossing through the middle of the probe volume, Figure 1, more relaxing limits are proposed. That is I_{p_1} will be accepted when $I_{p_1(min)} < I_{p_1} < I_{p_1(max)}$. Obviously, the broader the limits, the larger the error that can be allowed with the visibility technique.

Figure 2 shows three cases that illustrate the correcting properties of the V/I method. Figure 2a shows a droplet of size d_1 with visibility V_1 and intensity I_{p_1}. Since this last one is within established limits, the signal is accepted as valid. Figure 2b shows the signal produced by a droplet of diameter d_2 but the visibility was reduced to V_1 due to fringe contrast reduction. Since the visibility is V_1, this signal would be interpreted as having a diameter d_1. However, the peak intensity of the pedestal I_{p_2} corresponds to its true size (d_2) which is

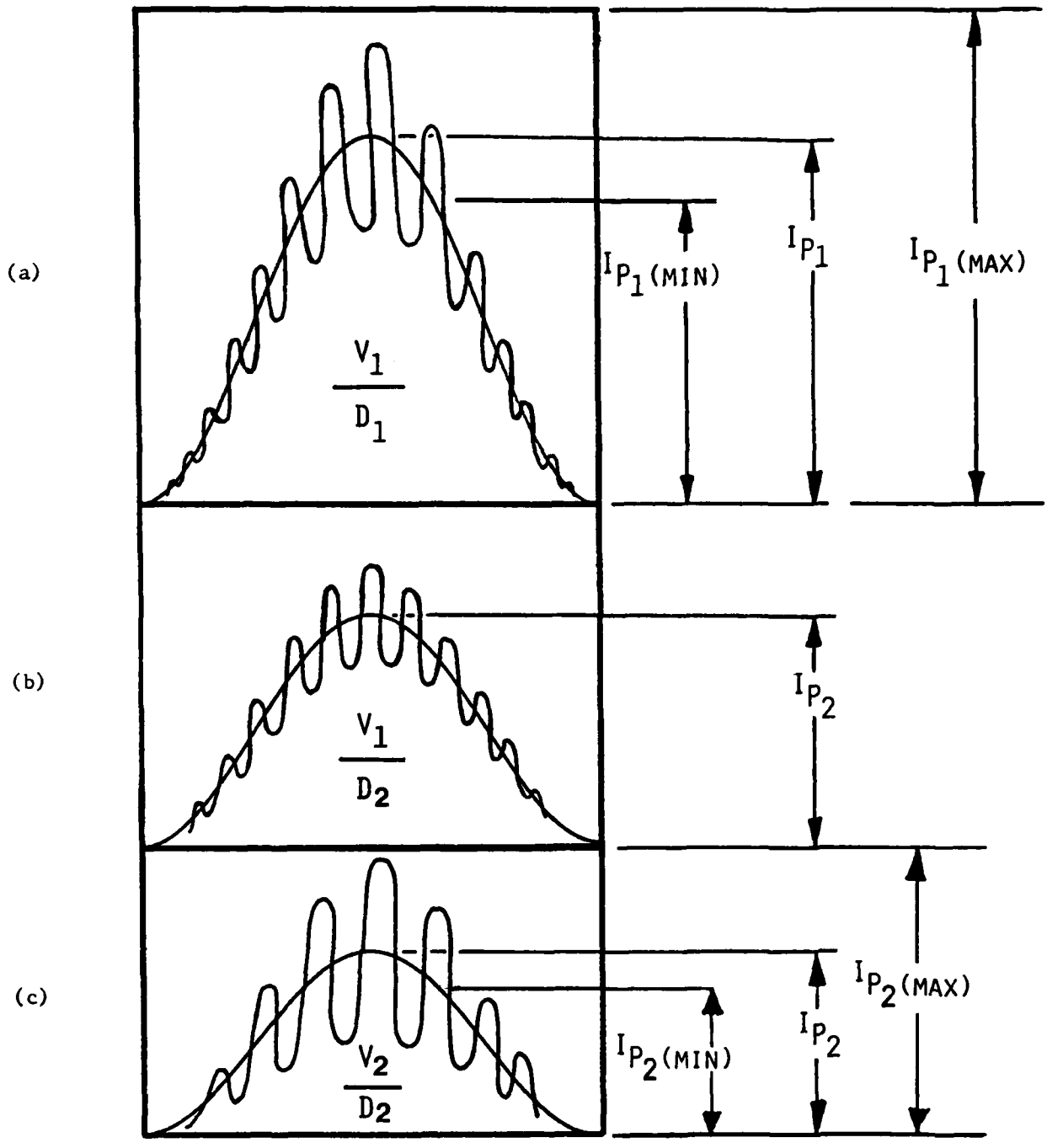

Figure 2. Visibility and Intensity of Two Size Droplets.
3(a) and 3(c) correspond to droplets traveling thru the middle of an undisturbed probe volume; 3(b) could be from a small droplet traveling thru the middle of a disturbed probe volume or a large droplet traveling thru the edge of the Gaussian probe volume.

smaller than $I_{p_1}(\min)$ (to which it is compared). Therefore, the signal is rejected. Figure 2c shows the signal of another droplet of diameter d_2 but with correct visibility V_2 and corresponding pedestal I_{p_2}. This last one will also be accepted.

Since the intensity limits are functions of droplet size, a variable filter like the one shown on Figure 3 is necessary. It contains the intensity limits $I_p(\min)$, $I_p(\max)$ corresponding to any visibility V. Figures 4a and 4b show the raw data and software filtered data of an intensity/visibility plot. Figure 4a shows that the intensity is bounded by $I_p(\max)$ (with a few exceptions due to light reradiated by upstream droplets). Points with different intensity/visibility combinations can be either due to droplets moving through the edge of the Gaussian intensity profile of the probe volume or to droplets with an erroneous visibility. By limiting the intensity of the pedestal for which a signal is considered valid, two things are accomplished: (1) the limits of the probe volume are carefully established; and, (2) most importantly, most of the signals with erroneous visibility are rejected.

Results

Experimental results are presented to illustrate the accuracy and resolution of the visibility/intensity technique, and how it compares with visibility only.

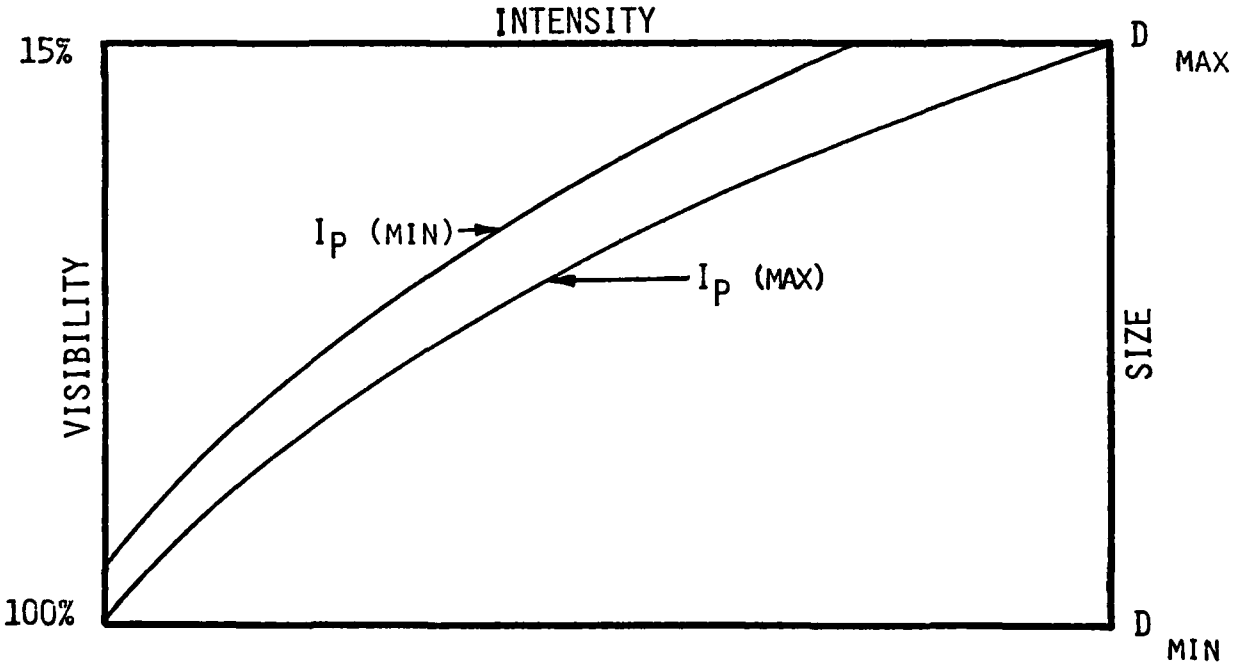

FIGURE 3. Variable Intensity vs. Visibility Software Filter

PRELIMINARY RESULTS OF VISIBILITY/INTENSITY ASSESSMENT

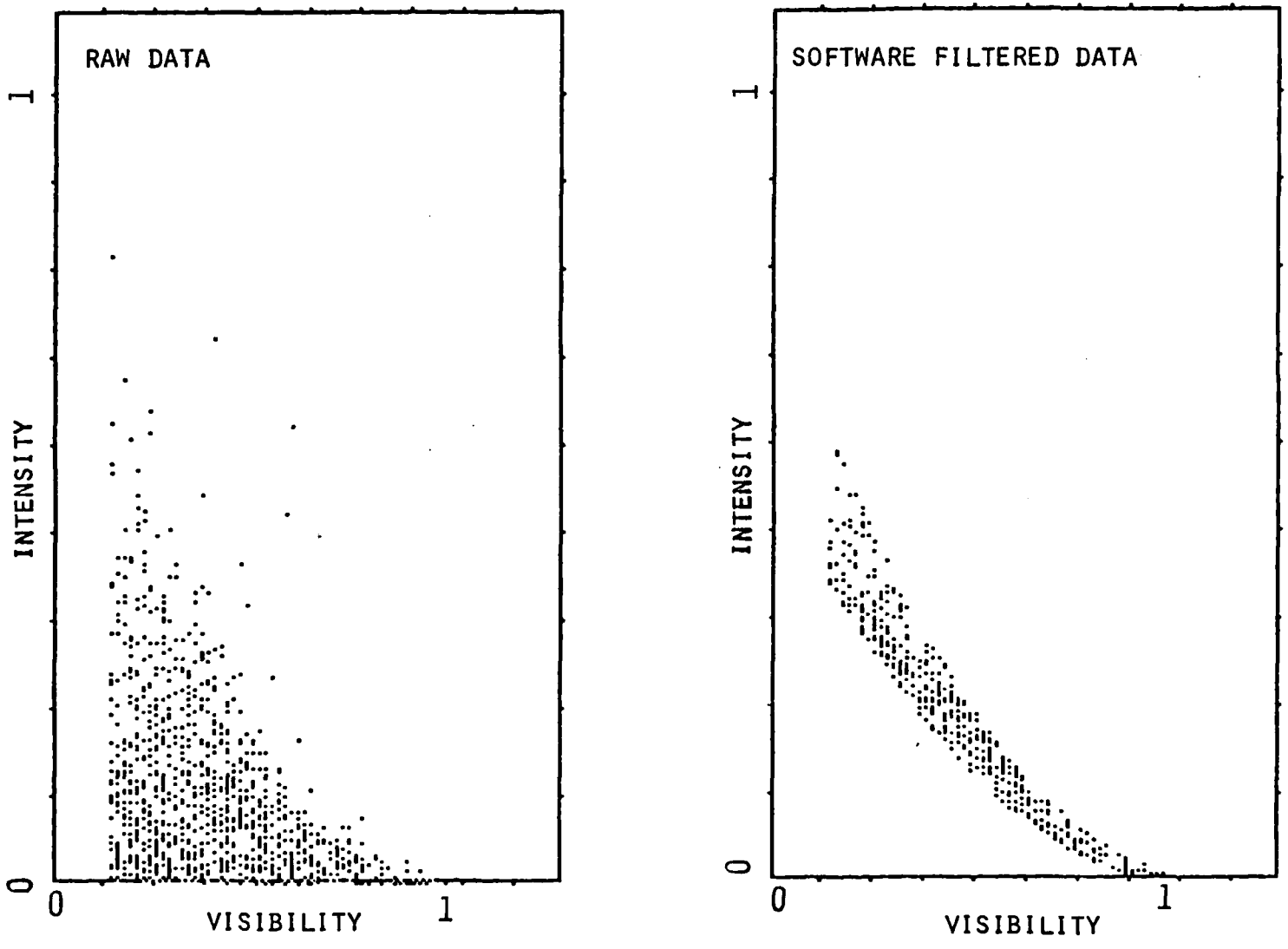

Figure 4. Visibility/Intensity Data of a Spray.

Effect of Beam Blockage on Size Distribution

The effect of a very dense spray blocking the laser beams before the probe volume was studied. Figure 5a shows the histogram produced when monodispersed droplets travel through the middle of an undisturbed probe volume. Figure 5b shows a histogram obtained with the visibility technique of the same monodispersed droplets but now the laser beams have traveled through a real spray before crossing. We made sure that the spray was not going into the probe volume. The fringe pattern produced by crossing two laser beams is well behaved and theoretically predicted in the undisturbed case. However, when the beams travel through a spray, this fringe pattern can be considerably altered due to random beam blockage. The result can be a distorted Doppler signal with a visibility, both lower and higher than that predicted theoretically. Considerable error in the size distribution will then be observed. The size of the error depends on the visibility itself. It is quite apparent from the histograms that what should be a monodispersed distribution is measured as a very broad one. The next histogram shown on Figure 5c shows the results obtained with V/I when the beams travel through the spray before crossing (same conditions as Figure 5b). Notice that a very narrow distribution is thus obtained.

Measurements with the Berglund Liu Droplet Generator

The calibration and verification source used in these experiments was the Berglund Liu monodisperse droplet generator. This generator can

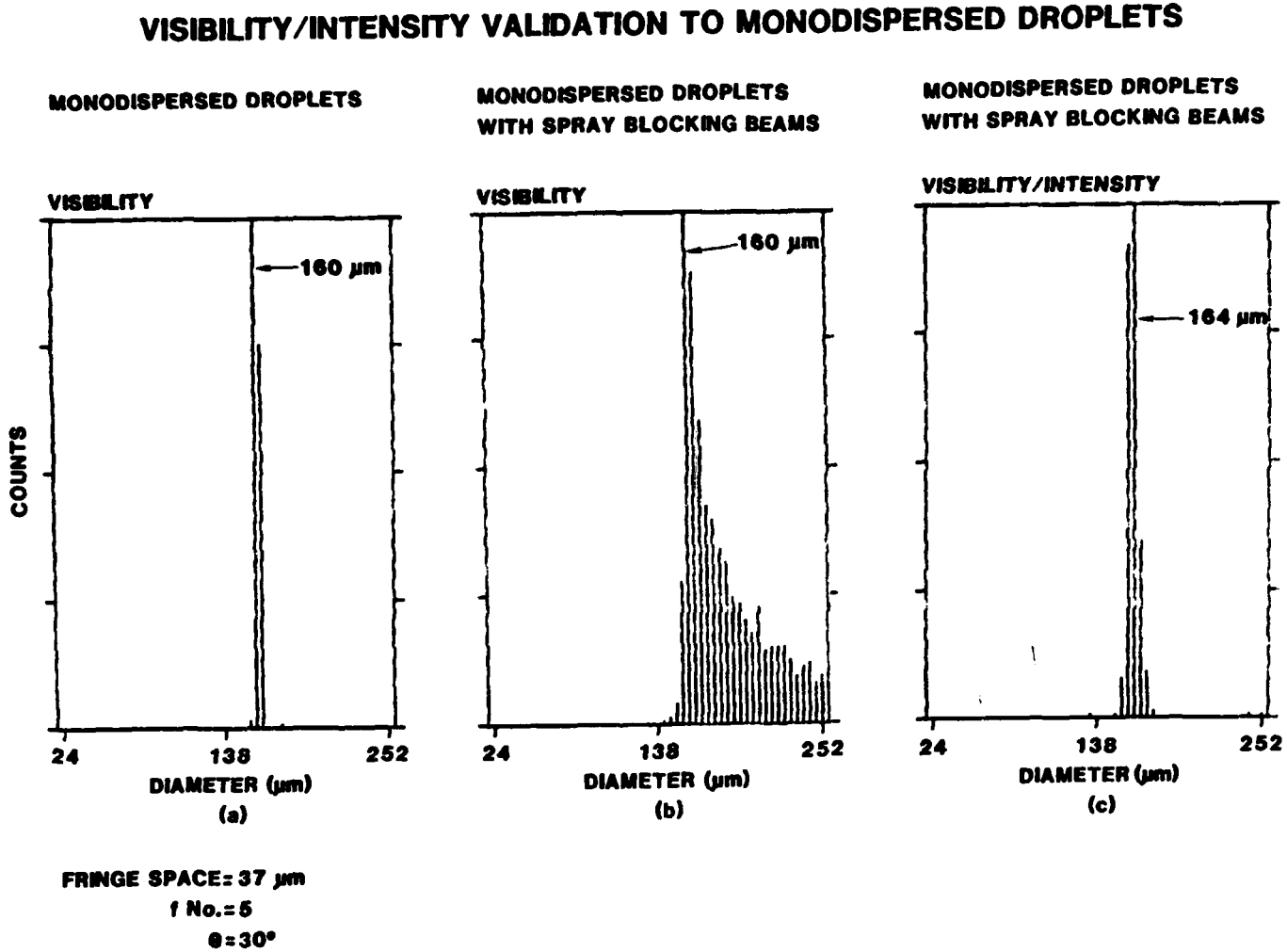

Figure 5. Size distributions of a monodispersed string of droplets.
(a) corresponds to undisturbed laser beams measured with either V or V/I.
(b) and (c) dense spray is blocking laser beams before crossing.

work in two modes: (a) it can generate a string of droplets of known size and equally spaced at the measurement point; (b) using a cap and dispersion air, these droplets can be dispersed into a spray of monodispersed droplets.

It has been observed in previous studies[8] that under some dispersion air conditions, some of the droplets will collide and form other droplets with double or even triple the volume. Therefore, if the primary droplet diameter is d_o, droplets with diameter $2^{1/3}d_o$ and $3^{1/3}\ d_o$ can be produced. It must be pointed out that in these studies, we did not obtain photographic measurements to verify the presence of the secondary droplets. The size of the primary droplets was accurately predicted from the flow rate and frequency of vibration of the pinhole.

One limitation imposed by the Berglund Liu is that it cannot produce droplets of a given size at arbitrary spacing. Since the measurement instrument requires the presence of only one droplet in the probe volume, that limits the size droplet that can be measured.

The procedure used in these experiments was to produce a string of large monodispersed droplets to calibrate the instrument. Then smaller droplets were produced by increasing the frequency of vibration of the orifice, and with the dispersion air a spray of these droplets was formed. Typical number density at the probe volume was 500 droplets/cm^3 and the diameter of the spray at the plane of measurements was about 4 mm.

A DSI system with V/I capability was used to obtain the data shown below.

Optical configuration:

- Collection angle of 30°
- Transmitting lens = 495 mm
- Waist diameter = 300 μm
- Fringe spacing = 13.6 μm
- Collection F# = 5

The high voltage to the photomultiplier was established with a droplet string of diameter 100 μm.

The size range of interest was 9 to 92 μm.

A spray of droplets with primary diameter of 53 μm was then produced using the Berglund Liu with a flow rate of 0.21 cc/min and frequency of 45.8K Hz and the dispersion air. For the conditions selected above, this size will produce a visibility of 58%.

Notice that for primary droplets of 53 μm, the droplets will have a diameter of $2^{1/3}$ x 53 = 66 μm, and the triplets' diameter will be $3^{1/3}$ x 53 = 76 μm.

Results are shown for both Visibility/Intensity and visibility only to provide some comparison.

Figure 6 shows the measurements of the monodispersed spray of 53 μm.

Figure 7a shows the data of the spray formed of primary droplets and doublets.

Figure 7b shows results similar to Figure 7a but obtained with visibility only. Notice how much broader the distributions are.

Figure 7c shows a spray containing primary droplets, doublets and triplets.

Figure 7d shows results similar to Figure 7c but obtained with visibility only. Notice that the distribution is broader and the resolution is not as fine.

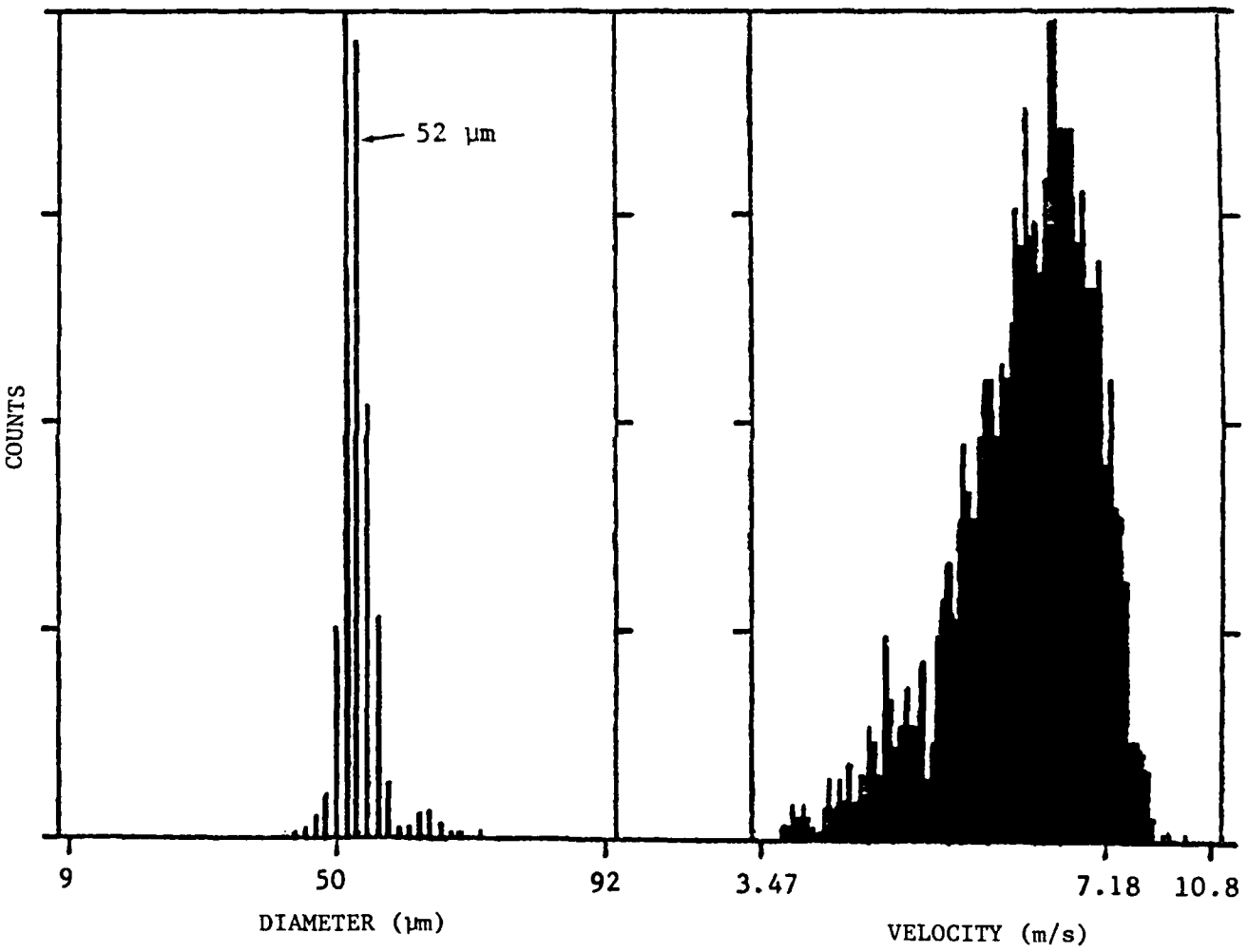

Figure 6. Visibility/Intensity Measurements of Monodispersed Spray.

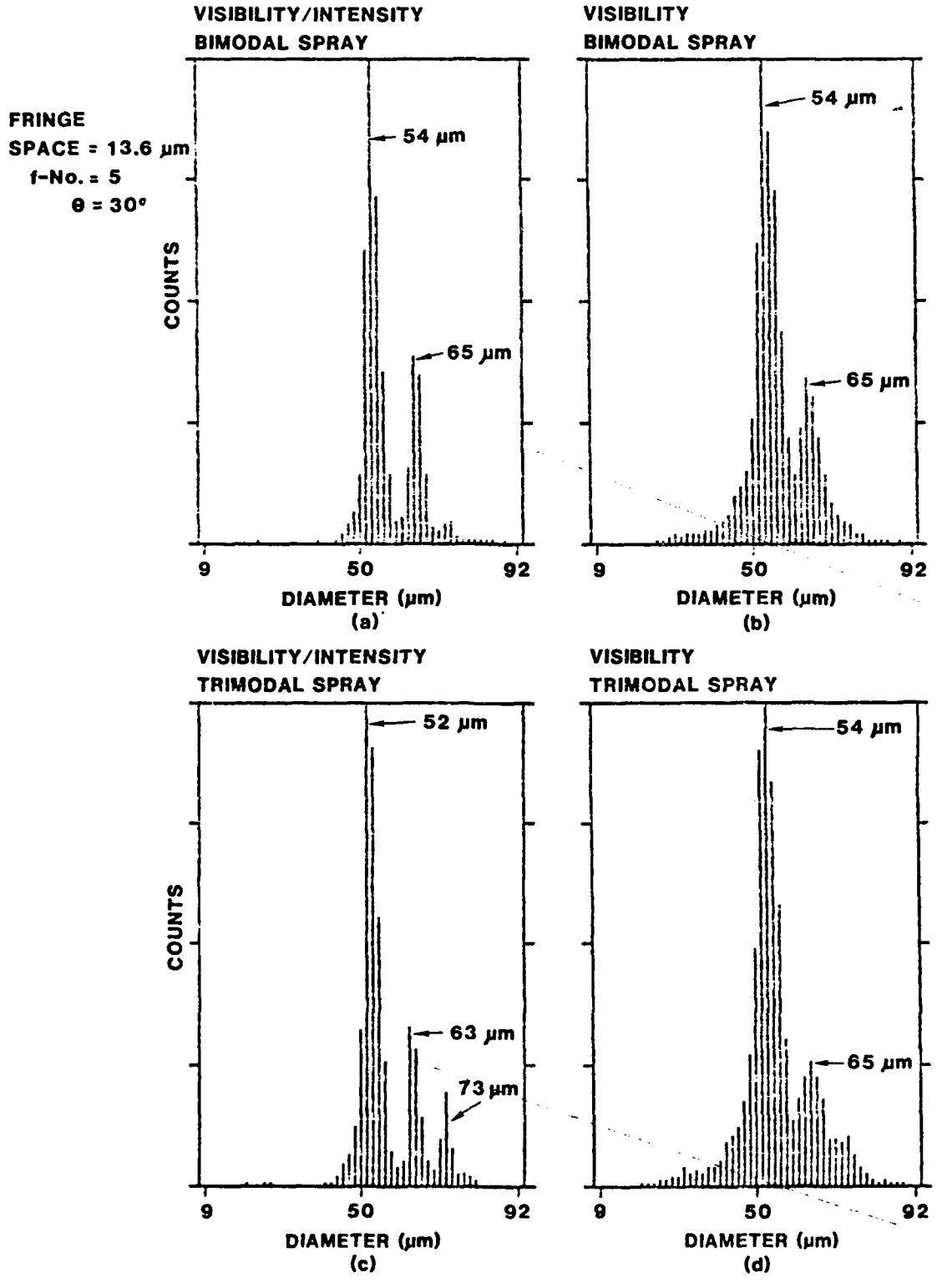

FIGURE 7. SIZE DISTRIBUTIONS OF BIMODAL AND TRIMODAL SPRAYS WITH VISIBILITY AND VISIBILITY/INTENSITY

Both the accuracy and resolution of these measurements are very good. The theoretically predicted sizes are 53 μm , 66 μm, and 76 μm. The corresponding measured diameters are (52 to 54), (63 to 65), and 73 μm.

Larger errors (about 20%) can be expected when measuring the size at a higher visibility (80%).

Conclusions

The simultaneous measurement of visibility and intensity to measure and validate the diameter of droplets in a spray is shown to be accurate and with high resolution. This technique extends the use of the visibility technique to more realistic environments and will avoid erroneous data by being selective during the data validation process.

Since many of the erroneous data are the result of high droplet concentration, the percent of signals rejected can be used to establish the limits of the technique.

An automatic calibration logic used to establish the gain of the photodetector makes the technique self-calibrating.

The technique, however, suffers of two serious limitations: first, it only works over a narrow size range of about 10:1; second, the rejected data may bias the size and velocity results.

References

1. W. M. Farmer, "Measurement of Particle Size, Number Density, and Velocity Using a Laser Interferometer", Applied Optics, Vol. 11, No. 11, (1972).

2. D. M. Robinson and W. P. Chu, Applied Optics, Vol. 14, 2177 (1975).

3. R. T. Adrian and K. L. Orloff, "Laser Anemometer Signals: Visibility Characteristics and Application to Particle Sizing", Applied Optics, Vol. 16, No. 3 (1977).

4. D. W. Roberds, "Particle Sizing Using Laser Interferometry", Applied Optics, Vol. 16, No. 7 (1976).

5. W. D. Bachalo, "Method for Measuring the Size and Velocity of Spheres by Dual-Beam Light Scatter Interferometry", Applied Optics, Vol. 19, No. 3 (1980).

6. J. D. Pendleton, "Mie and Refraction Theory Comparison for Particle Sizing with the Laser Velocimeter", Applied Optics, Vol. 21, No. 4. (1982).

7. M. L. Yeoman, H. J. White, B. J. Azzopadi, C. J. Bates, and P. J. Robets, "Optical Development and Application of a Two Colour LDA System for the Simultaneous Measurement of Particle Size and Particle Velocity", Presented in the Winter Annual Meeting of ASME, Engineering Applications of Laser Velocimetry, Phoenix, Arizona, November 14-19 (1982).

8. B. H. Liu, R. N. Berglund, J. K. Argawal, "Experimental Studies of Opticle Partile Counters", Atmospheric Environment, Vol. 8, pp. 717-732 (1974).

3.2 The IMAX Technique

A technique for measuring nonintrusively, and in real time, the size and velocity of droplets in a spray is presented. A small beam identifies the center of a larger beam, thus defining a region of almost uniform intensity, and only droplets crossing through such a center are measured. The size is obtained from the absolute scattered light, and the velocity from the modulated signal produced by the interferometric pattern. A self-calibrating algorithm is also discussed. Results are presented for a spray of predictable characteristics.

Introduction

A novel nonintrusive single particle counter (NSPC) to measure the size and velocity of particles in a two-phase flow is described here. This method bases the size information on the absolute light scattered by individual particles crossing through the middle of a Gaussian laser beam. To define the middle of the Gaussian profile, two laser beams of different diameters are crossed such that the small beam intersects the middle of the large beam. Thus an interference pattern of fringes is formed in the crossover, defining a region of almost uniform intensity in the large beam. Both, size and velocity information can be obtained from signals exhibiting adequate Doppler modulation. An alternative method consists of crossing two small beams of a given wavelength in the middle of a large beam of a different wavelength. NSPC's

find application in many areas where the spatial resolution of size and velocity distributions is needed. For example, fuel spray studies, aerosol studies, flue gas desulfurization, spray drying, paint sprays, and sizing biological structures. They are also very useful on in-line monitoring and quality control systems where no extraction of samples is desired.

Several NSPC's using absolute scattered light have been proposed and they can be divided into two groups. In the first group[1-3] Gaussian laser beams are used and various mathematical inversion techniques have been proposed to extract the true size distribution from the signal amplitude distribution. Several assumptions are needed to perform such inversion, such as assuming the form of the size distribution[1] or a uniform average velocity for all the particles regardless of size[2]. A method to account for the loss of collected light due to particles partially masked by a pinhole has also been described[3]. The second group of NSPC's uses a probe volume of known illumination to avoid the ambiguity of particle position. The technique described here falls in this group. Several approaches have been proposed[4-7] to accomplish this task. Apertures are used to cut off the edges of the Gaussian beam and thus image a probe volume of almost uniform illumination[4,5]. One of the apertures[4] had, in addition, two wedges that when properly oriented can be used to obtain the velocity vector in two components (magnitude and direction). Ring-shaped probe volumes have also been produced[6] by a TEM_{01} laser and a ring-shaped aperture. The measurement volume is defined by the intersection of apertures in front of two photomultipliers. A method[7] very similar to the two-color

method described here which evolved independently has also been used. Four beams of two different colors are crossed forming two fringe patterns of different size such that the small fringe pattern is in the middle of the large one. To extend the dynamic range of the visibility technique, they used visibility to cover part of the size range and intensity to cover the rest. The term visibility refers to the ratio of the modulated part of the signal to the pedestal of a Doppler signal.

Some of the differences between the latter method[7] and the one reported here are:

1) The technique reported here is based on a single color, and the two color system uses three beams instead of four;

2) Visibility is not used to obtain part of the size distribution;

3) Visibility alone cannot be used to calibrate attenuation, since the very attenuation reduces the fringe visibility and randomly modifies the phase of the beams. Instead a combination of visibility and intensity is used[8] to establish the validity of the signal and calibrate the attenuation.

The mathematical model presented here is for spherical particles much larger than the wavelength and we use diffraction, refraction and reflection to characterize the scattered light[9]. This results in closed form solutions of the dynamic range and error.

Results are presented for sprays of known characteristics.

Problem Statement

The method discussed here bases the size measurement on the absolute intensity scattered by the droplet crossing the probe volume, and

the velocity measurement on the classical Doppler signal. It is referred to as the IMAX method. In situ single particle counters are limited because of the nonuniform profile (typically Gaussian) of laser beams. Under this condition a particle crossing the middle of the beam will scatter more light than a similar particle crossing through the edge. Therefore, the relationship between size and scattered light is not unique.

To circumvent this problem, two beams of unequal size are crossed such that the small beam identifies the middle of the large beam and therefore, removing the Gaussian ambiguity. Laser beams are chosen because of their spatial and temporal coherence and because of their size. These beams will interfere where they cross and a fringe pattern will be formed in the middle of the large beam. Signals exhibiting an ac modulation will have crossed the fringe pattern and therefore, the middle of the large beam. Both size and velocity of individual spherical particles can be extracted from this signal.

At least two approaches can be used to implement the above concept. The first consists of crossing two laser beams of different diameters but with the same wavelength. In the second two small beams of one wavelength cross in the middle of a larger beam of another wavelength. These approaches will now be explained starting with the second.

Two-Color System

Figure 1 illustrates the probe volume of this method. A spherical particle crossing through the fringes will also cross through a

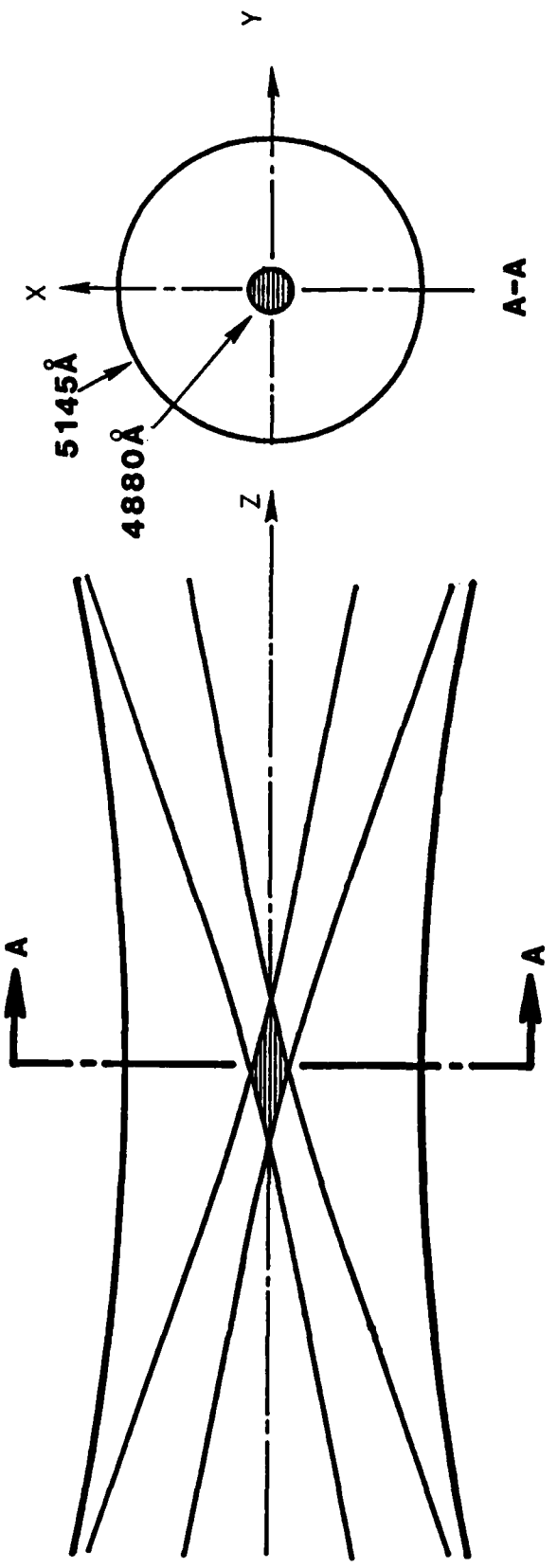

Figure 1. Probe Volume of Two-Color I_{max} Technique.

region of almost uniform intensity of the large beam. The ratio of the two beam diameters will establish the uniformity of the intensity incident on the droplet.

If we refer to the small beam as 1 and the large beam as 2, the intensity profiles in the probe volume can be spectrally separated, and given by:

$$I_1 = 2I_{o_1} \exp\left[\left(\frac{-2}{b_{o_1}^2}\right)\left(x^2+y^2+z^2\gamma^2/4\right)\right] \cdot \left[\cosh\left(\frac{2xz\gamma}{b_{o_1}^2}\right) + \cos\frac{4\pi x \sin\left(\frac{\gamma}{2}\right)}{\lambda}\right], \quad (1)$$

and

$$I_2 = I_{o_2} \exp\left[-\frac{2}{b_{o_2}^2}\left(x^2+y^2\right)\right] \quad . \quad (2)$$

Where I_o is the center intensity, γ is the intersection angle, b_o the waist radius, λ the laser wavelength, and x,y,z the coordinates. The z dependence of the large beam is neglibible. If we also assume that

$\frac{z\gamma}{2} \approx 0$ (which is an excellent assumption since a pinhole in the receiver will limit the value of z), the intensity scattered by a spherical particle is given by:

$$I_{s_1} = 2I_{o_1} K_{o_1} d^2 \exp\left[\left(-\frac{2}{b_{o_1}^2}\right)\left(x^2+y^2\right)\right]\left(1 + \cos 2\,\frac{\pi\gamma x}{\lambda} \cdot V\right) \quad , \quad (3)$$

and

$$I_{s_2} = I_{o_2} K_{o_2} d^2 \exp\left[\left(-\frac{2}{b_{o_2}^2}\right)\left(x^2+y^2\right)\right] \quad , \quad (4)$$

228615F32/14

where

$$Ko = \frac{1}{4r^2} \int_{A_{lens}} \left\{ \left[\varepsilon^2(\theta,n)\ D(\theta)\right]_{refraction} + \left[\varepsilon^2(\theta,n) D(\theta)\right]_{reflection} + \left[\frac{J_1^2\ (\alpha \sin\theta)}{\sin^2\theta}\right]_{diff.} \right\} dA \quad . \tag{5}$$

K_o is a scattering coefficient, D is the divergence, n the index of refraction, ε the fraction of energy for every ray reflected or refracted, d is the diameter of a spherical particle, V is its visibility, (defined as the ratio of the modulated signal to the pedestal) r the distance from the scattering center to the collecting lens, and θ the collection angle measured from the forward direction. It can be shown[9] that the contributions of these three terms is a function of angle. To keep the following analysis simple we will choose a collection angle θ of 30°. Assuming that the solid angle of the collecting lens is small with respect to θ we can then compare the intensities scattered at the discrete angle θ.

The refraction or reflection terms are given by:

$$i_R = \alpha^2 \varepsilon^2 D \quad ,$$

and the diffraction by:

$$i_D = \frac{\alpha^2}{\sin^2\theta} J_1^2\ (\alpha \sin\theta) \quad .$$

where $\alpha = \frac{\pi d}{\lambda}$ is the size parameter, and J_1 the Bessel's function of the first kind. Reference (9) shows that for S polarization:

$$i(\text{refraction}) = 1.0375\ \alpha^2$$

$$i(\text{reflection}) = 0.0785\ \alpha^2$$

and it can be calculated that

$$i_D(\alpha) < .088\ \alpha^2 \quad \text{for } \alpha > 49\ (d > 7.6\ \mu m).$$

At this angle the combined reflected and diffracted light represent 16% of the refracted light. Which implies that in general the three components must be taken into account. It is assumed that the collecting lens is in the plane of symmetry of the crossing beams. The above equations show that the scattered light intensity is proportional to the square of the diameter of the sphere. This approximation is only valid for diameters larger than about 10 wavelengths. Note that the angle θ (deviation of incident pencil of light) to an arbitrary position of the lens is different for both beams (except on the line of symmetry). However, the integrated value is the same as long as the collecting lens is in the plane of symmetry. In this technique the ac modulation of I_{s_1} is used to establish detectability of the signal and to measure the velocity. For a given threshold level, (minimum ac signal accepted by the electronics) the larger the dynamic size range, the farther from the center of the beam the largest particle can cross and still exhibit ac modulation and, therefore, be detectable. This will introduce an error in the measurement as will be discussed in the next section.

The peak to peak ac signal is then given by:

$$I_{ac_1} = 4\, I_{o_1} K_{o_1} V d^2 \exp\left[\left(-\frac{2}{b_{o_1}^2}\right)(x^2+y^2)\right] \quad , \tag{6}$$

and the pedestal is given by:

$$P_1 = 2 I_{o_1} K_{o_1} d^2 \exp\left[\left(-\frac{2}{b_{o_1}^2}\right)(x^2+y^2)\right] \quad . \tag{7}$$

Note that the pedestal is simply the sum of the Gaussian intensities without interference.

Dynamic size range and error analysis

There are two known sources of error in the IMAX method. First is the error introduced by beam blockage produced by other particles in the trajectory of the beams and scattered light. This one is difficult to quantify and will be discussed with the results. Second, since the small beam has a finite diameter the particles can travel a small distance away from the center of the big beam and still cross sufficient fringes to be detectable. The farther from the center it can be detectable, the larger the error it can produce. It will be shown here that this error increases with dynamic size range, and decreases with ratio of the large to small beam.

The dynamic range is limited by the electronic and optical noise. In general, we can establish that there is a threshold associated with the minimum processible ac signal, and a saturation level associated with the largest signal processible by the electronics. All the signals

accepted by the electronics must fall between these two limits. Equation (6) gives the peak to peak ac signal. Notice that both the diameter (d) and the visibility (V) influence the above expression.

To simplify this analysis we will neglect the contribution of diffraction at a collection angle of 30°. This assumption is reasonable for spheres larger than 7 μm where the contributions of reflection and diffraction are less than 16%. The dynamic range is actually larger when diffraction is included.

The minimum processible ac signal is produced by the smallest particle (with diameter d_{min}) crossing the probe volume at y = o and crossing the minimum number of fringes required by the electronics ($x = b_{o_1}$).

Therefore, $I_{ac_{min}} = 4I_{o_1}K_{o_1}d_{min}^2 \exp(-2)$ where it has been assumed that the visibility of the smallest particle is 1.

The maximum ac signal is produced by a droplet of diameter d_o (not necessarily d_{max}) and visibility V_o.

$$I_{ac_{max}} = 4I_{o_1}K_{o_1}d_o^2V_o \exp\left[\left(-\frac{2}{b_{o_1}^2}\right)(x^2+y^2)\right] \quad . \tag{8}$$

The farthest from the center this particle can be detected is when:

$$I_{ac_{max}} = I_{ac_{min}}$$

and it crosses sufficient number of fringe ($x = b_{o_1}$). Therefore,

$$4I_{o_1}K_{o_1}d_o^2 \exp\left[\left(-\frac{2}{b_{o_1}^2}\right)(b_{o_1}^2+y^2)\right] = 4I_{o_1}K_{o_1}d_{min}^2 \exp(-2) \quad .$$

Solving for the size range, we obtain:

$$\left(\frac{d_o}{d_{min}}\right)^2 = \frac{\exp(-2)}{V_o} \exp\left[\frac{2\left(b_{o_1}^2 + y^2\right)}{b_{o_1}^2}\right] = \frac{1}{V_o} \exp\left(\frac{2y^2}{b_{o_1}^2}\right) \quad ,$$

and

$$2y^2 = b_{o_1}^2 \ln\left[\left(\frac{d_o}{d_{min}}\right)^2 \frac{V_o}{\exp(-2)}\right] - 2\, b_{o_1}^2 \quad ,$$

which results in

$$2y^2 = b_{o_1}^2 \ln\left[V_o\left(\frac{d_o}{d_{min}}\right)^2\right] \quad . \tag{9}$$

The error in the size will be due to an error in the intensity scattered by the large beam when the particle crosses at $y > o$ (notice that the particle must cross through $x = 0$). If we state that the large beam is m times larger than the small one,

$$\frac{I_{s_2}}{I_{o_2} K_{o_2} d^2} = \exp\left(\frac{-2y^2}{m^2 b_{o_1}^2}\right) \quad . \tag{10}$$

To simplify the error analysis, let us assume that the optical parameters are chosen such that for any size range the visibility of the largest droplet is larger than zero.

Then the maximum ac signal is produced by a particle of diameter $d_o = 0.626\ d_{max}$ and its visibility is 43%.

Substituting these values into Equation 9, we obtain:

$$\frac{2y^2}{b_{o_1}^2} = \ln\left[.1685\ \left(\frac{d_{max}}{d_{min}}\right)^2\right] \quad .$$

The maximum errors resulting from the finite size of the beams can now be presented in tabular form.

m	d_{max}/d_{min}	$\frac{2y^2}{b_{o_1}^2}$	$\frac{I_{s_2}}{I_{o_2} K_{o_2}^2}$	max error
7	10	2.82	.94	3%
7	20	4.21	.92	4%
7	30	5.02	.90	5%
5	10	2.82	.89	5%
5	20	4.21	.85	8%
5	30	5.02	.82	10%

Single color system

Figure 2 shows a schematic representation of the probe volume formed by crossing two beams of the same wavelength but different diameters. There are several fundamental differences between this and the two color system: 1) Fringes are formed everywhere the large and small beams mix; 2) The pedestal of the large beams can not be spectrally separated but electronically filtered. The intensity distibution of either beam can be expressed as:

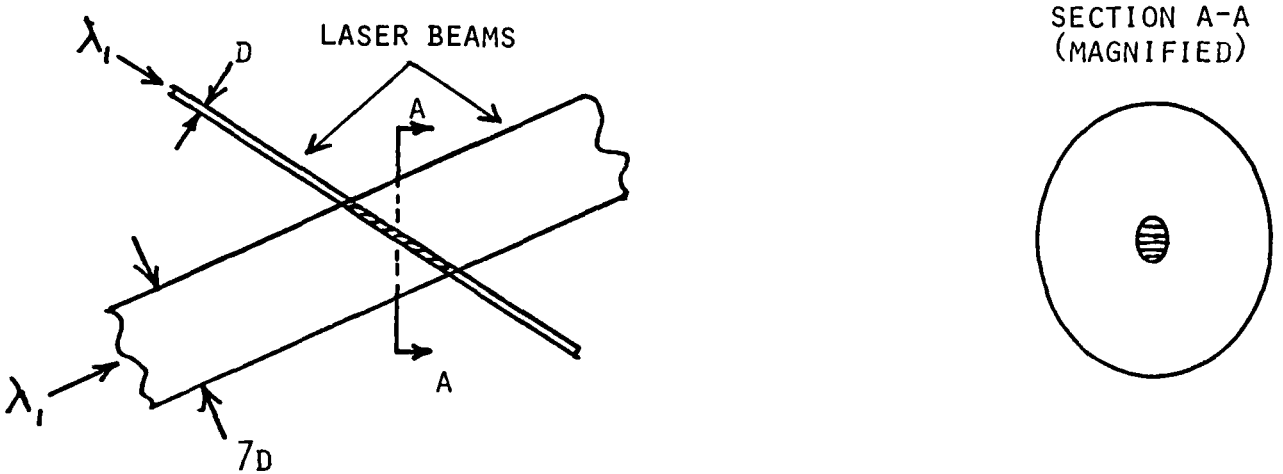

Figure 2. Probe Volume of Single-Color I_{max} Technique

$$I_1 = I_{o_1} \exp\left[-\frac{2}{b_{o_1}^2}(x^2+y^2)\right] \quad , \tag{11}$$

and

$$I_2 = I_{o_2} \exp\left[-\frac{2}{b_{o_2}^2}(x^2+y^2)\right] \quad . \tag{12}$$

The intensity scattered by the spherical particle can be expressed by:

$$I_s = I_{s_1} + I_{s_2} + 2\sqrt{I_{s_1} I_{s_2}}\cos\beta \cdot V$$

where

$$I_s = IK_o d^2 \quad ,$$

β is the phase angle, and again it is assumed that the collecting lens is on the plane of symmetry of the two crossing beams. The pedestal is given by

$$P = I_{s_1} + I_{s_2}$$

and the peak to peak ac intensity:

$$I_{ac} = 2\sqrt{I_{s_1} I_{s_2}}\, V \,(\cos\beta = 1) - 2\sqrt{I_{s_1} I_{s_2}}\, V \,(\cos\beta = -1)$$

$$= 4\sqrt{I_{s_1} I_{s_2}}\, V \quad .$$

228615F32/14

That is,

$$P = I_{o_1} K_o d^2 \exp\left[-\frac{2}{b_{o_1}^2}(x^2+y^2)\right] + I_{o_2} K_o d^2 \times \exp\left[-\frac{2}{b_{o_2}^2}(x^2+y^2)\right] \quad , \tag{13}$$

and

$$I_{ac} = 4K_o\sqrt{I_{o_1} I_{o_2}}\, d^2 V \exp\left[-\frac{(x^2+y^2)}{b_{o_1}^2} - \frac{(x^2+y^2)}{b_{o_2}^2}\right] \quad . \tag{14}$$

Following the same approach as before, and again neglecting the contribution of diffraction for the off-axis collection angle. If we let $m = b_{o_2}/b_{o_1}$, we obtain:

$$I_{ac_{min}} = 4K_o\sqrt{I_{o_1} I_{o_2}}\, d_{min}^2 \exp\left(-1 - \frac{1}{m^2}\right) \quad , \tag{15}$$

$$I_{ac_{max}} = 4K_o\sqrt{I_{o_1} I_{o_2}}\, d_o^2 V_o \exp\left[-\frac{(b_{o_1}^2+y^2)}{b_{o_1}^2} - \frac{(b_{o_1}^2+y^2)}{m^2 b_{o_1}^2}\right] \quad . \tag{16}$$

The variation in y will result in an error of the measured pedestal. If we can assume that m is large, then the pedestal of the large beam can be recovered by electronic filtering and it is given by the second term of Equation 13. This variation in y is obtained equating 15 and 16, and we obtain

$$y^2 = \frac{m^2 b_{o_1}^2}{m^2+1} \ln\left(\frac{d_o^2 V_o}{d_{min}^2}\right) \quad . \tag{17}$$

228615F32/14

The error in the size will result from droplets crossing the pedestal of the large beam at x = o and y given by Equation 17. That is:

$$\frac{I_{s_2}}{I_{o_2} K_o d^2} = \exp\left[\frac{-2y^2}{m^2 b_{o_1}^2}\right] \quad . \tag{18}$$

Making similar assumptions as before:

$$d_o = .626\, d_{max} \text{ and } V_o = 0.43$$

$$\therefore \frac{2y^2}{m^2 b_{o_1}^2} = \frac{2}{m^2+1} \ln\left[.1685 \left(\frac{d_{max}}{d_{min}}\right)^2\right] \quad . \tag{19}$$

The maximum errors resulting from the finite size of the beams can be presented in tabular form:

m	d_{max}/d_{min}	$\frac{2y^2}{m^2 b_{o_1}^2}$	$\frac{I_{s_2}}{I_{o_2} K_{o_2} d^2}$	max error
7	10	.113	.89	5%
7	20	.168	.84	8%
7	30	.2	.82	10%
5	10	.22	.80	10%
5	20	.32	.72	15%
5	30	.39	.68	18%

It should be pointed out that the technique discussed here bases the detectability of the signal on the modulated or ac part of the scattered light. It is, therefore, important that no zeros are present in the visibility function. There are two other aspects of the theoretical foundation upon which this technique is based which need to be taken into account. First, SPC's based on absolute scattered light require calibration at one datum point. This calibration can be difficult when measuring dense sprays and a method to obtain automatic calibration is discussed. Second, provision must be made to account for the dependence of the probe volume as a function of particle size. These two algorithms will now be discussed.

A Self-Calibrating Algorithm

The algorithm is based on measuring the visibility of any size class droplet. Combining the visibility and intensity[8] of the signal a very accurate measurement of the size can be made. Knowing the size of the chosen corresponding visibility one can then establish the amplitude of the pedestal of this signal by adjusting the gain of the photo detector. The logic is as follows: for a given visibility (chosen in the most accurate region of the visibility function) there is an associated size and, therefore, an intensity scattered from the large beam. Since the intensity of this large beam is almost uniform the scattered light associated with the chosen visibility will be almost constant in the absence of errors in the visibility. There are, however, errors associated with measuring visibility in a dense spray and these points are rejected by V/I[8]. The process is an iterative one where V/I is

implemented by choosing several narrow intensity bands to establish points out of control. The gain to the photo-detector is adjusted until the majority of the points fall in the pre-established intensity band corresponding to the measured size.

The Probe Volume

The dynamic range exercise indicated that droplets that scatter light with large modulation are detectable over a larger region than those that scatter light with little modulation. As a result, the probe volume or region of detectability is a function of droplet size. Algorithms have been presented[10] to define the probe volume in LDV type systems. A very simple algorithm will be presented here for the two color system and off-axis collection.

Notice that only the small beams define the probe volume in this case and, therefore, the probe volume will be a standard LDV type volume. The approach followed will be very similar to the one described in Reference (10).

There are two signal levels imposed by the electronics: the saturation (I_{max}) and the threshold (I_{min}). The intensity to the peak of the ac modulation (I_{peak}) of the largest signal must be less than I_{max}, and the smallest detectable signal must be larger than I_{min} (defined peak to peak).

$$I_{peak_1} = 2I_{o_1} K_{o_1} d_o^2 (1+V_o) < I_{max} \quad . \tag{20}$$

where d_o produces the largest signal within the detectable size range, and V_o is its corresponding visibility.

Solving for I_{o_1} we obtain:

$$I_{o_1} = \frac{I_{max}}{2K_{o_1} d_o^2 (1+V_o)} \quad . \tag{21}$$

This expression can now be substituted in Equation 6 to obtain:

$$I_{ac_1} = \frac{2d^2 V I_{max}}{d_o^2 (1+V_o)} \exp\left[\left(-\frac{2}{b_{o_1}^2}\right)(x^2+y^2)\right] \quad , \tag{22}$$

and the detectability criterion establishes that $I_{ac_1} \geq I_{min}$ and that sufficient fringes are crossed. If we assume that the number of fringes processed by the electronics is equal to that in the waist diameter, $x = b_{o_1}$.

Solving for y in Equation (22) we obtain:

$$y \leq \sqrt{-\frac{b_{o_1}^2}{2} \ln\left[\frac{I_{min}}{2I_{max}}\left(\frac{d_o}{d}\right)^2 \frac{(1+V_o)}{V}\right] - b_{o_1}^2} \quad . \tag{23}$$

The cross-sectional area of sensitivity for an off-axis pinhole limited signal can be approximated by:

$$A(d) = \frac{2D_p y}{\sin\theta} \cdot \frac{f_1}{f_2} \quad , \tag{24}$$

where D_p is the pinhole diameter and f_1/f_2 determines the magnification of the receiving optics. The effect of the pinhole and the coordinate system are illustrated on Figure 3.

As seen by Equation (23) and (24) the area of detectability (in the yz plane) is only a function of droplet size and corresponding visibility. This area can now be normalized and provide a weighting function to size distributions otherwise biased to the large signals.

This weighting factor is given by:

$$w(d) = \frac{A(d)}{A_{max}} \quad .$$

The number density of any size droplet can also be calculated by dividing the number of counts of the given size by its corresponding sampling volume (SV).

The sampling volume is a cylinder with cross-section A(d) and length equal to the droplet velocity (U(d)) multiplied by the effective sampling time (T).

That is $SV(d) = A(d)U(d)T$, and $T = TS - \sum_{i=1}^{M} N\ \tau D_i - M\tau_o$,

where TS is the total sampling time to collect M samples, N is the number of fringes, τD_i is the Doppler period of sample i and τ_o is the processor's dead time after every sample.

The number density of size d is then given by:

$$ND(d) = \frac{N(d)}{A_{max}U(d)T} \quad , \tag{25}$$

where n(d) is the raw count of size d.

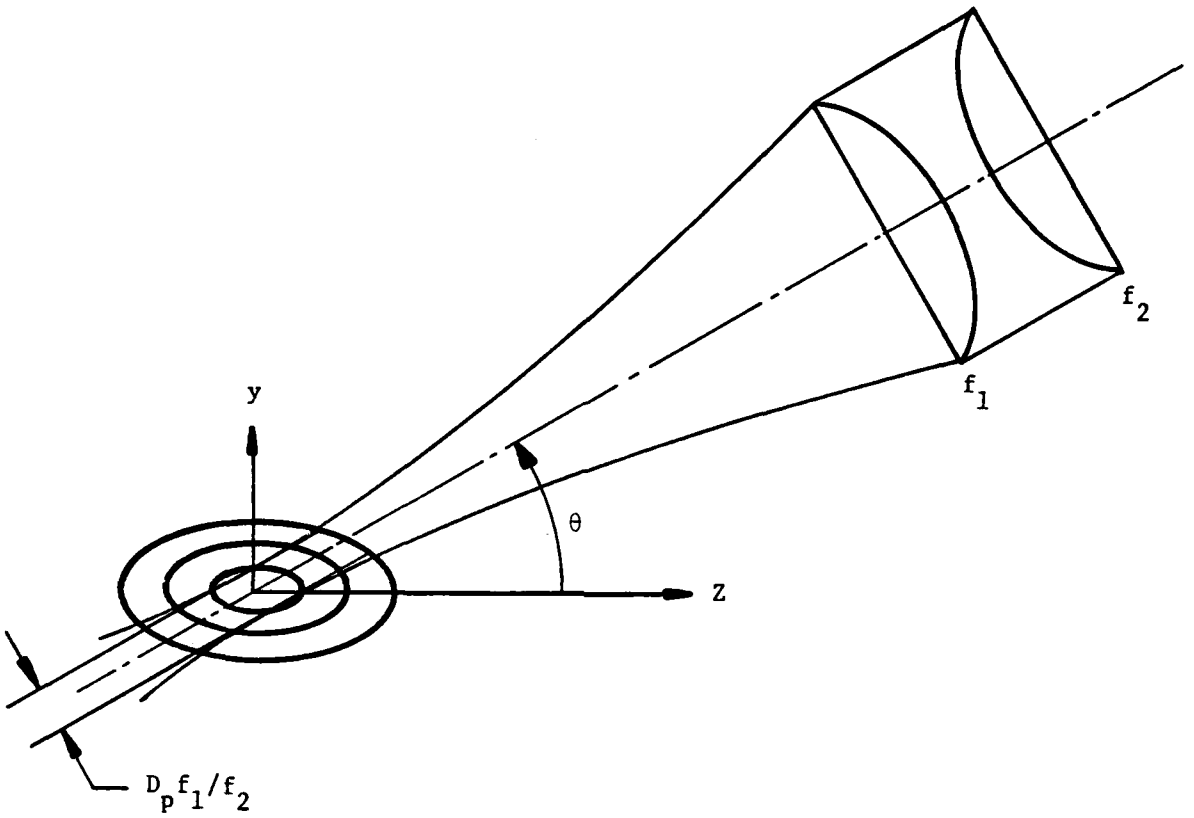

FIGURE 3. SCHEMATIC REPRESENTATION OF DUAL BEAM PROBE VOLUME LIMITED BY A PINHOLE.

Description of Apparatus

An apparatus was designed and built based on the concepts presented earlier. In its simplest form this apparatus consists of: 1) Optics (transmitter and receiver); 2) Electronic processor; 3) Data management system (data handling and output devices). Figure 4 shows a schematic diagram of a two-color breadboard optical system. An argon ion laser provides the light source. The beam colors are separated by the dispersion prism and two of these colors (the 5145Å shown by the broken line, and the 4880Å shown by the solid line) are used to define the probe volume. A beam expander formed by lenses L1 and L2 define the beam ratio parameter m. A compensated beamsplitter splits the blue beam into two beams and the transmitting lens L3 focuses and crosses these two blue beams in the middle of the green beam. The receiving optics use a dichroic mirror to separate the two colors of the scattered light. The probe volume is imaged on pinholes in front of two PMT's and interference filters are used to perfectly separate the two colors. The outputs of the two PMT's are then inputs to the electronic processor. Figure 5 shows these outputs for a series of monodisperse droplets. This electronic processor consists of two major components: a frequency counter, and a pulse height analyzer. The frequency counter uses the same principles as an LDV processor, and in this case it is a modified VP-1001 (SDL). The output of the blue PMT is the input to this processor.

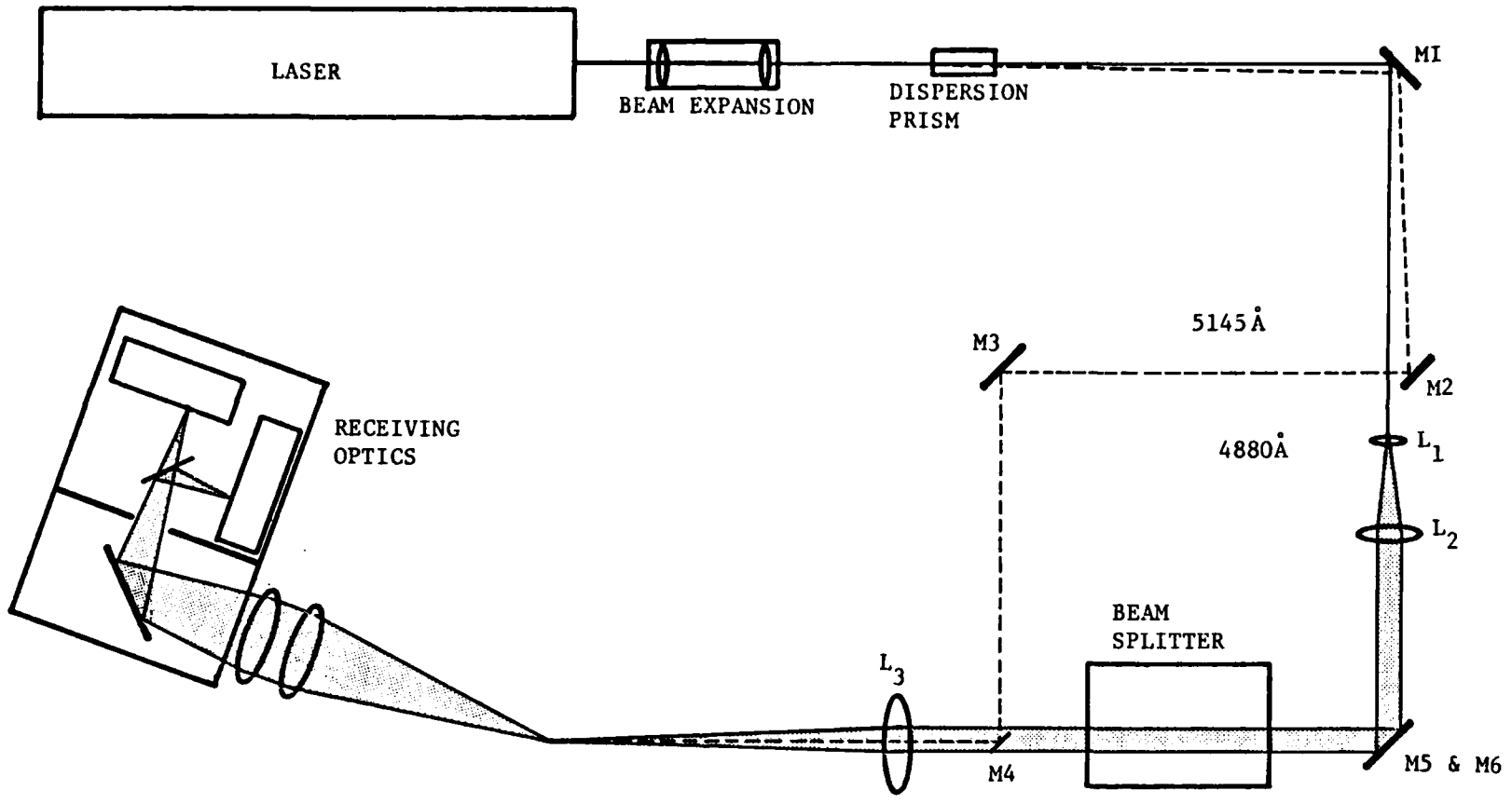

FIGURE 4. SCHEMATIC IMAX BREADBOARD SYSTEM

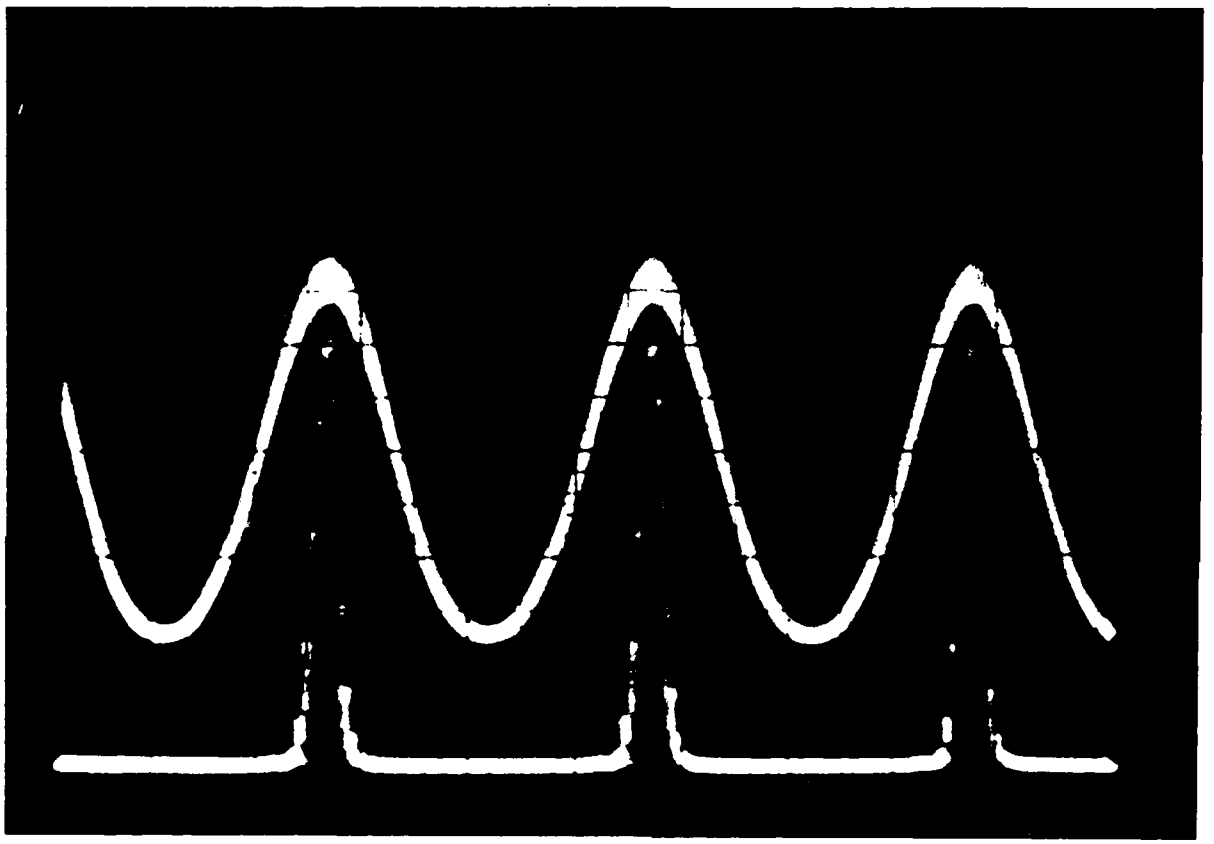

FIGURE 5. OSCILLOSCOPE TRACE OF SIGNALS PRODUCED BY A MONODISPERSE STRING OF DROPLETS

Its functions are:

1. Establish the threshold (I_{min}).
2. Measure the time of N fringes with $I_{ac} > I_{min}$.
3. Regulate the PMT high voltage, and
4. Bandpass the signal to reduce unwanted noise.

The output of the green PMT is input to the pulse height analyzer. As can be observed on Figure 5, this signal has a simple Gaussian profile as given by Equation (4). This pulse height analyzer is triggered by the frequency counter when signals exceed the threshold (I_{min}). It measures the peak intensity of such signal, and the validation is established in the frequency counter by measuring a preestablished number of fringes (typically 12). Figure 6 shows a schematic representation of the processing logic.

The information of Doppler frequency and peak intensity is digitized and two PROMS establish the bin numbers of a velocity and a size histograms. A microprocessor based data management system accepts this information and handles the data. The data handling consists of real time display of the size and velocity histograms, data storage, analysis, and output (via printer or CRT). One of the programs to analyze the data computes the probe volume coordinate y as given by Equation (23). This is used to correct the data by the probability of detection. Sample rates of several KHz are possible with this system.

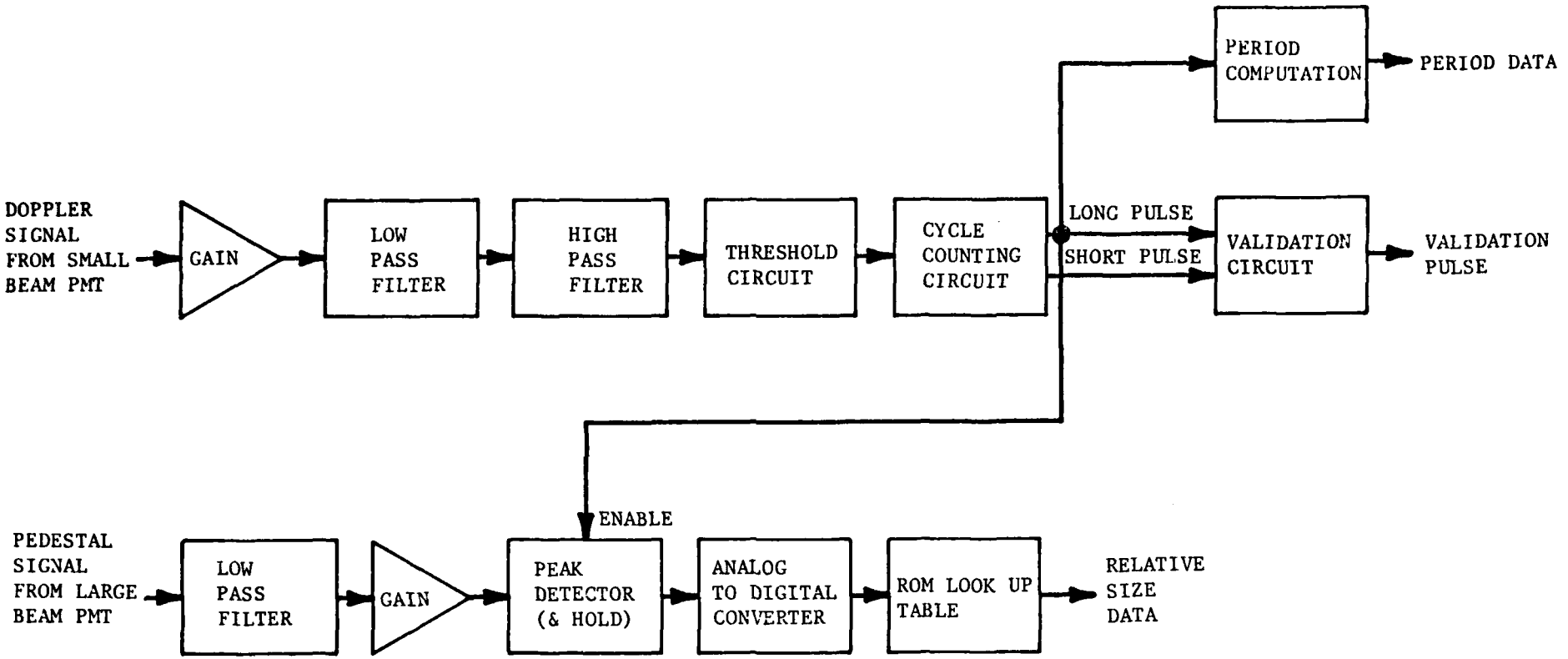

FIGURE 6. ELECTRONICS BLOCK DIAGRAM
DROPLET SIZING, TWO COLOR IMAX TECHNIQUE

Results

A vibrating orifice droplet generator was used to produce strings and sprays of known size droplets. This generator produces a string of droplets of equal size and spacing. These droplets can be dispersed with external air to produce a spray of monodisperse droplets, or under some dispersion conditions the primary droplets will collide and form doublets and triplets.[11] The procedure used in these experiments was to produce a string of large monodisperse droplets to calibrate the instrument. Smaller droplets were then produced by increasing the frequency of vibration of the orifice, and with the dispersion air a spray of these droplets was formed. The spray angle was about 10° and the number density was typically 500/cm^3. The optical configuration consisted of a transmitting lens of 711 mm, m = 7, blue waist diameter of 100 μm, receiving angle of 20°, and receiving lenses of 300/495 mm. The calibration point was provided by a string of 110 μm droplets produced with a flow rate of 0.21 cm^3/min and a frequency of 5 KHz. Note that the droplet size can be precisely estimated given the flow rate and number of equal droplets produced. Figure 7 shows the measured size and velocity. A spray of primary droplets of 49 μm (produced with a flow rate of 0.21 cm^3/min and frequency of 56.9 KHz) was then produced with the dispersion air. Figure 8a shows the measurements of the spray of primary droplets. Figure 8b shows the measurements of a spray formed of primary droplets and doublets. The sizes predicted given the flow rate and frequency of droplet generation are 49 μm and 62 μm. The sizes measured with the NSPC were 46 μm and 57 μm respectively. Figure 8c extends the measurements of 8b to the presence of triplets. The

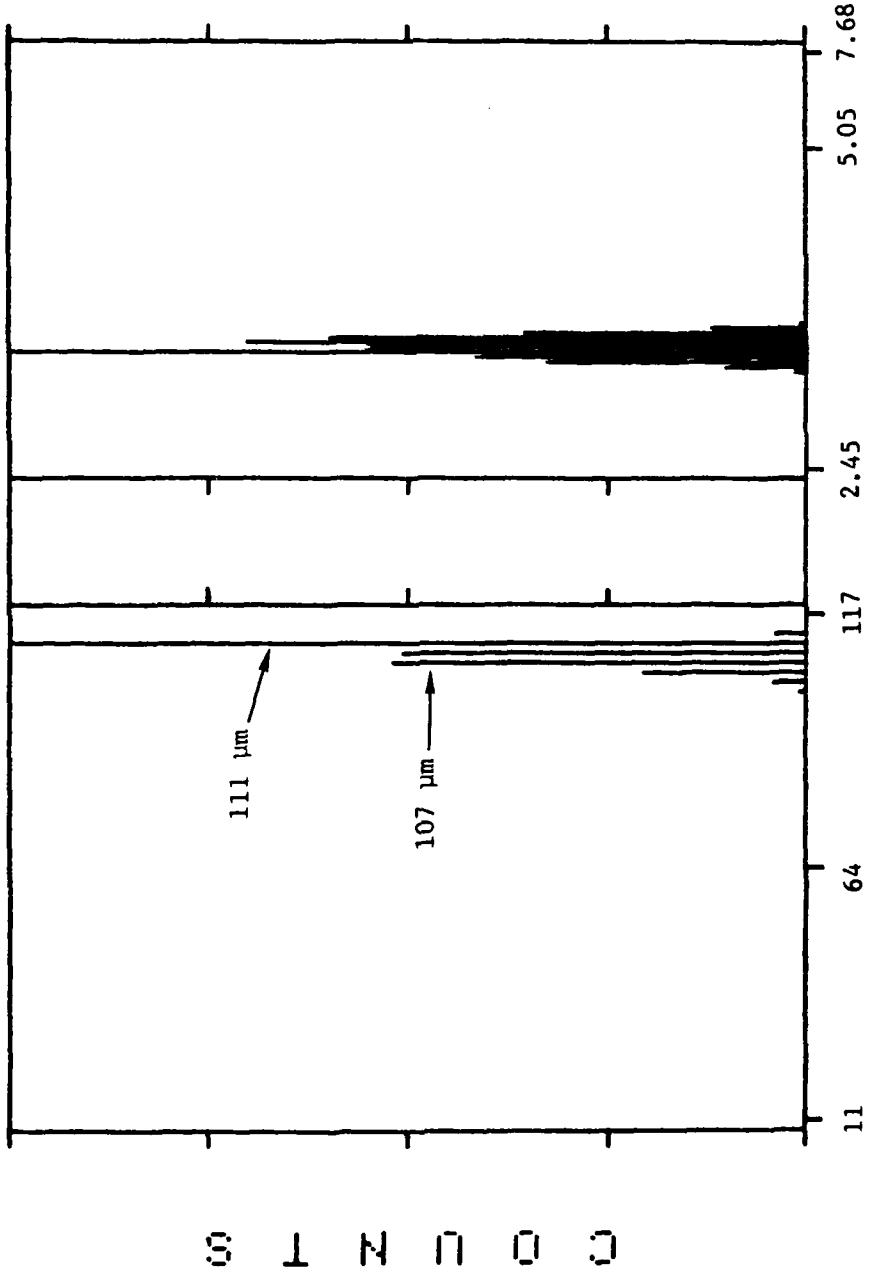

Figure 7. I_{max} Measurements of a String of Monodisperse Droplets.

IMAX DROPLET SIZE MEASUREMENTS

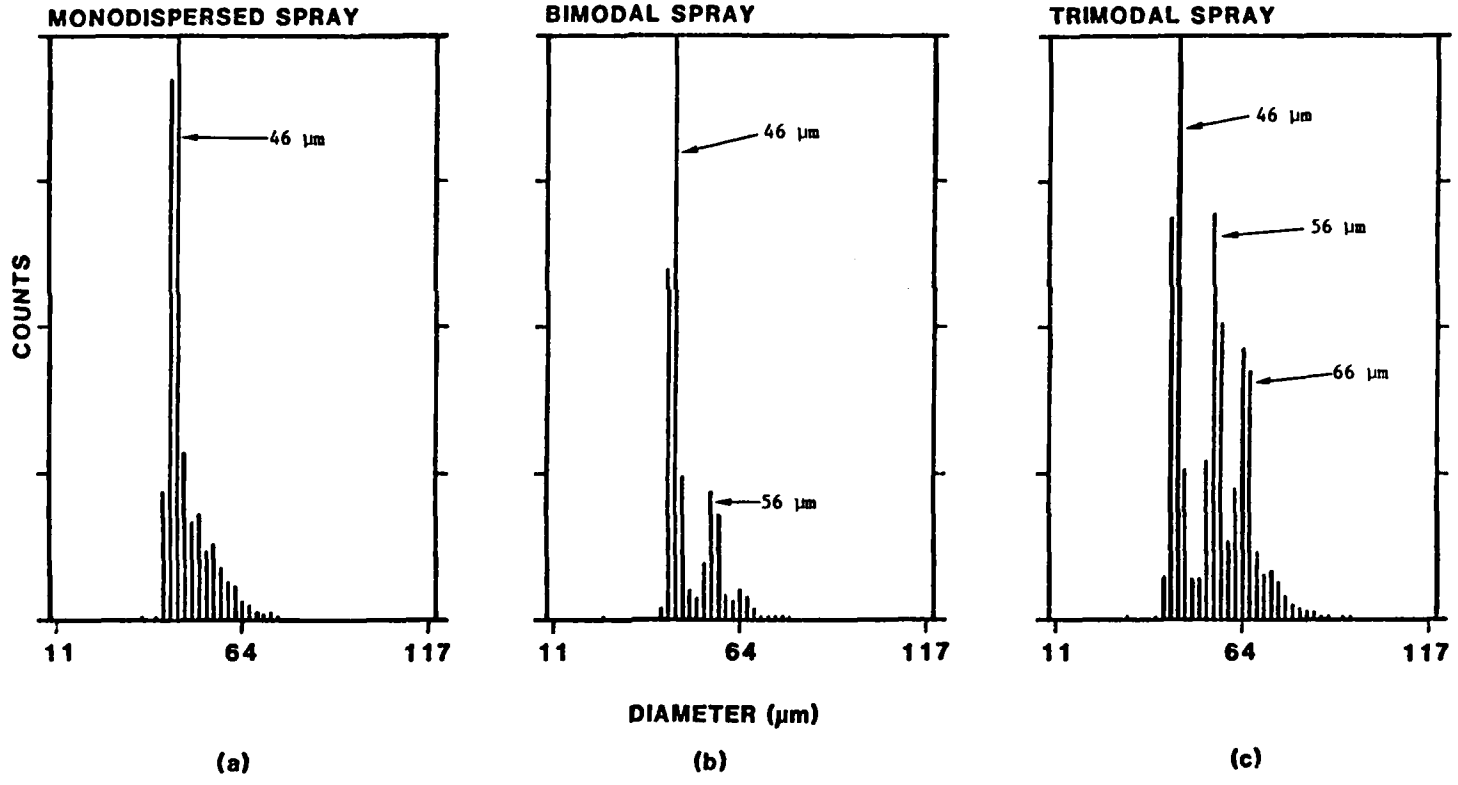

Figure 8.

predicted sizes in this case are 49 μm, 62 μm and 70 μm. Note that the diameters of the doublets and triplets measured with the NSPC are related to the primary droplets by $2^{1/3}$ and $3^{1/3}$ respectively.

Effect of Beam Blockage on Size Distribution

The effect of spray blocking the laser beams before they cross on the size distribution measured with IMAX was explored. A size range of 10 to 100 μm was used in this case, and the monodisperse droplet size was 73 μm.

Figure 9a shows the measurement of the monodisperse string of droplets.

Figure 9b shows similar results but a spray is blocking the laser beams. Two effects can be noted: the peak of the distribution dropped to 69 μm (5%) and the spread of the distribution is +5 μm, -7 μm (+7%, -10%), to the $1/e^2$. It should be noted that once the high voltage is corrected to account for the beam blockage, the broadening should have very little effect in the distribution of a polydispersed spray.

Conclusions

This concept extends the well-established laser Doppler velocimetry to allow the simultaneous measurement of size and velocity of individual droplets crossing a defined region in space. The results show the high resolution with which the system can measure droplets of different size classes. This is expected given that for this technique the resolution is constant throughout the size spectrum. The accuracy of the system is satisfactory for engineering purposes (about 10 percent).

EFFECT OF BEAM BLOCKAGE ON SIZE DISTRIBUTION

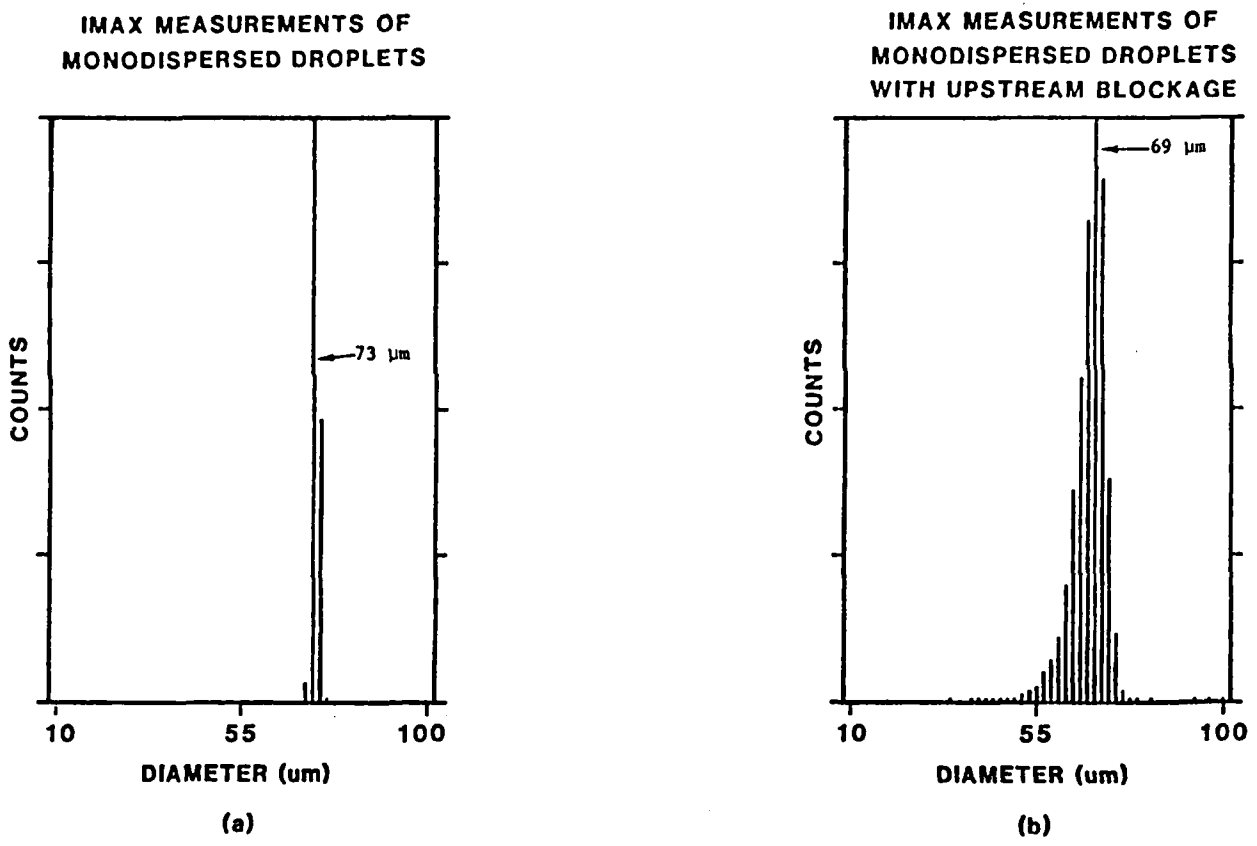

FIGURE 9.

Signal to noise considerations indicate that the dynamic size range capability of the instrument can be in excess of 100:1. However, practical limitations in the electronics and the need to make measurements in high number density flows indicate that a more realistic dynamic size range is 30:1. The capability to measure velocity is based on the well-established LDV concept. The big advantage offered by this system is the ability to simultaneously measure the size and the velocity of individual droplets with high resolution over a large dynamic range.

Also, it is expected that particles of slight irregular shape can be measured with this system by collecting and analyzing the diffracted component of the scattered light.

References

1. A.J. Yule, N.A. Chigier, S. Atakan, and A. Ungut, J. Energy 1, 220-228 (1977).

2. D. Holve and S.A. Self, Appl. Opt. 18 (1979).

3. Y. Mizutani, H. Kodama and K. Miyasaka, Combustion and Flame 44:85-95 (1982).

4. A. Men', Y. Krimerman, and D. Adler, J. Phys. E.:Sci. Instrum. 14 (1981).

5. P.R. Ereaut, A. Ungut, A.J. Yule, N. Chigier, Proceedings from "The 2nd International Conference of Liquid Atomization and Spray Systems," p. 261 (1982).

6. W.J. Glantschnig, M.W. Golay, S.H. Chen, and F.R. Best, Appl. Opt. 21 (1982).

7. M.L. Yeoman, B.J. Azzopardi, H.J. White, C.J. Bates and P.J. Roberts, "Eng. Appl. of Laser Velocimetry" Winter Annual Meeting ASME. Phoenix, Arizona, November 14-19 (1982).

8. C.F. Hess "A Technique Combining the Visibility of a Doppler Signal with a Peak Intensity of the Pedestal to Measure the Size and Velocity of Droplets in a Spray," to be presented in AIAA 22nd Aerospace Sciences Meeting, Jan. 9-12 (1984).

9. H.C. van de Hulst, "Light Scattering by Small Particles" John Wiley and Sons, 1957, Chap. 12.

10. D.W. Roberts, C.W. Brasier, and B.W. Bomar, Opt. Eng. 18 (1979).

11. B.Y.H. Liu, R.N. Berglund, T.K. Argawal, Atmospheric Environment, 18, p. 717 (1974).

3.3 The IMAX Apparatus

In this subsection we describe an instrument developed for NASA Lewis which is based on the IMAX technique. This system is referred to as the Advanced Droplet Sizing System (ADSS). Also in this section we include spray data obtained with the above system using a spray systems pressure nozzle TG0.3.

ADSS

Figure 1 shows the transmitter and receiver. The transmitter houses an argon-ion laser, which provides the light source, and all the required optics to separate the two colors used (5145 A and 4880 A) to form the probe volume of interest. The receiver is essentially a telescope with two photomultipliers to collect the light scattered by particles crossing the sample volume. This beam is split into two via a beamsplitter and a mirror system; each beam is focused on the pinhole of the corresponding PMT housing. The colors are separated by means of narrow band filters internal to the PMT housings. The outputs of the two PMTs are then electronically processed and information of the size and velocity of individual spheres crossing the probe volume is thus obtained. An electronic processor was developed for this purpose, and a dedicated microprocessor was interfaced to store, display and analyze the acquired data. Sample rates of several KHz are possible with this system. Figure 2 shows the electronic equipment used for data processing. It should be noted that the system uses a VP1001 processor, and a newly developed V-I/IMAX interface.

Figure 1. Transmitter and Receiver Units of the Advanced Droplet Sizing System (ADSS) used for IMAX Measurement.

86-2286-15F

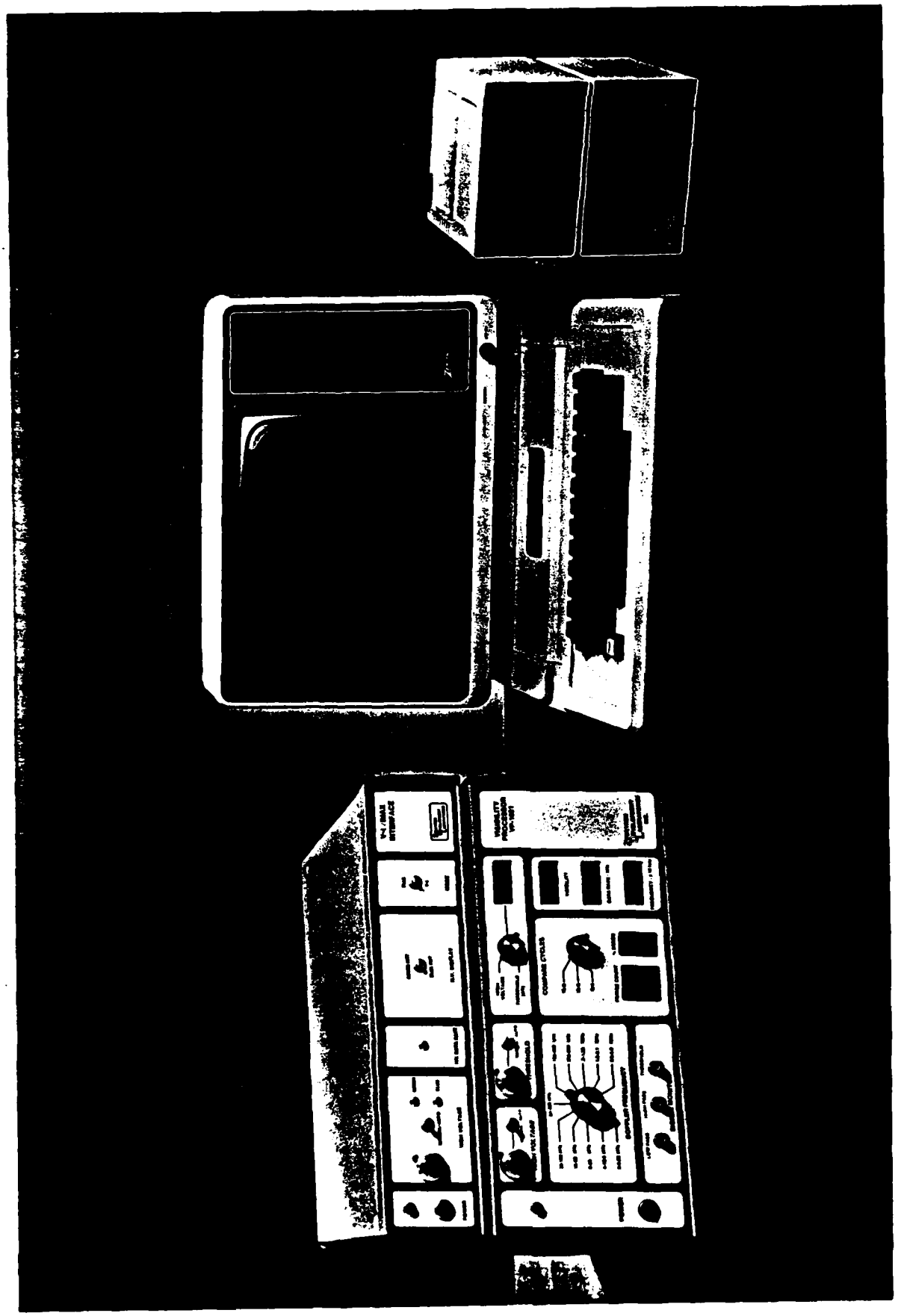

Figure 2. Photograph of the ADSS Electronics.

Spray Results

The following results correspond to a spray produced by a pressure nozzle (spraying systems TG0.3 at 50 psi and 50 mm from the tip). These results are adequate to show trends and gross changes in the distributions. However, considerable transient variations were observed in both the size and velocity distributions. These variations were the result of changes in the spray pattern produced by the above mentioned nozzle. Simple visual observations of the spray pattern indicated changes from conical to flatted sprays.

The first set of measurements are shown on Figures 3a, 3b, 4a and 4b. They were made at a radial position of 0 and 10 mm. Figures 3a and 4a show the raw data while Figures 3b and 4b show the probe volume corrected data. Comparing the raw and the probe volume corrected data it is quite apparent how signal detectability influences the number of counts in the histograms. For instance, the ability to detect a 25 μm droplet with a size range of 20 to 200 μm is much more limited than with a size range of 5 to 50 μm. This change in sensitivity is what the probe volume is all about and it is characteristic of any optical technique (for instance, in photography the data rate must be corrected by the depth of field).

The trend shown in Figures 3b and 4b is the expected one. That is, there are more small droplets in the middle of the spray than on the edge.

In order to test the resolution of the system, data were obtained using three different size ranges: 5 to 50 μm; 10 to 100 μm; and 20 to 200 μm. This is one of the most difficult self-consistency tests

imposed on any technique, and most available techniques will show a shift on the predicted data. IMAX shows excellent matching of the data in the overlapping region as illustrated in Figures 3b and 4b.

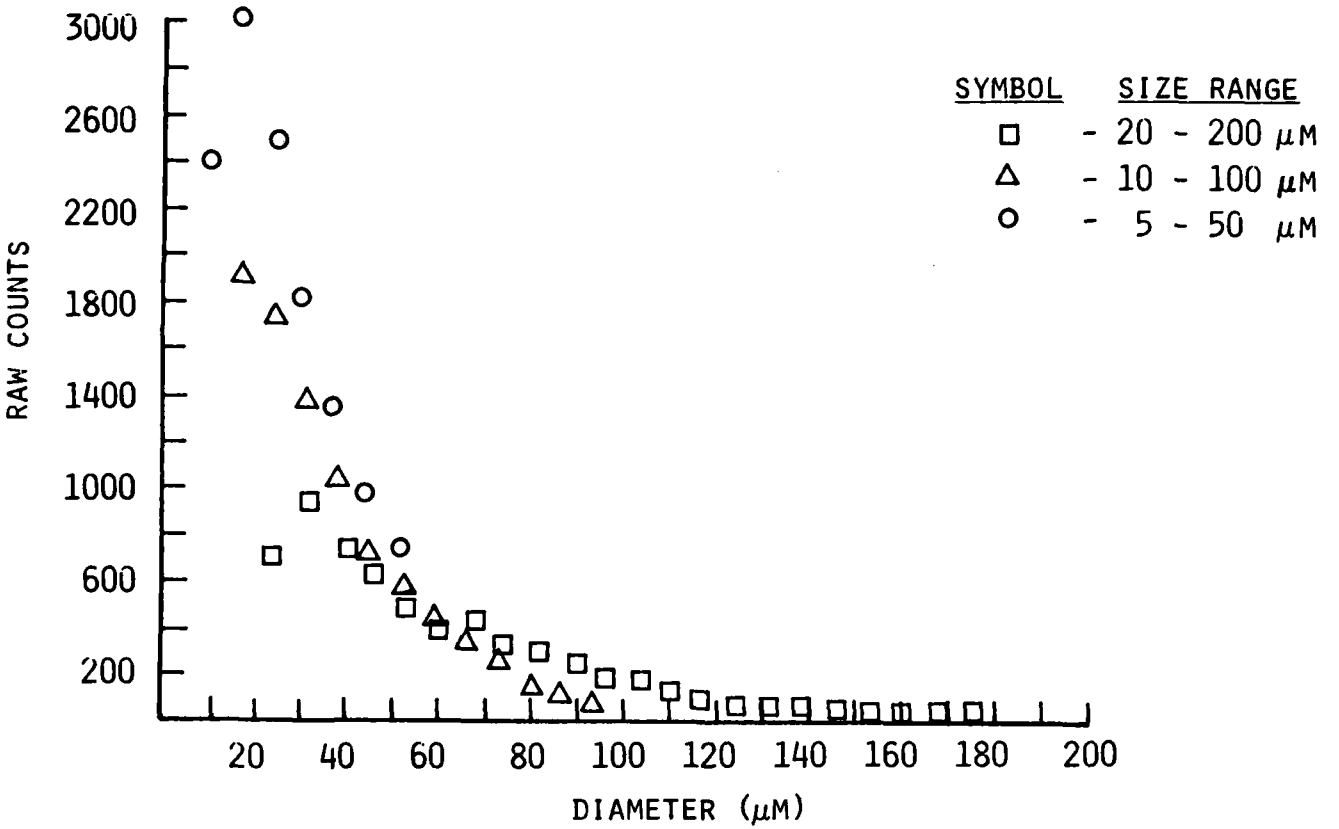

Figure 3a. IMAX Measurements of a Spray at a Radial Position of 0 mm. Uncorrected Size Distribution.

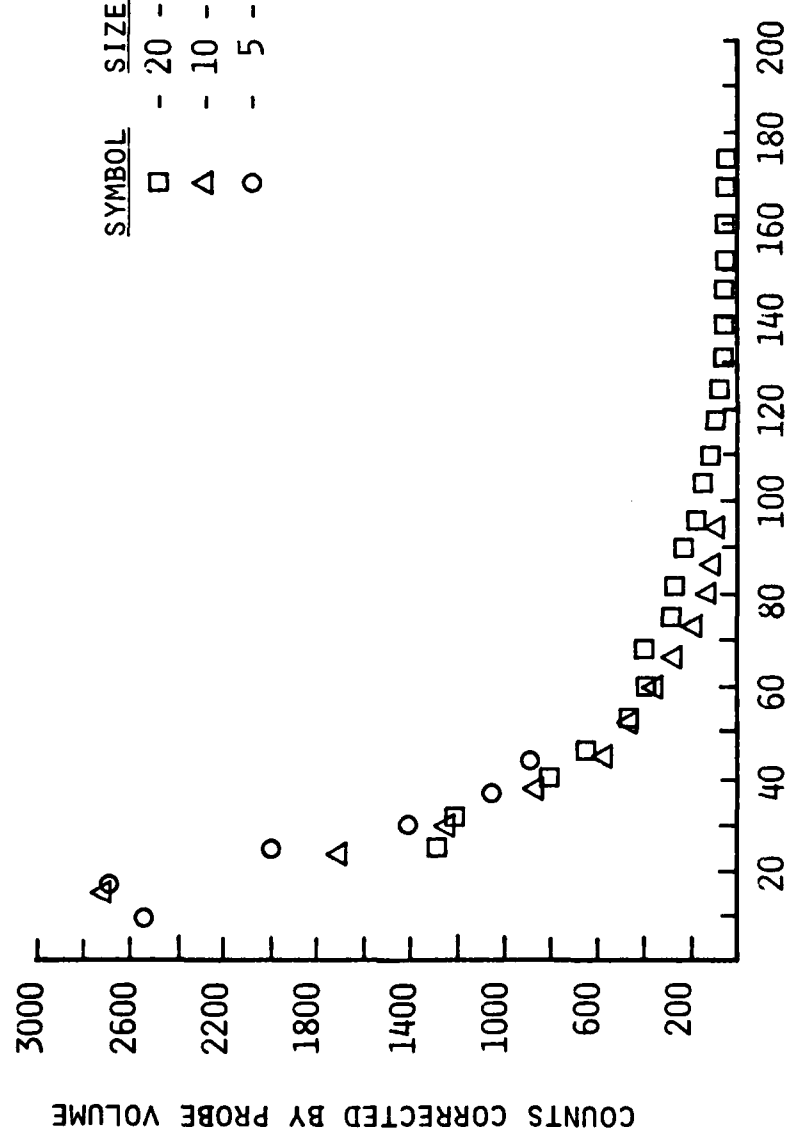

Figure 3b. IMAX Measurements of a Spray at a Radial Position of 0 mm. Probe Volume Corrected Size Distribution.

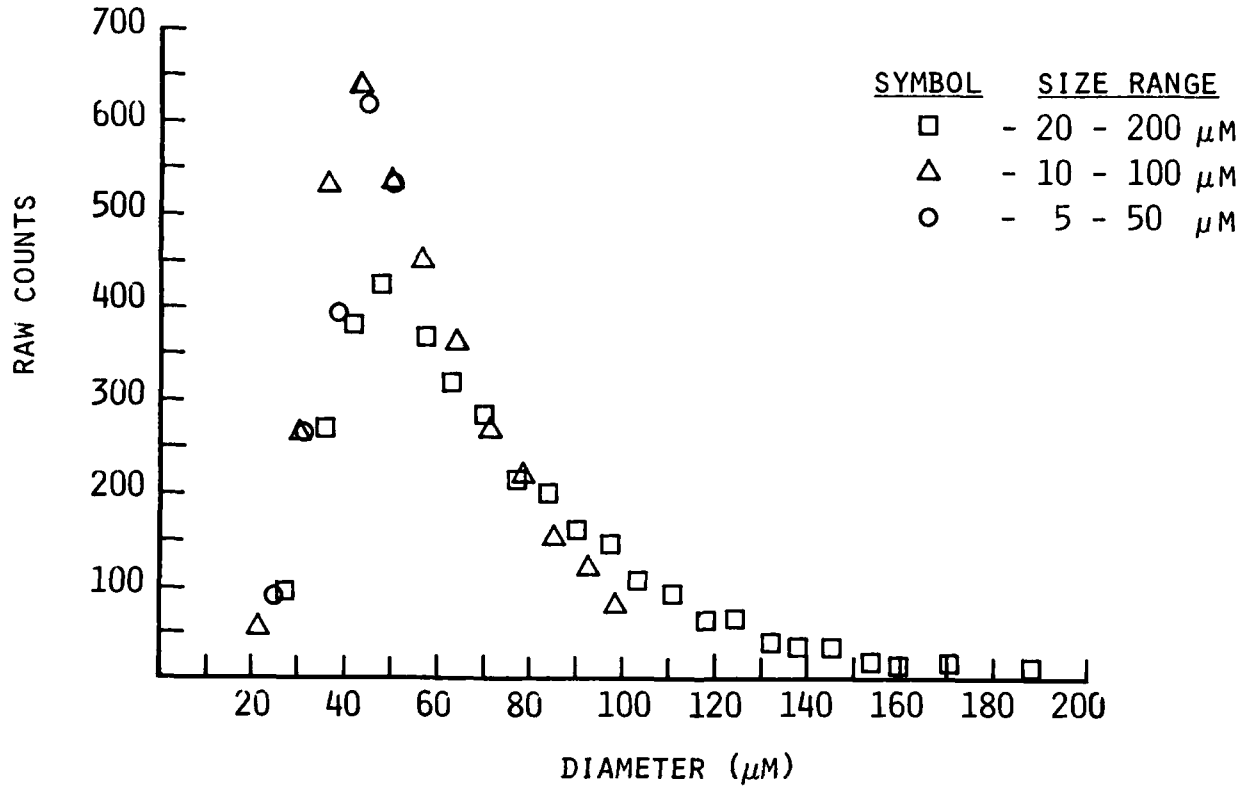

Figure 4a. IMAX Measurements of a Spray at a Radial Position of 10 mm. Uncorrected Size Distribution.

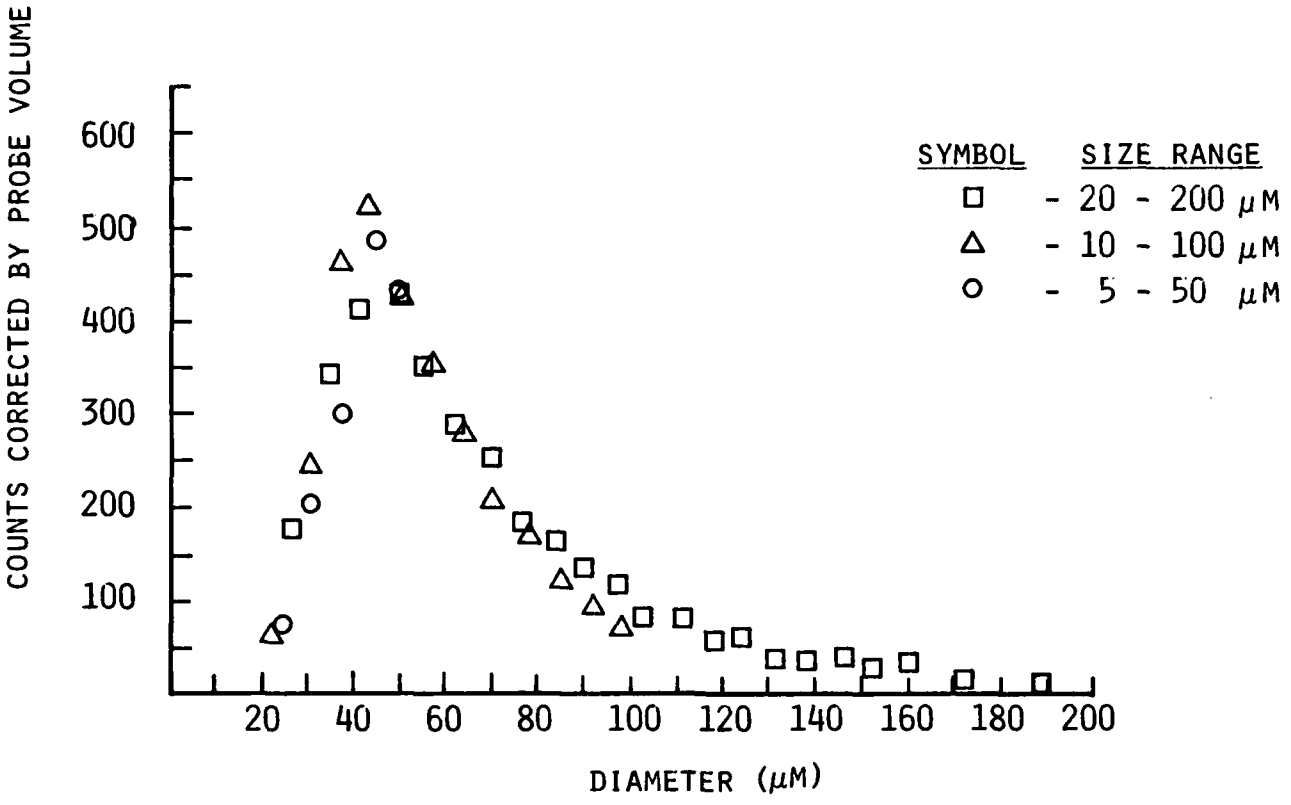

Figure 4b. IMAX Measurements of a Spray at a Radial Position of 10 mm. Probe Volume Corrected Size Distribution.

3.4 The PIMAX Technique

PIMAX is a variation of IMAX where two polarizations instead of two colors are used. That is, two beams of a given polarization cross in the center of a larger beam with normal polarization. This technique was studied experimentally, and the results were compared to the theoretical predictions.

It was found that it was almost as good as IMAX with some crosstalk between polarizations which for the most part could be filtered out.

The obvious advantage of PIMAX is that it requires a single color laser (which is smaller and cheaper) and simpler optics.

In this subsection we discuss the experimental apparatus, the probe volume size, and spray data.

Apparatus and Experimental Facility

Figure 1 shows a schematic of this optical system, which consists of a transmitter and a receiver positioned 5° off axis. The transmitter uses a 5 mW He-Ne laser which is focused on a diffraction grating (DG) by lens L_1. The zero order beam goes through a beam compressor formed by L_4 and L_5 and its polarization is rotated by PR. Lens L_3 focuses and crosses all three beams to form the probe volume. The scattered light is collected by L6 and focused onto the photomultipliers by L_7. A cube polarizer (CP) divides efficiently the scattered light into its two polarization components. In addition, a polarization filter was placed in front of the PMT which looks at the big beam (BPMT) to reduce the crosstalk between the two polarizations.

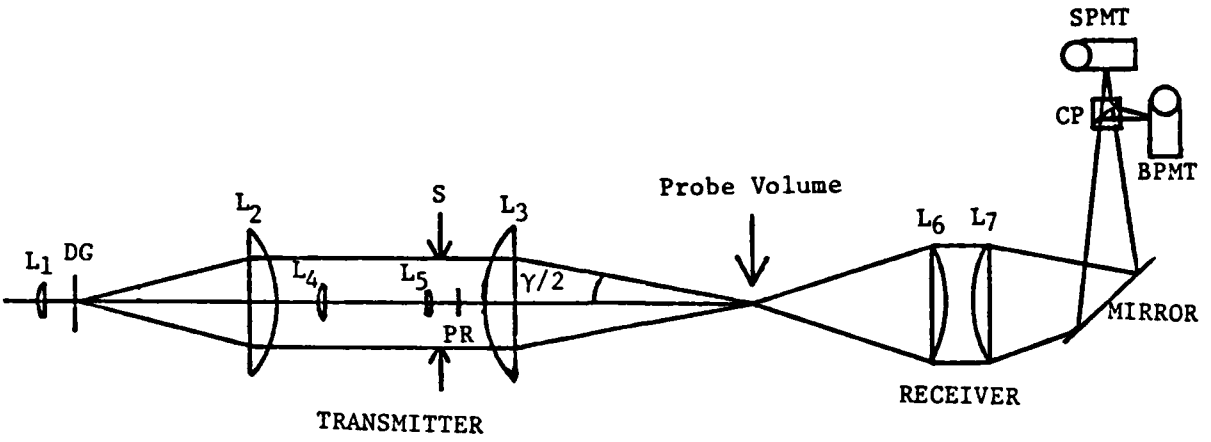

Achromatic Lens	Focal Length (mm)
L_1	35
L_2	220
L_3	500
L_4	112
L_5	16
L_6	300
L_7	500

CP: Cube Polarizer

DG: Diffraction Grating
100 lines/mm

PR: Polarization Rotator

Figure 1. Schematic of PIMAX system with compact transmitter.

The outputs of the photomultipliers are input to an electronic breadboard which measures the Doppler period and the peak intensity of each scattering center.

Experimental Determination of the PIMAX Probe Volume

Optical probe volumes with nonuniform intensity distribution droplets that scatter light with large modulation are detectable over a larger region than those that scatter light with little modulation. As a result, the probe volume or region of detectablity is a function of droplet size. The derivation of the equation that relates the size dimension y of the probe volume to the droplet diameter d is given in the previous subsection. This equation restated here, is now experimentally verified. It is given by:

$$y < \sqrt{\frac{-b_{0_1}^2}{2} \ln\left[\frac{I_{min}}{2I_{max}} \left(\frac{d_o}{d}\right)^2 \left(\frac{1+V_o}{v}\right)\right] - b_{0_1}^2}$$

To experimentally measure the y dimension of the probe volume in the scattering plane and perpendicular to the transmitted laser beams, the Berglund-Liu droplet generator was used. This produced a steady and stable string of monodispersed water droplets. The droplet generator was mounted on a precision x-y micrometric traverse so that the droplets could be positioned anywhere in the probe volume. The orifice of the Berglund-Liu generator was placed as close to the probe volume as possible to minimize errors due to wander of the string of droplets; data was also repeated several times to further reduce the errors.

A very difficult part of this experiment was determining the edge of the probe volume for any particular size droplet. Theoretically, the edge of the probe volume is calculated by the expression given for y. Experimentally, there is a region near the edge of the PV where the rate of acquistion drops off. That is, some of the signals (droplets) are processed by the electronics and some are not. The electronics impose an upper limit on the data rate of about 6 kHz, while the drops can be generated at a frequency of up to 60 kHz.

In defining the edge of the probe volume the data rate of signal acceptance was observed. One criterion corresponded to the location where the data rate dropped to about 90% of the maximum rate. Another criterion corresponded to a data rate very close to zero. Notice that in principle all the measured droplets are identical and traveling exactly through the same trajectory. Therefore, the data rate should be either zero or have a fixed constant value. In actuality the droplet trajectory can change by a few microns, therefore, causing some droplets to cross inside the probe volume while others cross outside. In addition, the droplets could vary in size, although we have no evidence of this.

The droplet generator was traversed from the position of peak intensity to the position of 90% data rate, and then zero data rate. The respective relative movements were recorded in each case. The 90% data rate corresponds to a conservatively small probe volume referred to in Figure 2 as y_{small}, while the zero data rate corresponds to a conservatively large probe volume and is indicated as y_{large}. Also shown on Figure 2 are the average of y_{small} and y_{large}, and the theoretically

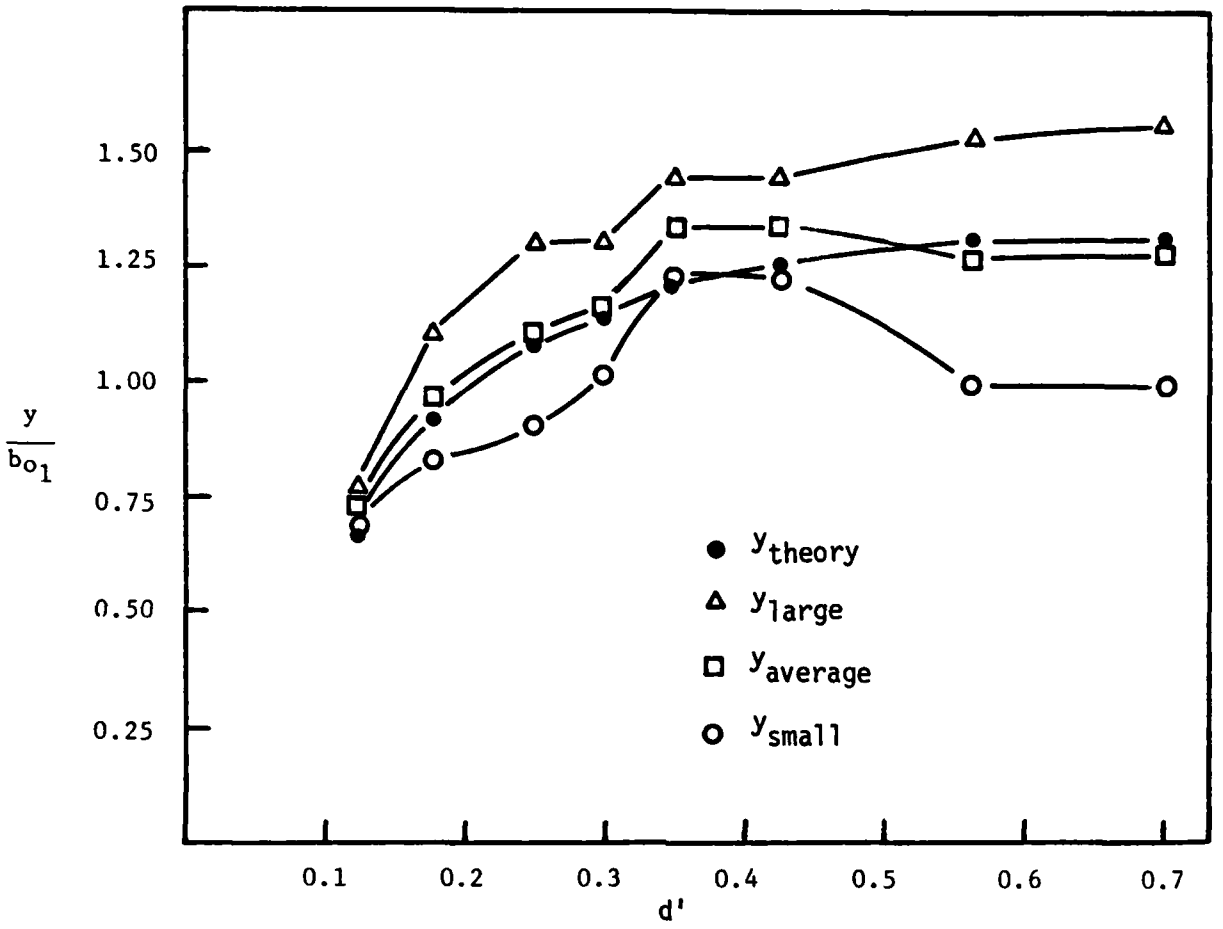

Figure 2.
PROBE VOLUME AS A FUNCTION OF PARTICLE SIZE

predicted value. It can be deducted from this figure that there is a good agreement between the theoretical and the average experimental values.

Polarization Crosstalk

The accuracy of the PIMAX technique can be reduced if the scattered light is elliptically polarized and the polarization separators are not efficient. In a two-color system the separation of the colors is trivial and the problem of crosstalk need not be considered. There are several reasons that can unpolarize the signal, therefore, reducing the separation. They are: 1) particles disturbing the laser beam; 2) scattering plane can be at an angle other than 0° or 90° with the incident polarization; 3) polarization separators are inefficient. Several tests were conducted to establish the reasons and level of the crosstalk. This crosstalk was shown to be very small in the PIMAX system accounting for about 3% error in the particle size and have no measurable effect in the velocity. This error could be virtually eliminated by placing the receiver on the plane of the laser beams, thus reducing the ellipticity of the polarization.

Experimental Results

Pre-Calibration Procedure

The calibration of the PIMAX relies on the accuracy of producing a reference size droplet. These droplets were produced with a Berglund-Liu generator, and their size could be predicted knowing the flow rate

and droplet generation frequency. To test the accuracy of the Berglund-Liu generator the droplets were also photographed and their size obtained from a magnified negative. The droplets were measured with PIMAX before and after photographing them to insure consistency. The procedure for this experiment was to first produce a string of large monodisperse droplets to calibrate the PIMAX system. These large monodisperse droplets are normally formed by smaller, unstable droplets colliding into each other in the first 2 cm of the droplet string.

Smaller droplets were then produced by increasing the frequency of the orifice vibration. These were stable and monodisperse at the point of inception and produced a well-behaved monodisperse spray with the aid of dispersion air which could then be measured with the calibrated PIMAX system.

For the spray produced with the assistance of dispersion air the angle was about 10° and the number density typically 500/cm^3. The PIMAX optical configuration consisted of a transmitting lens of 711 mm, small beam diameter of 80 μm, receiving angle of 20°, and receiving lenses of 300/495 mm.

The photographic system (Figure 3) consisted of a stroboscopic light source which illuminated a string of monodisperse droplets produced by a Berglund-Liu droplet generator. The scattered light from this string of droplets was collected by a 55 mm Olympus f 1.2 lens. The collected light was then relayed to a 490 mm lens which focused the image onto the film plane of an Olympus OM-2 body.

The Olympus camera was mounted on a rack and pinion rail for focusing. Since this was a constant magnification system, the movement

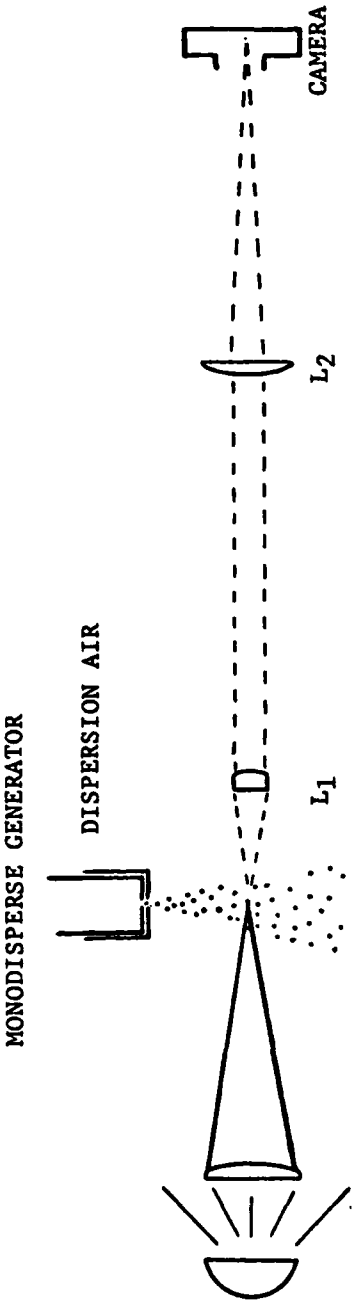

Figure 3. Schematic of Photographic System.

of the camera did not affect the magnification of the droplets. The total system magnification from the droplet to the image on the film plane was approximately nine. A resolution chart (U.S.A.F. 1951) was also photographed with the same system and used as an absolute scale to calculate the droplet magnification. It also served to determine the resolution of the optical system.

It was estimated that the resolution was less than 2.2 μm but larger than .8 μm due to noise in the system.

The stroboscope (Gen Rod 1539) was used on its highest frequency setting, having a flash duration of 800 ns at 1/3 of the peak intensity. This exposure time was short enough to "freeze" the droplets which were traveling at about 6 to 10 m/s. The decay of the strobe flash left a faint "ghost image" of approximately 3 droplet diameters. The procedure for the flash photograph was to open the shutter in a darkened room, remotely fire the stobe once, then close the shutter. An 8" focal length lens was used to focus the strobe light on the droplet stream to maximize illumination.

The film used was Kodak Technical Pan Film 2415 which is an extremely fine grain film (320 lines/mm). The film was given an exposure index of 50 and developed for 12 minutes at 75° in D-76 developer. This developing time was used to produce an optimum optical density of .5, as measured on a densitometer, and a contrast index of 2.5.

Two size droplets were photographed: an 80 μm droplet string produced with a flow rate of 0.3 cm^3/min and a frequency of 18.6 kHz, and a 52 μm produced with the same flow rate and a frequency of 69.4 kHz. The corresponding sizes obtained photographically are 78 μm

and 50 μm. Figures 4a and 4b show the photographs of the corresponding droplet strings. The 52 μm droplets were then dispersed with air to form a monodisperse spray. Here the photographic technique was more tedious since very few particles were in focus. Figure 4c shows a photograph of two of these droplets. The estimated size was also 50 μm. We could, therefore, conclude that the Berg-Liu predicted size is photographically confirmed to 4% error. The size and velocity histograms measured with PIMAX of a 59 μm droplet (as predicted by the Berglund-Liu) are shown on Figure 5.

The following table shows the size predicted by the Berglund-Liu generator, and measured with the PIMAX system. Included are the measurements of the spray produced with the aid of dispersion air.

Droplets	Mode	$d_{predicted}$ (μm)	$d_{meas.}$ (μm)	error (%)
Monodisperse	String	59	60	+1.7
	Spray	59	58	-1.7
	String	54	53	-1.9
	Spray	54	53	-1.9
	String	52	51	-1.9
	Spray	52	49	-5.6

Dynamic Size Range

The dynamic size range is defined as the ratio of maximum to minimum size measurable by a system with a given single configuration. The actual values of the extrema can change depending on the chosen

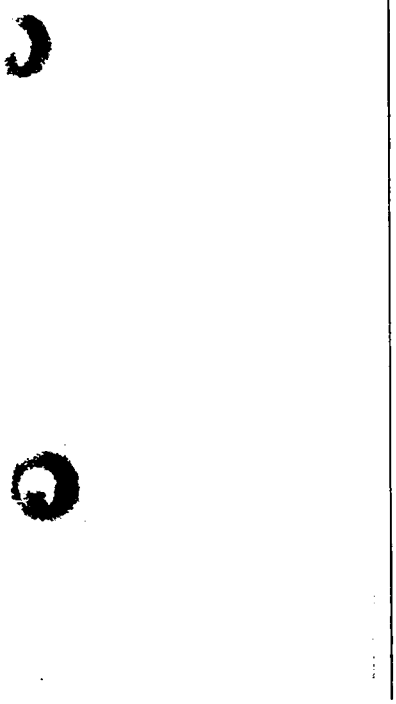

Figure 4a. Photograph of 80μm droplet string.

Figure 4b. Photograph of 52μm droplet string.

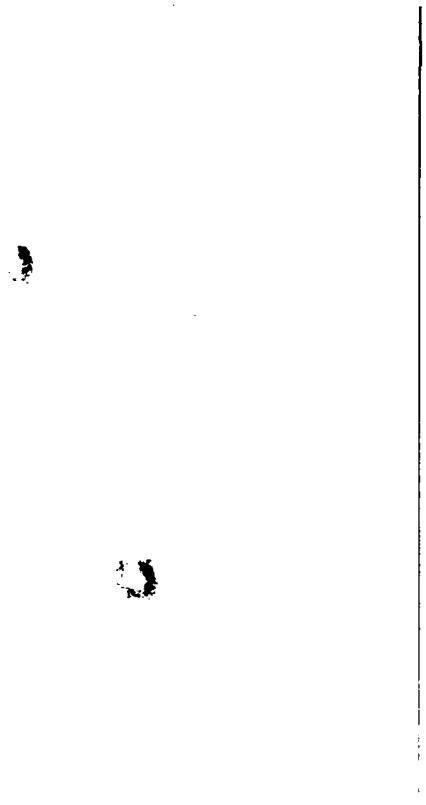

Figure 4c. Photograph of 52μm droplet spray.

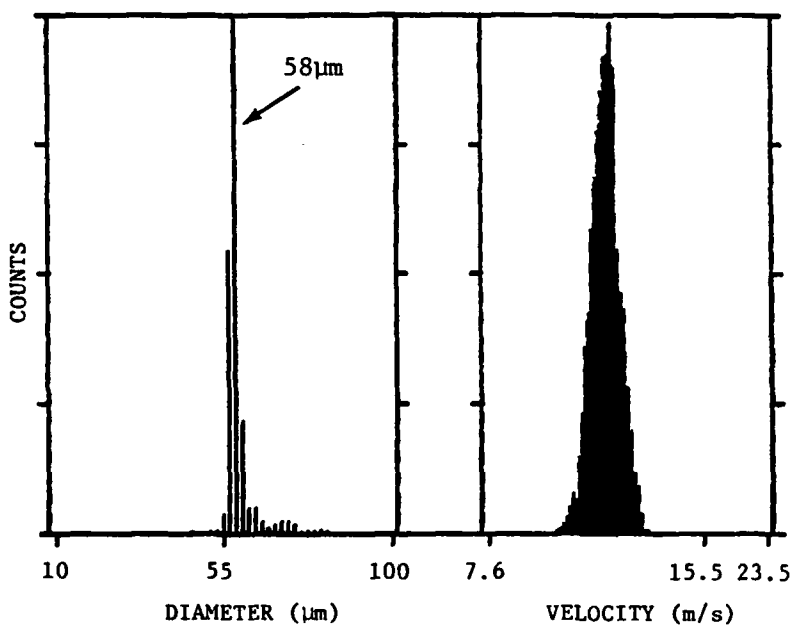

Figure 5. Size and Velocity histogram of a monodisperse spray of 58 μm droplets.

configuration. For fuel sprays, as an example, the dynamic size range should be about 30:1. Therefore, an instrument with a narrower dynamic range would need two or more configuations to resolve the spray.

To establish the dynamic size range particles of various sizes should be measured and so should their signal-to-noise ratio. Thus, the minimum measurable size is established for a given upper limit.

In the present experiments the variety of sizes that could be generated was limited. Therefore, the approach taken was to simulate different size particles, given a stable droplet string. First, it is important to recognize that the scattered light signal is characterized by its amplitude and visibility. Both of these parameters were independently controlled during this experiment, primarily by masking the receiver and attenuating the laser beam. The S/N was estimated from the velocity histogram given that the stable droplet string produced a single velocity value. The signals of the simulated small particles had optical noise which was interpreted by the electronics as a broad velocity distribution. Using the velocity broadening as the criterion for signal acceptability, the maximum dynamic size range was estimated at 100:1 for a 25 mW He-Ne laser.

Spray Results

A Parker-Hannifin simplex spray nozzle (Part No. 673005IM7) was characterized with the new PIMAX system. Three aspects of this work are described here. First, the effect of the probe volume correction in the size distribution is established. Two positions of the spray (the center and a radial position of 10 mm) were chosen for these studies.

Second, the system's self-consistency is illustrated by acquiring and displaying the data in two overlapping size ranges (10 - 100 μm and 15 - 150 μm). Third, the spray is mapped as a function of radial position and pressure for an axial position of 50 mm.

Figures 6a and 6b show the raw counts and probe volume corrected counts of the size distribution of droplets in the center of the spray for a pressure of 50 psi. Both the raw and corrected counts are normalized by the time of collection and the size bin width. Notice that this latter is just proportional to the size range in question. The corrected counts are, in addition, normalized by the weighting function of the probe volume. Two key ideas are conveyed in these figures: First, probe volume correction is needed to unbias size distributions obtained with nonuniform intensity laser beams; second, broad size distribution can be resolved with a series of overlapping ranges.

It should be noted from Figures 6a and 6b that very little correction is required for the large diameters. This is not a general statement and it depends on the ac modulation (given by the product of the pedestal and the visibility) associated with any size droplet. In the reported experiments, we chose a size versus modulation dependence which would make the large droplets less subject to threshold variations. Nevertheless, there is a consistent error in the corrected counts of the large droplets, showing that the number of large droplets measured in the 10 - 100 μm size range is larger than the equivalent measurement in the 15 - 150 μm range. This will require further research in instrument sensitivity and experimental procedure. The size distributions obtained with the two ranges are, however, very similar,

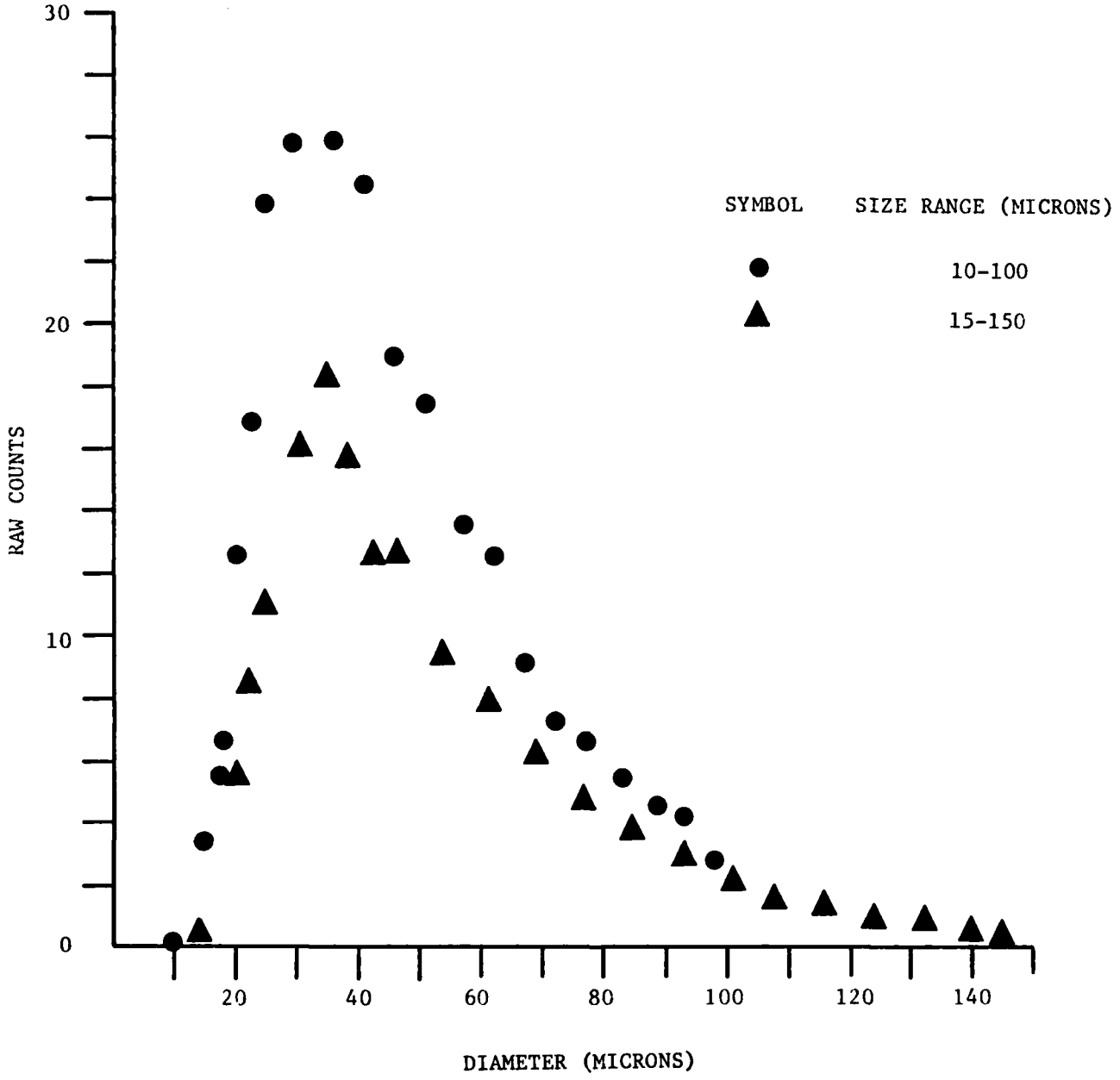

Figure 6a. PIMAX measurements of a spray (produced by a Parker Hannifin nozzle No. 6730051M7 with water at 50 psi) at a radial position of 0 mm and axial position of 50 mm - uncorrected.

85-2286-12

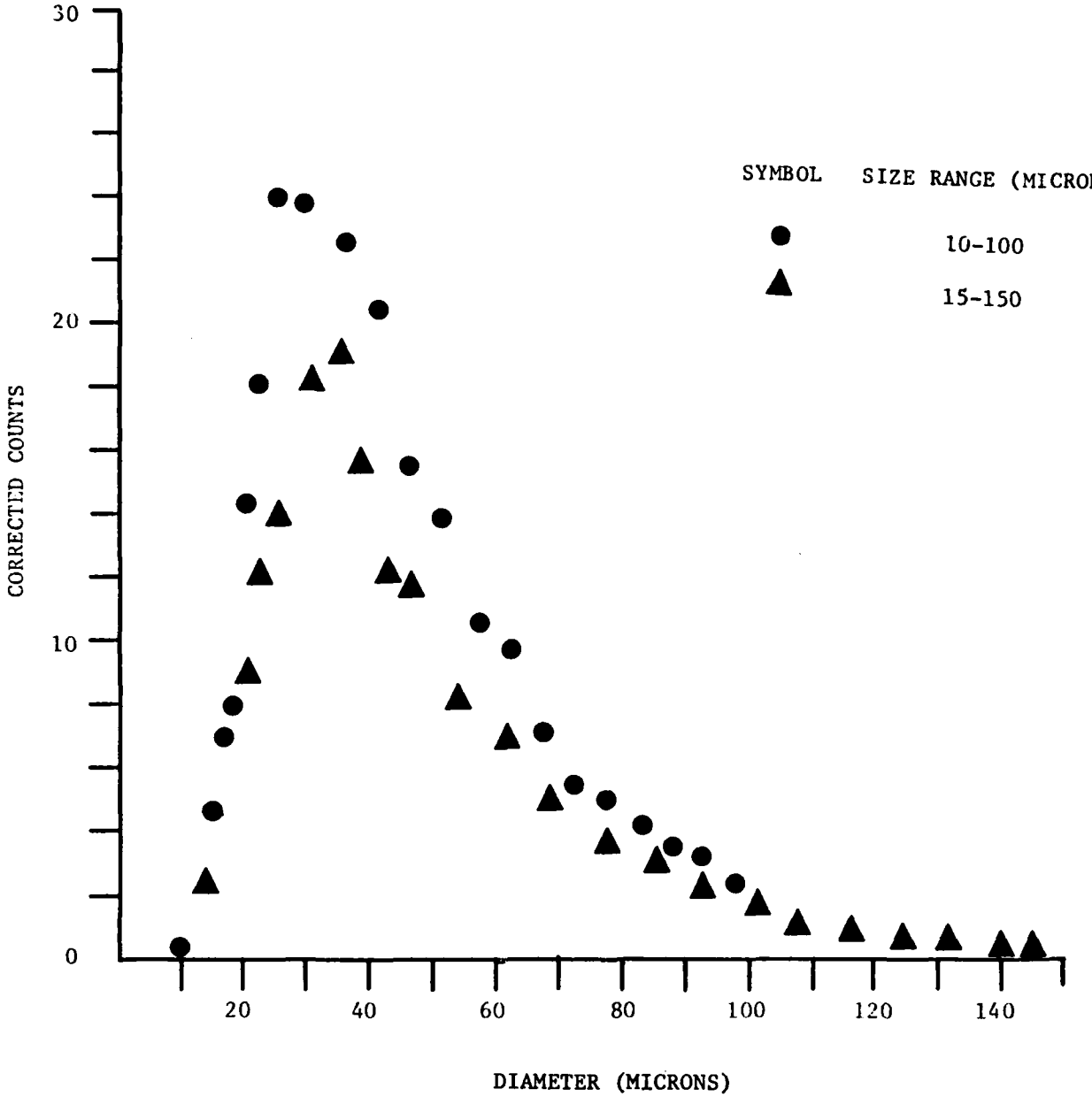

Figure 6b. PIMAX measurements of a spray (produced by a Parker Hannifin nozzle No. 6730051M7 with water at 50 psi) at a radial position of 0 mm and axial position of 50 mm - probe volume corrected.

and the effect of the probe volume is very noticeable in the small size end. Raw and corrected data are also shown on Figures 7a and 7b corresponding to a radial position of 10 mm and the same pressure (50 psi) and axial position (50 mm) as before. Here, there is less discrepancy in the counts of the large droplets and more in the small droplets. The trend in the size distribution is the same that was reported before. Namely, there are more small particles in the middle of the spray than at the edge.

Size distributions were obtained at five radial positions and the results are shown on Figures 8a and b. The first shows the variation of peak diameter at 50 psi and 60 psi. As can be observed, the peak of the distribution changes almost a factor of 2 between a radial position of zero and -10 mm. It can also be observed by comparing the data of -10 mm with that of +10 mm that the spray is not symmetrical. Figure 8b shows the variation of SMD as a function of radial position for the same two pressures. As can be observed, there is a distinct difference in SMD for the two pressures. In addition, there is some dependence of the SMD in the radial position. Notice that these values cannot be directly compared to spatial measurements (such as flash photography for there is a strong correlation between size and velocity.

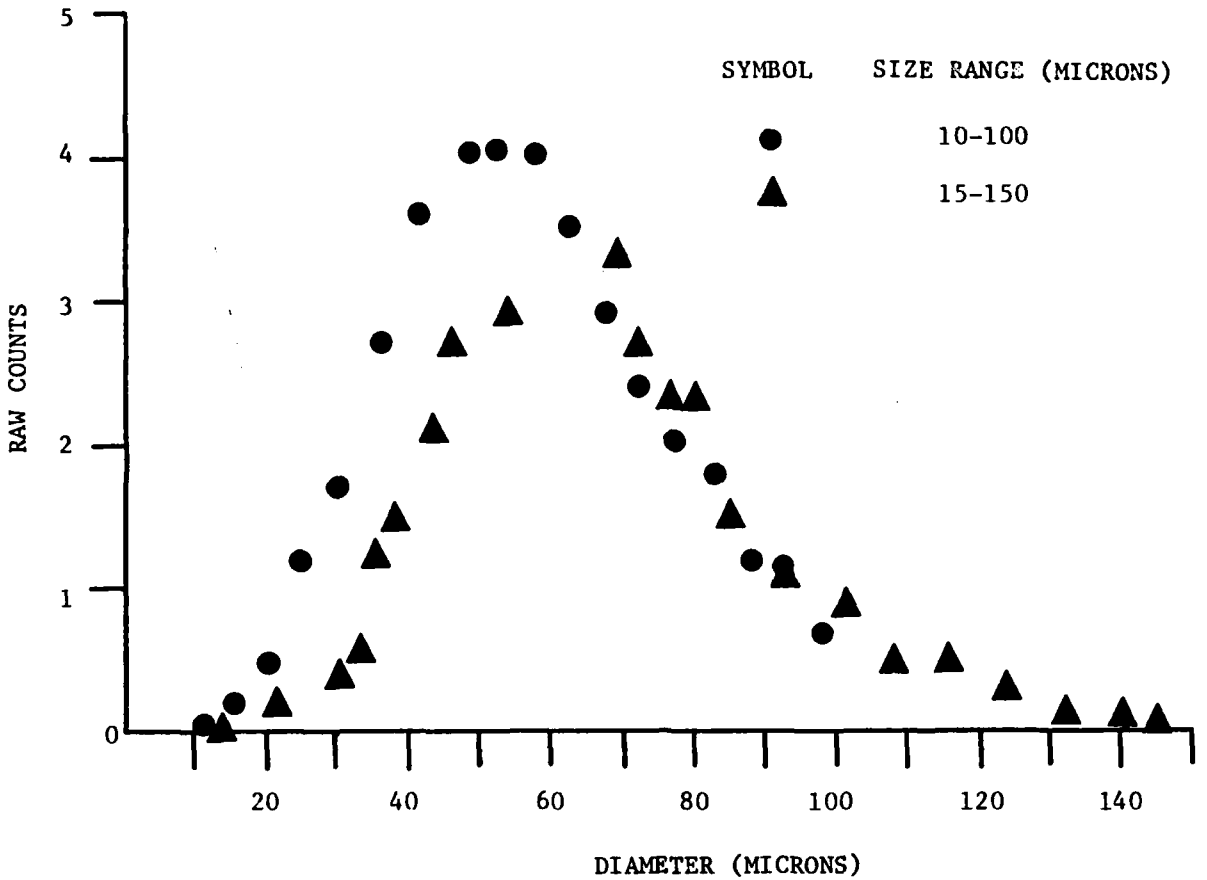

Figure 7a. PIMAX measurements of a spray (produced by a Parker Hannifin nozzle No. 6730051M7 with water at 50 psi) at a radial position of 10 mm and axial position of 50 mm - uncorrected.

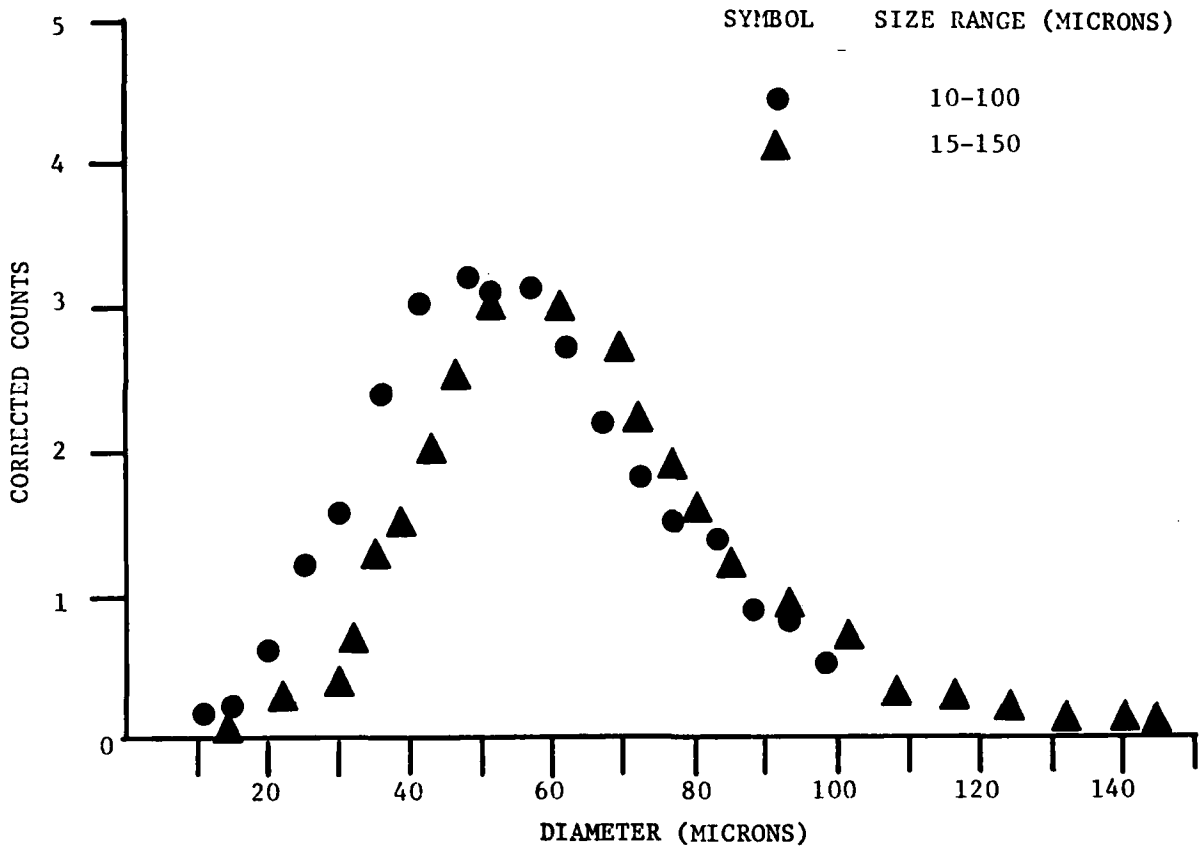

Figure 7b. PIMAX measurements of a spray (produced by a Parker Hannifin nozzle No. 6730051M7 with water at 50 psi) at a radial position of 10 mm and axial position of 50 mm - probe volume corrected.

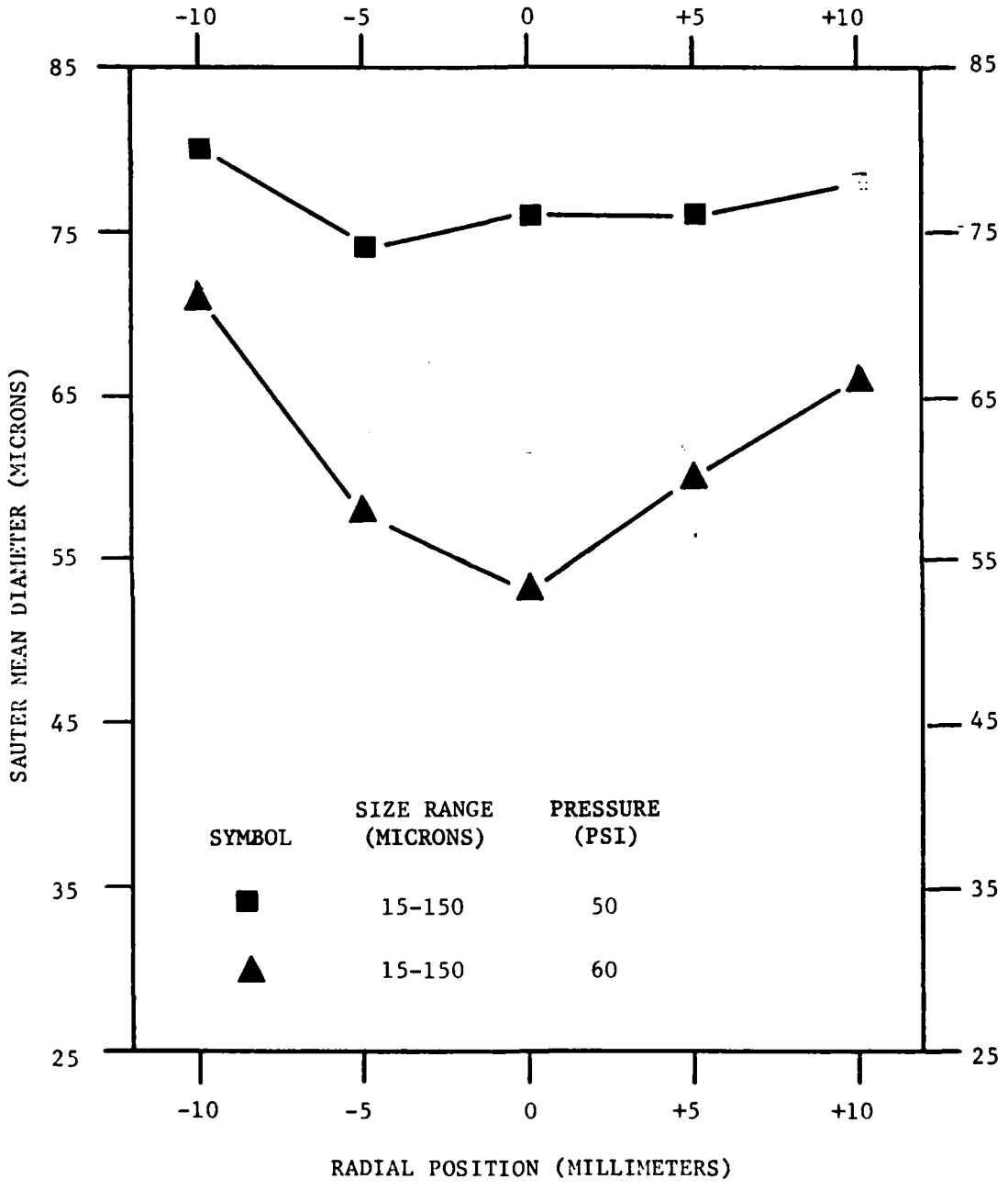

Figure 8a. Variation of characteristic diameter of spray with radial position and pressure - peak diameter.

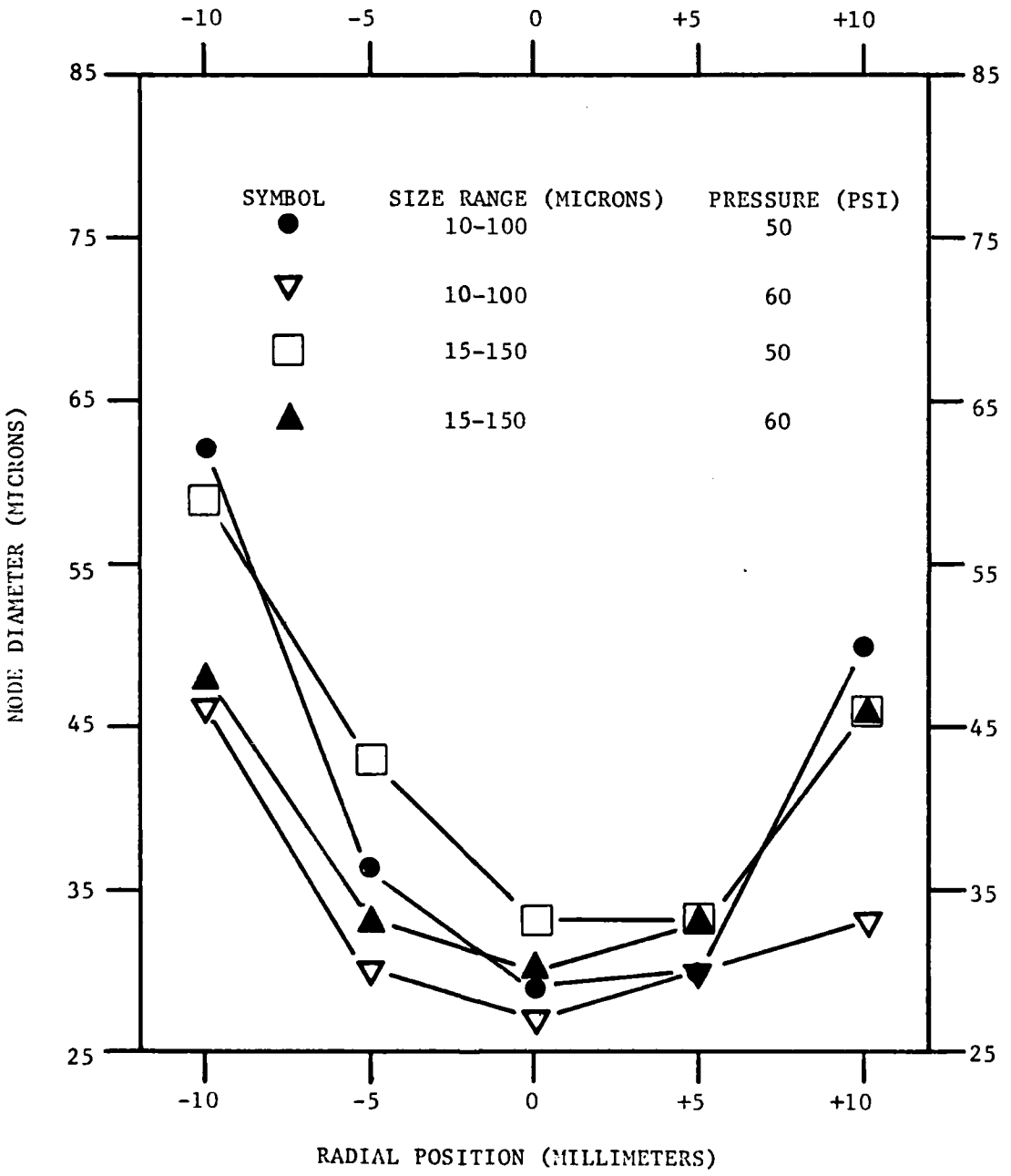

Figure 8b. Variation of characteristic diameter of spray with radial position and pressure - Sauter mean diameter.

3.5 Measurement of Submicron Particles

The measurement of particles near the wavelength has always been a necessary yet challenging task. We experimented with IMAX/PIMAX and found that it worked very well in the size range of about 0.5 μm to several microns. Obviously here, the full Mie[1] scattering equations had to be solved since ray optics are no longer applicable..

We tested this concept with PIMAX as shown on Figure 1.

It should be pointed out that this application was sponsored by AEDC since they are interestd in establishing the effect of particle size in LDV applications. This was only possible because of the previous developments under the AFOSR program and we find it appropriate to include it in this Final Report.

Theory

If we refer to the small beam as 1 and the large beam as 2, the intensity profiles in the probe volume can be separated by their polarization and given by:

$$I_1 = 2I_{o_1} \exp\left(\frac{-2}{b_{o_1}^2}\right)\left[x^2+y^2+z^2\gamma^2/4\right] \cdot$$

$$\left[\cosh\left(\frac{2xz\gamma}{b_{o_1}^2}\right) + \cos\frac{4\pi x \sin\left(\frac{\gamma}{2}\right)}{\lambda}\right], \qquad (1)$$

and

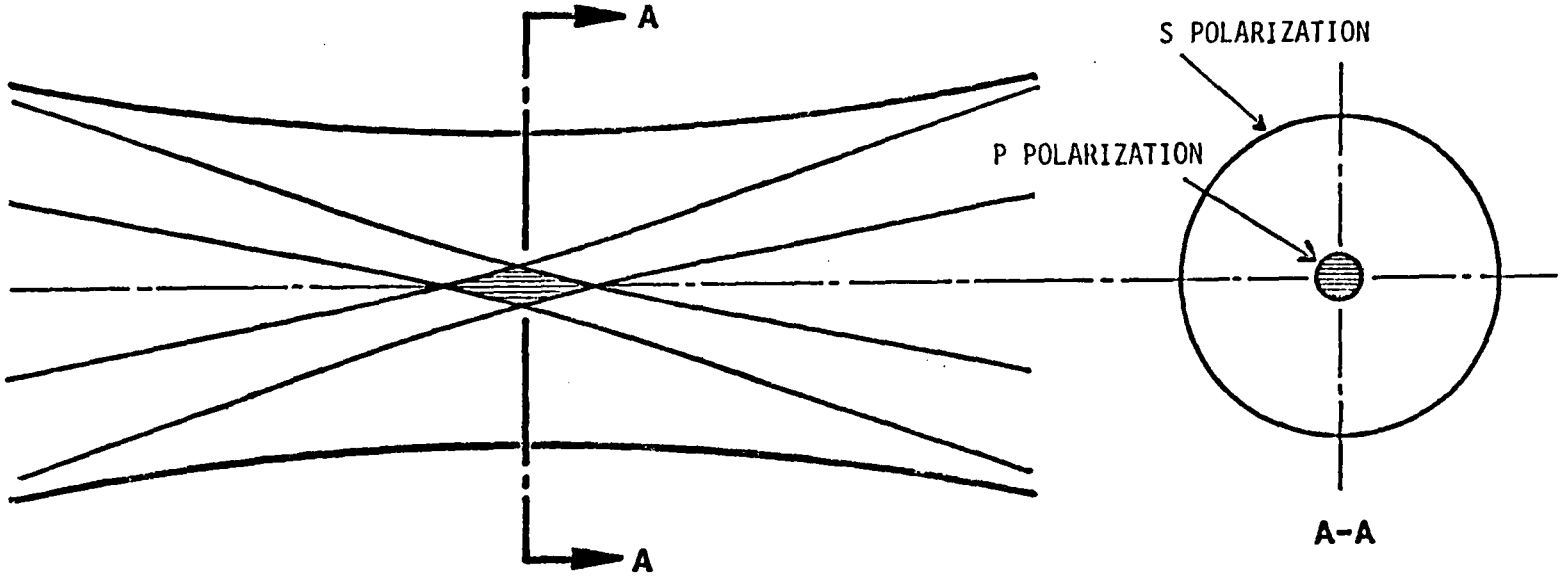

FIGURE 1. PROBE VOLUME OF TWO POLARIZATION PIMAX TECHNIQUE

$$I_2 = I_{o_2} \exp\left[-\frac{2}{b_{o_2}^2}(x^2+y^2)\right] \quad . \tag{2}$$

Where I_o is the center intensity, γ is the intersection angle, b_o the waist radius, λ the laser wavelength, and x,y,z the coordinates. The z dependence of the large beam is negligible. If we also assume that $\frac{z\gamma}{2} \approx 0$ (which is an excellent assumption since a pinhole in the receiver will limit the value of z), the intensity scattered by a spherical particle is given by:

$$I_{s_1} = 2I_{o_1} K_1(d,n,\theta,\Omega,\lambda,P)G_1 \exp\left[\left(-\frac{2}{b_{o_1}^2}\right)(x^2+y^2)\right]$$

$$\left[1 + \cos 2\frac{\pi\gamma x}{\lambda} \cdot V\right], \tag{3}$$

and

$$I_{s_2} = I_{o_2} K_2(d,n,\theta,\Omega,\lambda,S)G_2$$

$$\exp\left[\left(-\frac{2}{b_{o_1}^2}\right)(x^2+y^2)\right] \quad , \tag{4}$$

where

K is the scattering cross-section as obtained by the Lorentz-Mie theory[2]. It is a complex function of size d, the index of refraction n, the collection angle θ, the solid angle of collection Ω, the wavelength λ and the polarization. Here it is assumed that the small beams

have a polarization parallel to the scattering plane while the polarization of the big beam is perpendicular. G is the gain function of the instrument, and V is the visibility of the measured particle.

It should be pointed out that the visibility of the particle is not an adequate parameter to obtain the size, given that many of the particles of interest are below 3 μm and, in general, many of the particles will be submicron.

Equation (3) gives the signal response of the laser Doppler velocimeter which will establish the detectability of the signal. The processing logic will be the following: signals exhibiting ac modulation will have crossed the fringe pattern which is located in the middle of the large beam. Therefore, signals validated by the laser velocimeter correspond to particles crossing the middle of the large beam and their scattered light can be inverted to size since the Gaussian ambiguity is removed. In Equation (4) the exponent can therefore be approximated as unity and we get

$$I_{S_2} = I_{o_2} K_2 G_2 \quad . \tag{5}$$

The K_2 coefficients will be obtained from Lorentz-Mie scattering using a modified version of the numerical program developed by Dave[3]. Equation (5) can then be solved for the particle size which is contained in K_2 $(d,n,\theta,\Omega,\lambda,S)$.

Numerical Computations of the Scattering Functions

To obtain the particle diameter, d, it is necessary to know the functional relationship of K_2 $(d,n,\theta,\Omega,\lambda,S)$. This function can be quite complex and it is necessary to find the conditions under which the ambiguities, if any, are within tolerable error margins. The computations were made in a PDP11 computer. Parametric studies were conducted to establish optimum experimental conditions. These parameters include the angle of collection (θ). The solid angle of collection (Ω) and index of refraction ($n_1 - in_2$). The results show that near forward scattering angles of collection ($\theta < 5°$) offer the best optical characteristics.

Since the index of refraction of the particles present in LDV applications may be quite different, it is important to establish conditions which are less sensitive to these variations. Both real (n_1) and imaginary (n_2) parts of the refractive indices were varied to check the sensitivity of these parameters. Figures 2 and 3 show the scattered intensity as a function of the particle size parameter α for different values of n_1 and n_2 at different scattered angles.

It can be concluded from these calculations that shallow angles of collection ($< 5°$) offer the most favorable conditions.

The calibration of the system was conducted with known size polystyrene particles, therefore the scattering function corresponding to these particles was also evaluated. The results are shown on Figure 4 and, as before, the shallow angles offer the best conditions.

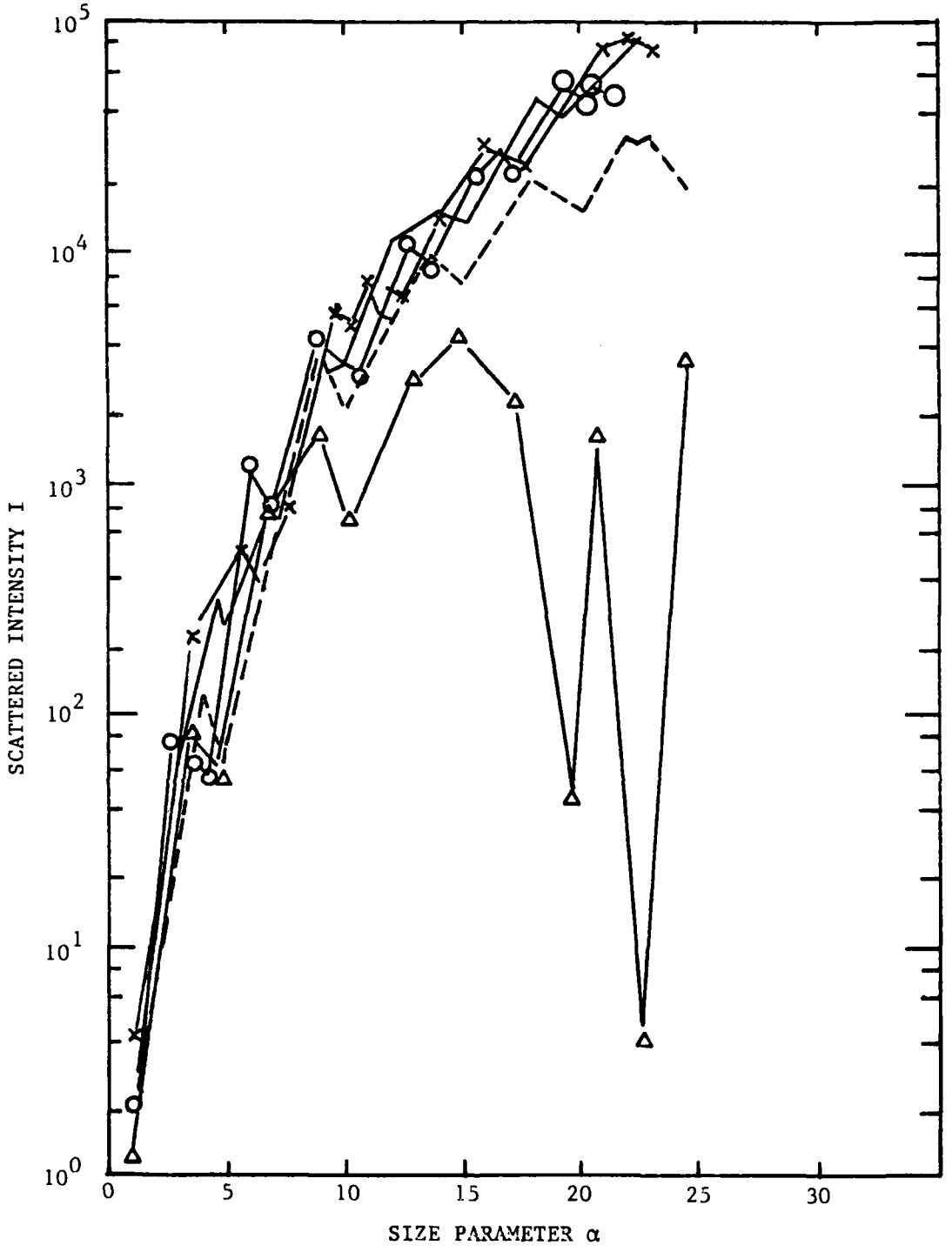

Figure 2. Perpendicularly polarized scattered light intensity as a function of the size parameter α

$\theta = 0°$: (x-x-x ($\tilde{n} = 1.56 - i2.9 \times 10^{-7}$), ——— ($\tilde{n} = 1.66 - i2.9 \times 10^{-7}$), 0 - 0 - 0 ($\tilde{n} = 1.96 - i2.9 \times 10^{-7}$) $\theta = 5°$: (----- $\tilde{n} = 1.66$), $\theta = 10°$: (Δ - Δ - Δ $\tilde{n} = 1.66$)

AD-A173 100 DROPLET SIZING RESEARCH PROGRAM(U) SPECTRON DEVELOPMENT 2/2
LABS INC COSTA MESA CA C F WESS 10 MAR 86
SDL-86-2286-15F AFOSR-TR-86-0875 F49620-83-C-0060
UNCLASSIFIED F/G 4/1 NL

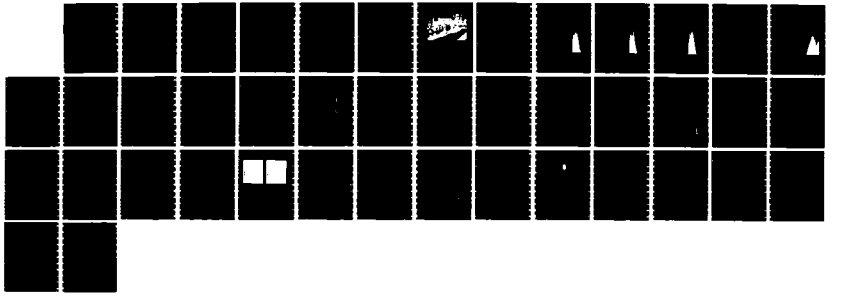

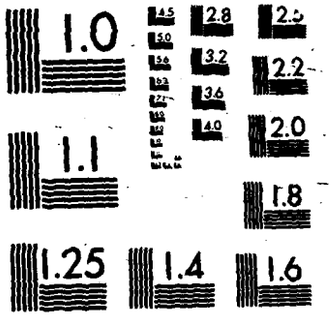
1.0
1.1
1.25
1.4
1.6
1.8
2.0
2.2
2.5
2.8
3.2
3.6
4.0
4.5
5.0
5.6
6.3
7.1
8.0
9.0

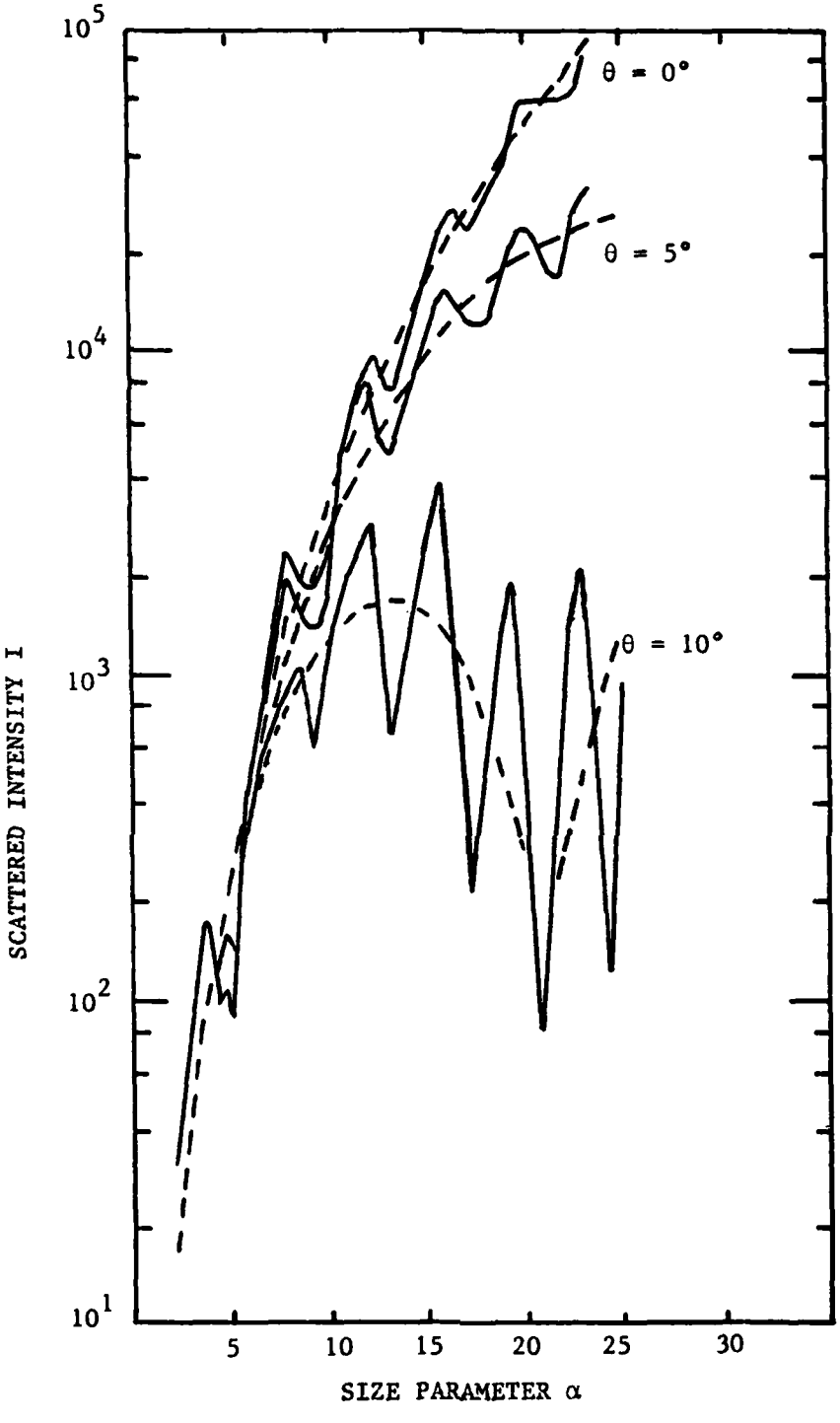

Figure 3. Perpendicularly polarized scattered light intensity as a function of the size parameter α for different refractive indices (---- $\mathfrak{n}$ = 1.75, ---- $\mathfrak{n}$ = 1.75 - 10.29) at angles 0°, 5° and 10°.

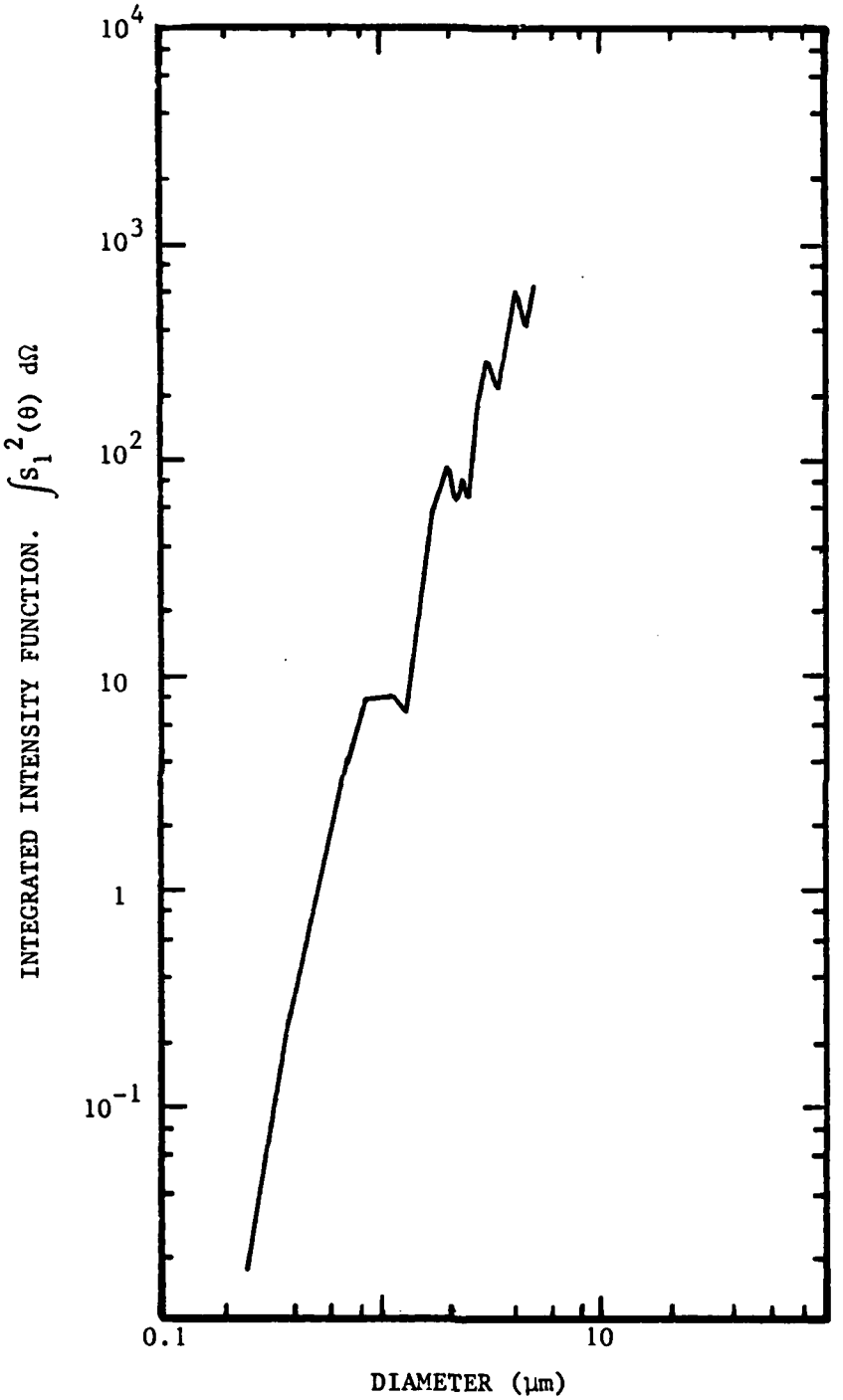

Figure 4. Integrated intensity function for θ = 5° and F/5 lens for polystyrene microspheres, (n = 1.59) as a function of diameter.

Apparatus and Experimental Facility

Figure 5 shows a schematic of the optical system used in the experiments. The system consists of a transmitter and a receiver positioned 5° off axis. The transmitter uses a 5 mW He-Ne laser. The laser beam is focused on a diffraction grating (DG) by Lens L_1, and the three major orders are collimated by Lens L_2. The zero order beam goes through a beam compressor formed by L_4 and L_5 and its polarization is rotated by PR. Lens L_3 focuses and crosses all three beams to form a probe volume like the one shown in Figure 1. The light scattered by particles crossing the probe volume is collected by L_6 and focused onto the photomultipliers by L_7. A cube polarizer (CP) divides efficiently the scattered light into its two polarization components. In addition, a polarization filter was placed in front of the PMT which looks at the big beam (BPMT) to reduce the cross talk between the two polarizations.

The size of the probe volume was typically 600 μm for the large beam and 86 μm for the small ones. The fringe spacing was 10.7 μm. To reduce the size of the probe volume we used a slit in front of the BPMT. The width of this slit was typically equal to the diameter of the small probe volume (100 μm) and its length was about four times longer to avoid signal masking. Thus, the probe volume was about 10^{-5} cm^3 which, in general, is quite adequate for LDV applications.

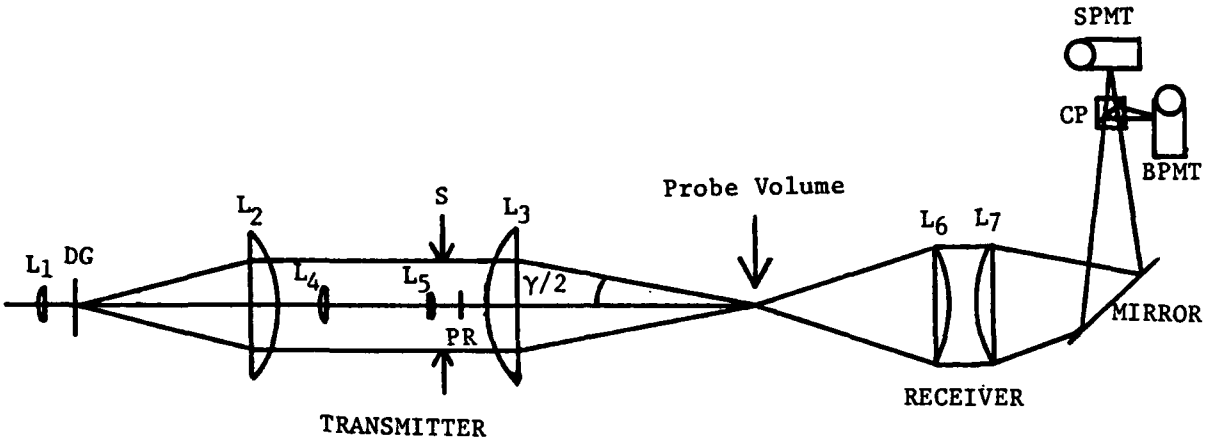

Achromatic Lens	Focal Length (mm)
L_1	35
L_2	220
L_3	112
L_5	16
L_6	300
L_7	500

CP: Cube Polarizer
DG: Diffraction Grating
100 lines/mm
PR: Polarization Rotator

Figure 5. Schematic of PIMAX system

228615F35/29

The Particle Generator

The particle size of interest is that corresponding to typical LDV applications. We used polystyrene particles of 1.1 μm, 1.7 μm, 2.7 μm and 3.3 μm in diameter. These are latex particles made by Dow Chemicals of good size uniformity and of spherical shape. The particles come suspended in water with a concentration of 10% by weight. A few droplets of the particle suspension were introduced and diluted in a nebulizer. An air compressor provided the air flow to produce a mist carrying the polystyrene particles out of the nebulizer and into a heated chamber. There the water was evaporated and the particles were sprayed over the probe volume.

Different size particles could be introduced into the nebulizer thus producing monodisperse, bimodal, trimodal and quadramodal distributions. The compressor was also used to trap the particles after they passed through the probe volume to avoid contaminating the surrounding environment. Figure 6 shows a photograph of the optics and the particle generator.

An alternative apparatus was also constructed to introduce glass beads into the probe volume. The glass beads come in dry containers and their size distribution was reasonably broad. A test tube with a stopper was used to contain the glass beads. Two glass tubes protruded through the stopper and flex tubing was connected at the end of each glass tube. One of the flex tubes was connected to a nitrogen tank via a pressure regulator and a flow meter. The other flex tube discharged the glass beads into the probe volume. The flow rate of nitrogen could

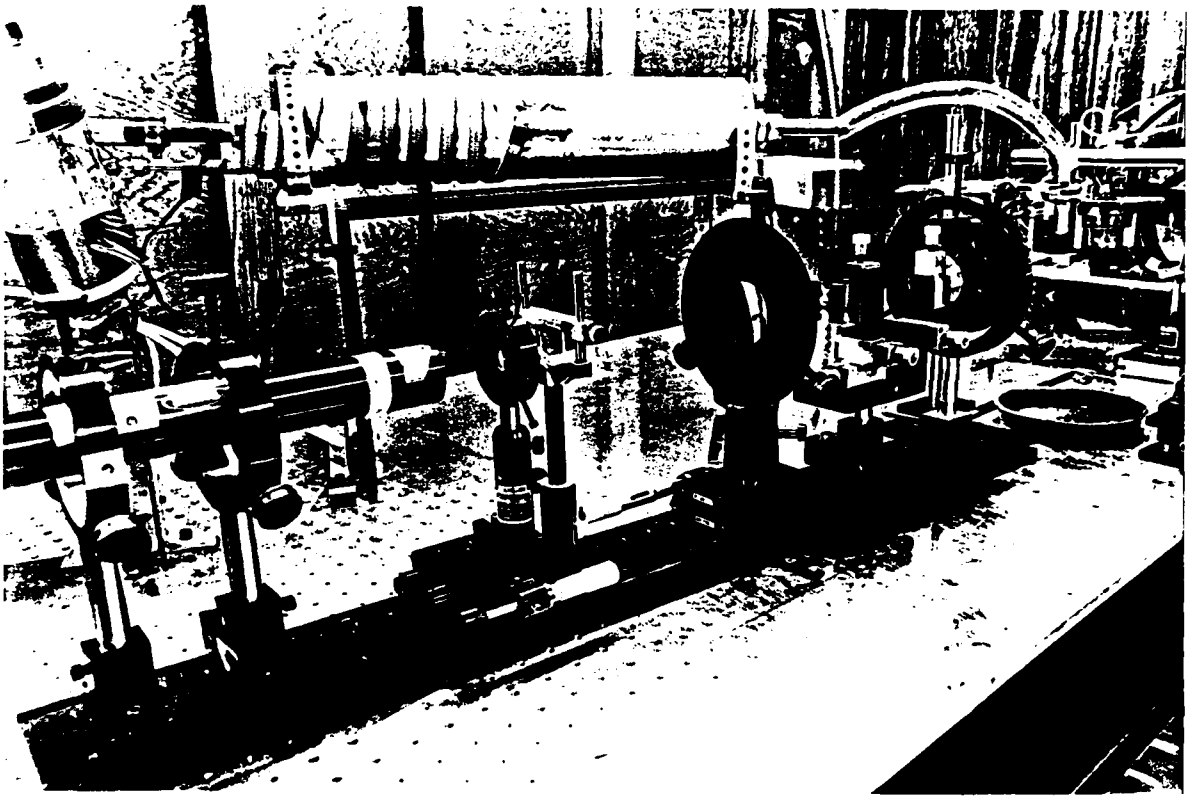

Figure 6. Photograph of PIMAX transmitter and particle generator.

be regulated very carefully and thus, the flow velocity at the exit of the flexible tube could be reproduced.

Experimental Results

The system was calibrated and tested with polystyrene latex particles of uniform and known size distributions. The size and uniformity of the particles were checked with a microscope and agreed with the manufacturer's specifications.

Size and velocity distributions of the polystyrene particles flowing out of the heating chamber were obtained with the optical system described above. Figure 7a shows the distributions corresponding to 1.74 μm and 3.3 μm. The calibration high voltage of 500 V was established based on the 1.74 μm. The arrow with the 3.3 μm mark indicates the value predicted by the Mie calculations. In Figure 7b an intermediate size of 2.7 μm was added and the calibration high voltage was changed to 550 V to decrease the size range. As before the calibration was based on the 1.74 μm, and the arrows point at the numerically predicted values. The 3.3 μm was measured very accurately, but the measurement of the 2.7 μm particles was off by two bins. This error was consistent and very repeatable. We attribute it to the oscillations found in the scattering function. Figure 7c shows the distributions corresponding to four different latex particles. As before the calibration was obtained with the 1.74 μm particles. The calibration high voltage is 550 V. It must be pointed out that the size histograms are

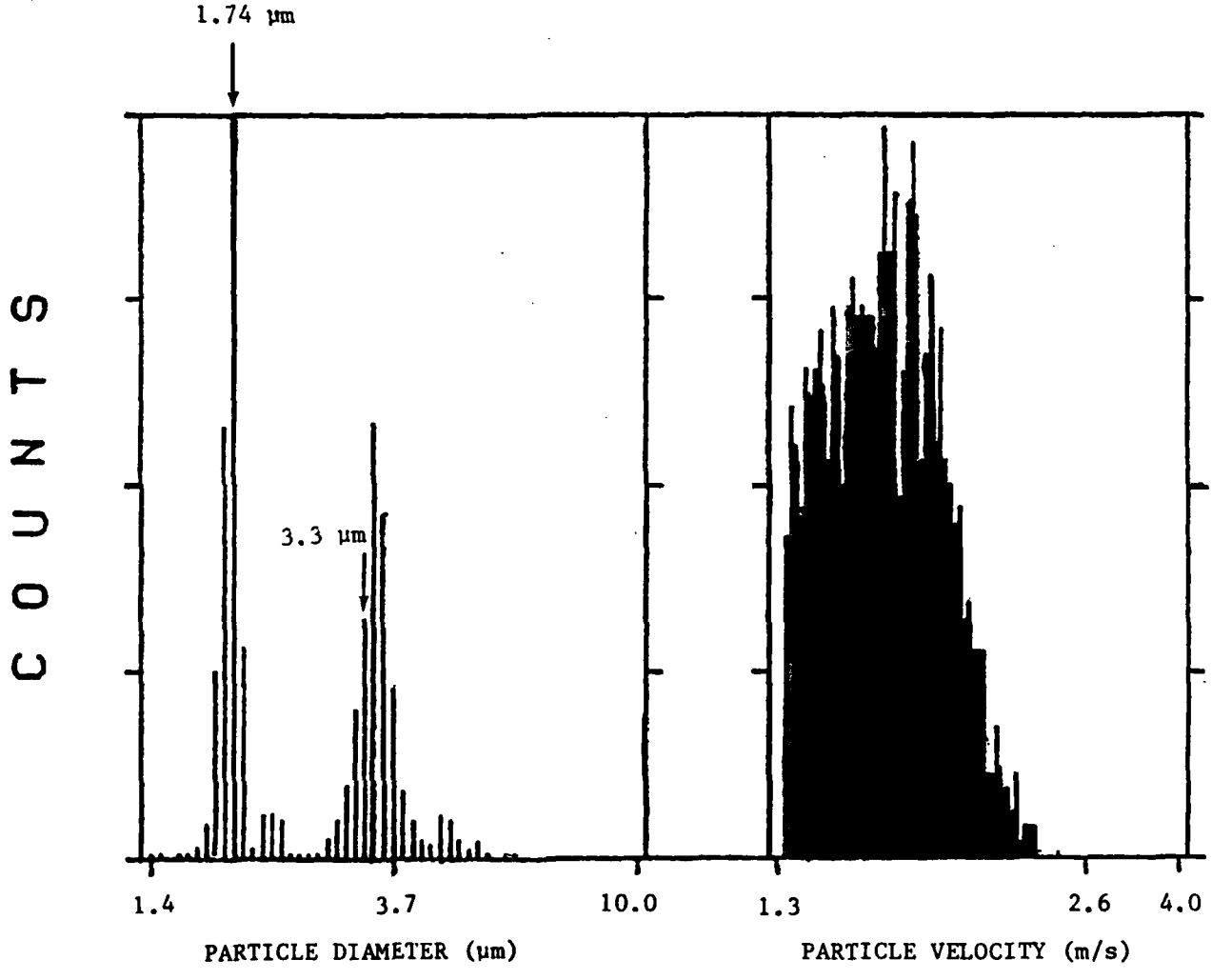

Figure 7a.

SIZE AND VELOCITY HISTOGRAM OF 1.74 µm AND 3.3 µm POLYSTYRENE SPHERES IN AIR. PHOTOMULTIPLIER TUBE HIGH VOLTAGE = 500 VOLTS.

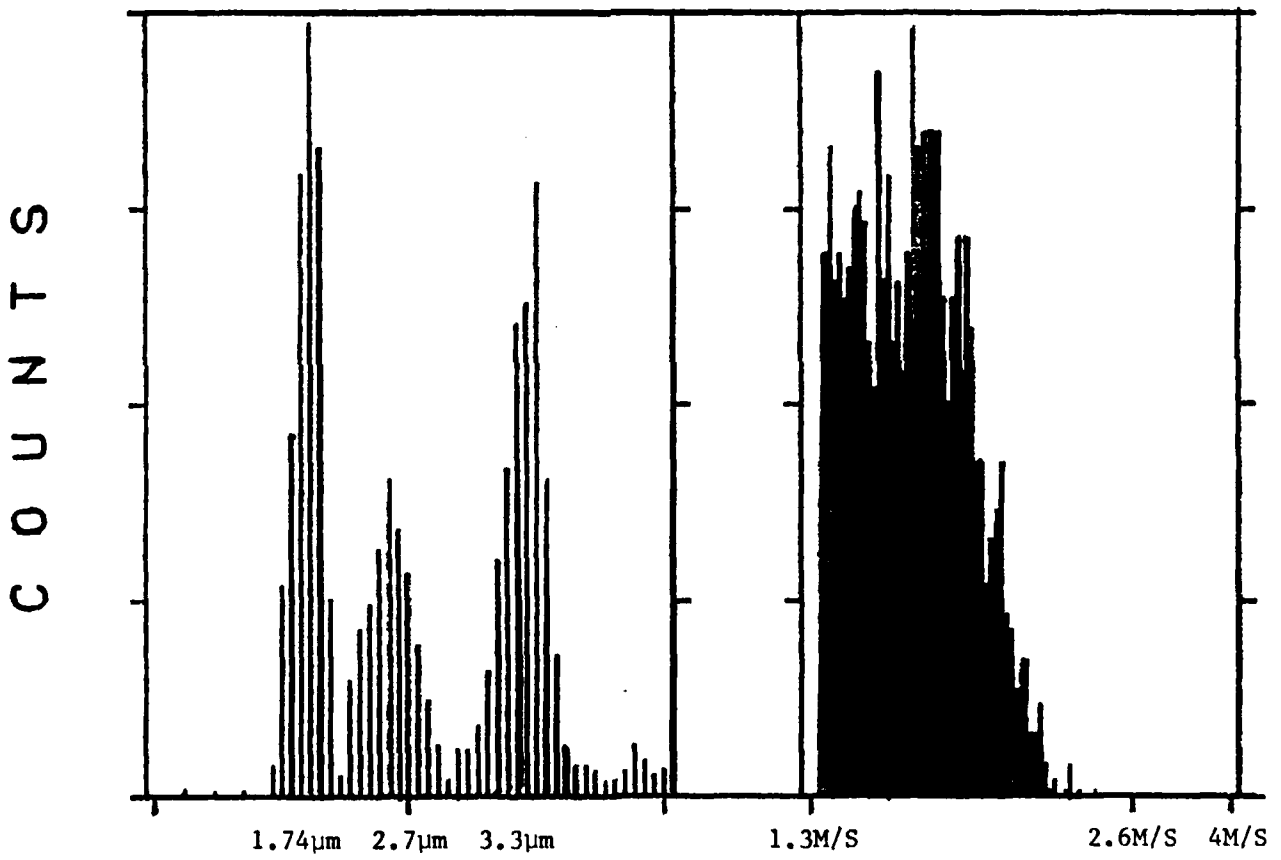

Figure 7b.

SIZE AND VELOCITY HISTOGRAMS OF 3.3 μm, 2.7 μm, AND 1.74 μm DIAMETER SPHERES IN AIR - PHOTOMULTIPLIER TUBE HIGH VOLTAGE = 550 VOLTS.

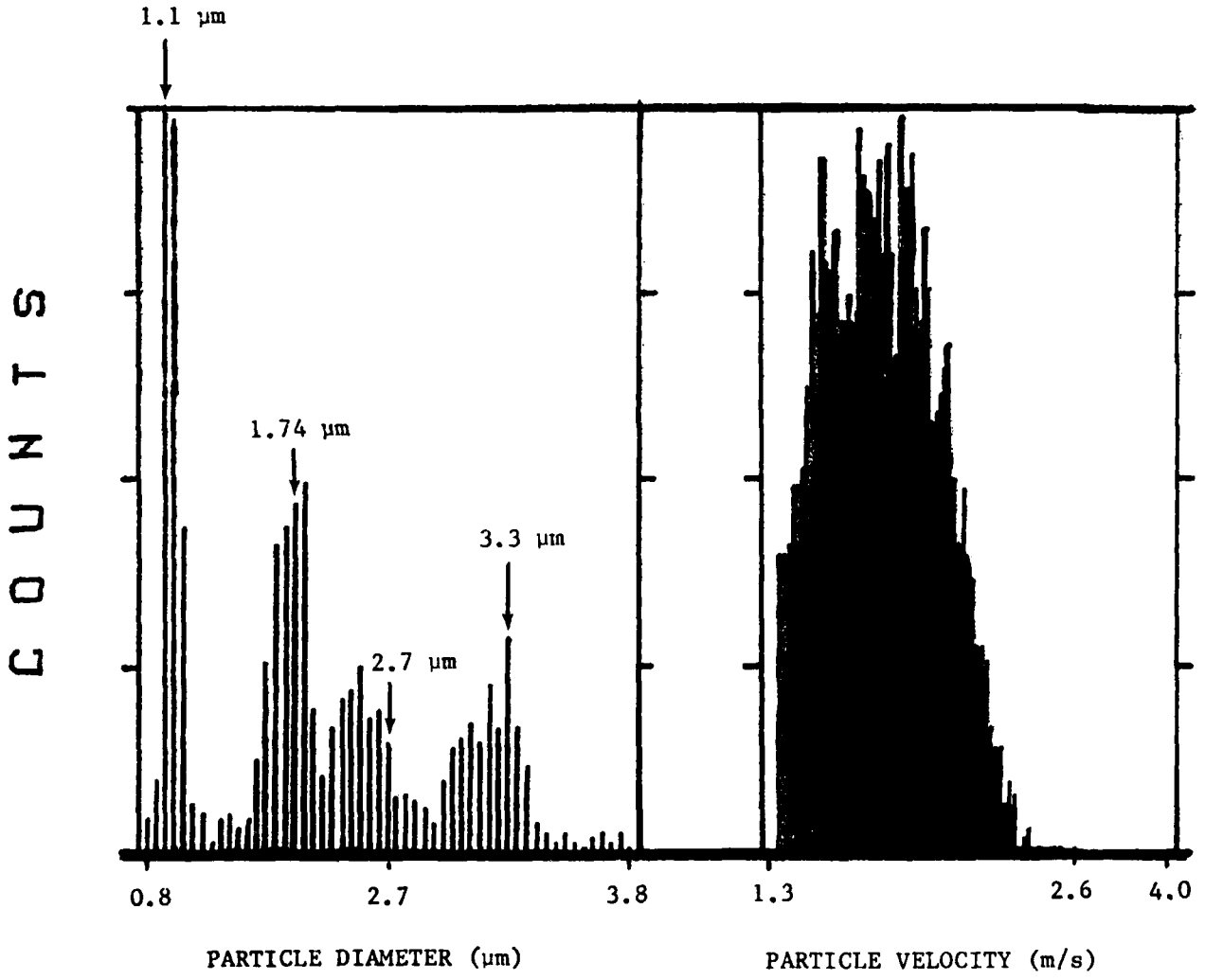

Figure 7c.

SIZE AND VELOCITY HISTOGRAMS OF 1.1 µm, 1.74 µm, 2.7 µm, and 3.3 µm POLYSTYRENE SPHERES IN AIR. PHOTOMULTIPLIER HIGH VOLTAGE = 550 VOLTS.

divided into 53 equal size bins. Therefore, distributions on the large diameter end will appear broader than those in the small diameter end.

These results indicate that the technique and instrument can accurately discriminate the particles by their size in LDV applications. Unfortunately, since all the particles are rather small and the flow velocity is also small and constant, all the particles moved at about the same velocity. Therefore, no velocity/size discrimination could be established. To illustrate this last point we used very large glass beads which would not follow the flow. Two different size classes were simultaneously introduced into the test tube and entrained into a constant nitrogen flow. These particles were sprayed over the probe volume and their size and velocity histograms are shown on Figure 8. Notice the bimodal size distribution and the corresponding bimodal velocity distribution. Although not obvious from this figure the small particles are moving faster than the big ones. This is better illustrated in Figure 9 which shows a velocity/size distribution of the entrained small and large glass beads. It can be deducted that the small glass beads are moving at about 13 m/s while the large ones are moving at about 8 m/s.

This particle size range is not expected in LDV applications but the experiment illustrates the kind of error that can be incurred in the flow velocity measurement if no consideration is given to the particle size.

An aspect of the PIMAX technique that needs to be considered is the crosstalk between the two polarizations. To establish this crosstalk a series of tests were conducted. First, the polarization ratio of

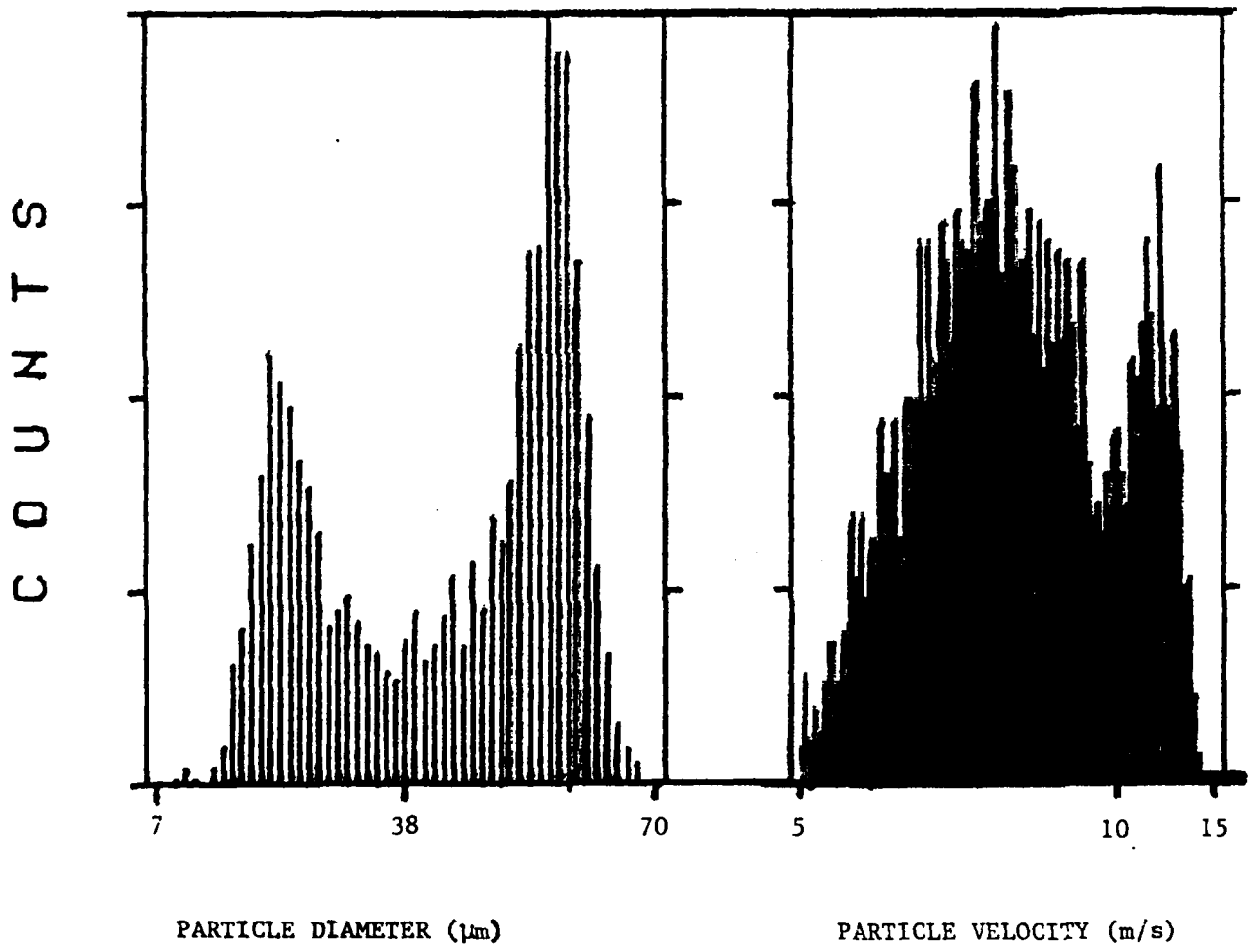

Figure 8.

SIZE AND VELOCITY HISTOGRAMS OF SMALL AND LARGE GLASS BEADS ENTRAINED IN AN AIR JET.

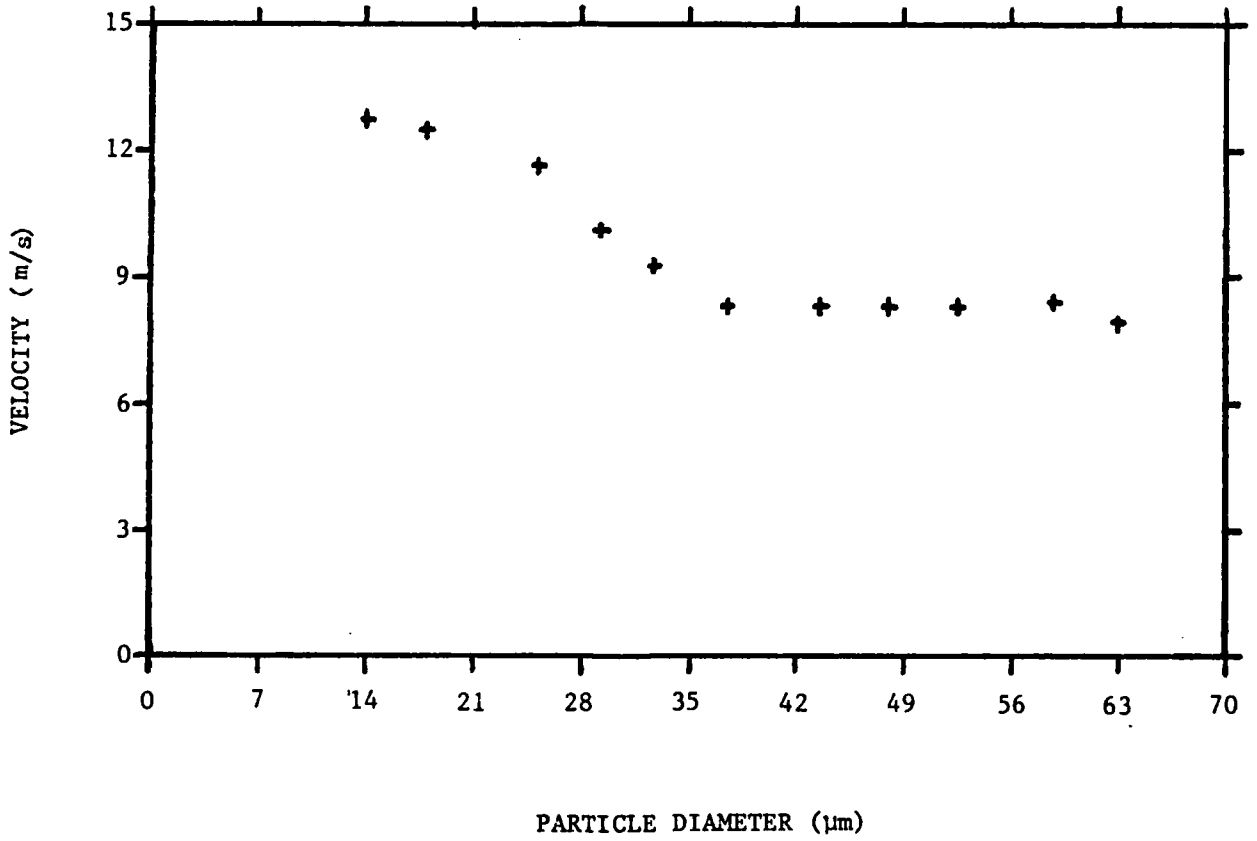

Figure 9.

VELOCITY DISTRIBUTION OF SMALL AND LARGE GLASS BEADS ENTRAINED IN AN AIR JET.

the transmitted laser beams was measured with and without particle extinction. To produce a substantial particle interference a fuel spray was used to attenuate the laser beam by 10%. Very little change in the polarization ratio was measured which is of no surprise since the light scattered in the forward direction carries the same polarization as the incident radiation. A second set of tests was also conducted. Monodisperse droplets produced by a Berglund-Liu generator scattered light which could be analyzed by the receiving optics. One PMT measured the S-polarized light while the other measured the P-polarized light. We blocked the large beam which is S-polarized and illuminated the particles with the small P-polarized beams. The scattered light was measured in the PMT intended for the S-polarized light. The crosstalk was about 4% at large (20°) angles and smaller at shallow angles. This crosstalk could be virtually eliminated by placing a polarizing filter in front of the PMT. It should be noted that the intensity into the small and large beams may not necessarily be the same and, therefore, the crosstalk will be proportional to the intensity ratio. For the small particles of interest in LDV and at shallow angles of collection this crosstalk is negligible.

References

1. Mie, G., "Beiträge zue optik trüber Medien; Speziell Koloidaller Metallösungen", Ann. Physik, 25, 377 (1908).
2. van de Hulst, H. C., "Light Scattering by Small Particles" Wiley, New York, 1962, Chapter 9.
3. Dave, T. V., "Subroutine for computing the parameters of the electromagnetic radiation scattered by a sphere", IBM Scientific Center, Report No. 320-3237 (1968).

3.6 Measurement of Nonspherical Drops

Another study which spun directly from the AFOSR research involves the measurement of nonspherical drops. This is also of interest to NASA and the Department of Commerce for their interest in atmospheric phenomena. Again, we feel it appropriate to include this work in this Final Report since it shows AFOSR how its program has been synergistic with other work of interest to other agencies.

This work is also very important to AFOSR, particularly for the measurement of dense sprays where the shape of the droplets is not necessarily spherical.

In this subsection, we discussed specifically how a top hat laser beam can be used to measure spheroids and its application to the measurement of heavy rain which is of interest to NASA Langley.

Introduction

A technique to measure raindrops during very heavy rain is discussed, and results from an experimental study are presented.

It has been postulated[1] that heavy rain, especially accompanied by wind shear, is responsible for many accidents during aircraft landing and takeoff. To quantify this effect, wind tunnel measurements will be conducted at NASA Langley to model real situations. The size and velocity of droplets in the free stream are required inputs to these models. Techniques are therefore needed to measure very large size droplets (up to seven or eight mm) in very large liquid water content (up to 40 gr/m^3) environments.

There are three major problems in characterizing raindrops in heavy rain using optical methods. First, the shape of the natural raindrops may be nonspherical especially for large size droplets.[2] Since light scattering theories assume for the most part that the droplets are spherical, errors will be incurred when inverting the scattered light information. The selection of optical conditions to minimize this error becomes an important aspect of this work.

In the size range of interest (>100 μm) the scattered light can be divided into three components[3]: diffraction, reflection, and refraction. The first is in the forward direction and cannot be completely separated from the unscattered beam. The last two are more sensitive to shape and must be interpreted carefully.

Second, the large range of droplet size encountered in heavy rain[4] can also impose difficulty in the size measurement. In order to measure a particular size range, a suitable size probe volume is required. This probe volume can, however, impose limitations in the number density of smaller droplets.

Finally, beam blockage and interference due to the presence of upstream droplets along the beams can affect the measurements. Beam blockage and interference introduce instantaneous fluctuations to the constant intensity laser beams. These fluctuations not only broaden the size histogram but also reduce the data rate of collection. We demonstrated that a laser Top Hat technique can be used to obtain the required measurements. This method based on the absolute scattered light from constant intensity laser beams can measure droplets in the 0.1 mm to 10 mm size range moving at very high speeds.

Description of Apparatus

Figure 1 shows a schematic diagram of a Top Hat optical system and the associated electronics. Two cylindrical lenses L1 and L2 expand approximately 8 times one dimension of a 1.25 mm diameter He-Ne laser beam. This expanded laser beam was masked with a 3 mm slit placed after the cylindrical lens L2. A spherical lens L3 and a beam splitter were placed such that the mask was imaged at the center of the spray. This was accomplished by placing a thin hair at the mask and searching for its sharp image at the conjugate plane. The two beams coming out of the beamsplitter were crossed there thus defining a probe volume with interference fringes. F/5 receiving optics placed at 90° imaged the probe volume on a pinhole in front of the PMT thus limiting its length. The output of the PMT was connected to a VP1001 signal processor which was interfaced to a computer. The velocity of the droplets was measured from the Doppler frequency and the size was measured from the peak of the absolute scattered light using a pulse height analyzer. A low pass filter eliminated the ac component of the signals measured by the pulse height analyzer.

Size and velocity histograms of the droplets crossing the probe volume were displaced in real time and stored for further analysis.

Description of Experiments

Three kinds of experiments were conducted to establish the feasiblity of the Top Hat technique in measuring heavy rain. These experiments were designed to address the following issues:

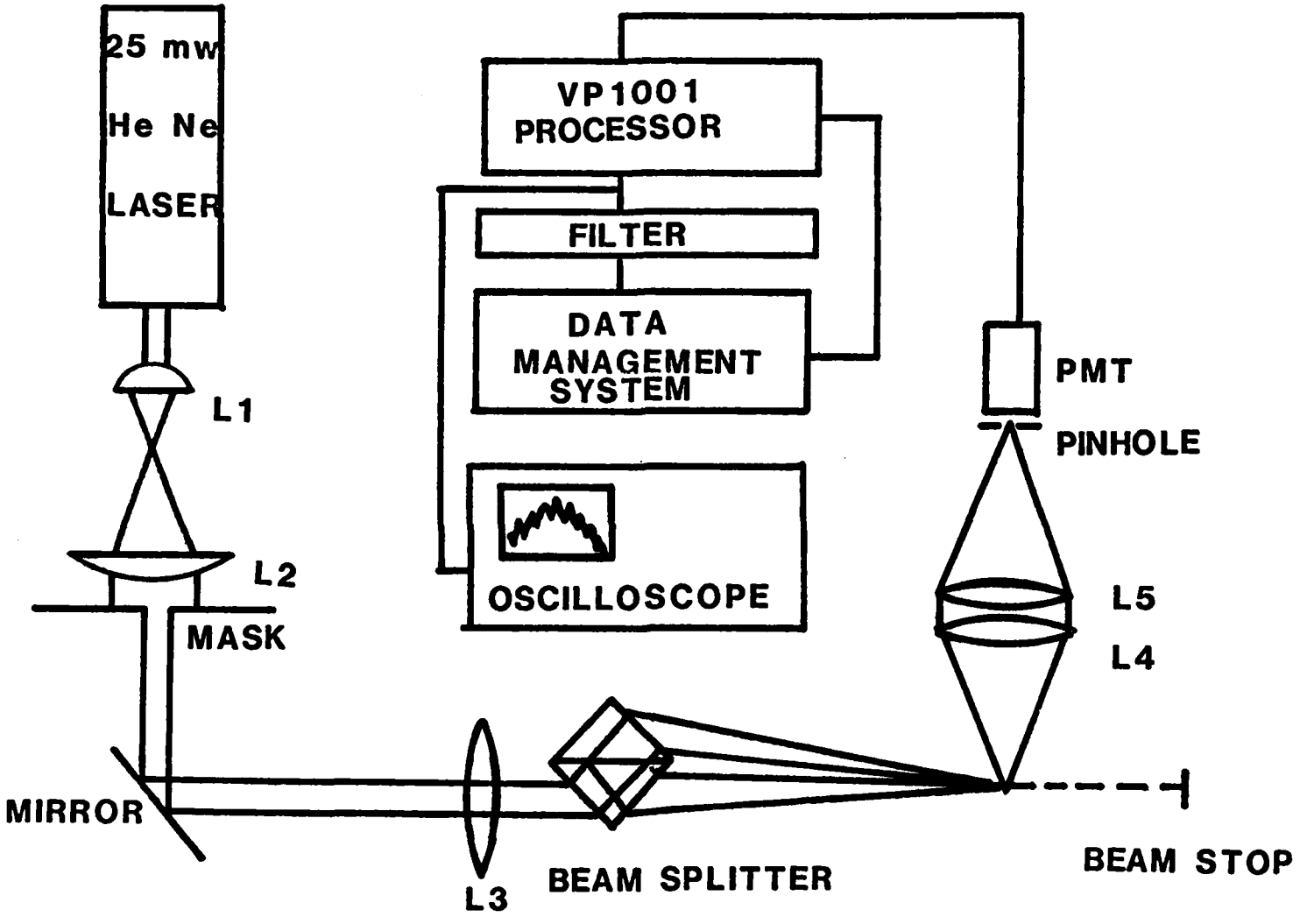

Figure 1. Schematic diagram of Top Hat measurement system.

a. The ability to measure a spray produced by a BURR 2 (this is a nomenclature adopted by JPL to define multitube nozzles - see Paper 0291 of this session) nozzle in the 300 to 9000 μm range.

b. The effect of spray interference on monodisperse and polydisperse sprays.

c. The effect of droplet asphericity on the scattered light.

The first type of experiment was conducted using a single orifice of a 5 orifice BURR 2 nozzle. This restriction was imposed by the size of our laboratory which, unfortunately, is not designed to handle the five orifices at full blast. Visual inspection of the spray indicated that well established droplet regimes existed 2 m from the nozzle tip. We, therefore, installed the nozzle at 4 m from the floor and sprayed down. Measurements were performed at about 2.65 m from the nozzle tip. A pressure gauge next to the nozzle was used to monitor the discharge pressure during measurements. The spray was discharged into a 50 gal. bucket with a submersible pump to dispose off the water. The spray flow rate could be easily established with a stop watch and volume measurement. The optics remained fixed during the experiments and imaged at a predetermined position within the spray.

To assess the effect of spray interference, the laser beams traveled through the "rain spray" and formed the probe volume after the

spray. At the probe volume we measured monodisperse drops of known size (typically 2.8 mm) or another spray produced by a Spray Systems pressure nozzle. Typical LWC during the spray measurements and laser interference experiments were about 90 gr/m^3, which is considerably larger than that encountered under the heaviest of rains. There were two reasons for testing the feasibility of the technique under such large LWC. First, this was the normal level encountered at 3 m from the nozzle tip. Second, we postulated that if we could perform adequate measurements under this heavy particle loading, the technique would most definitely work in the wind tunnel experiments.

The last set of experiments were conducted to qualify the effect of droplet nonsphericity in the scattered light. Photographs of the spray indicated that many of the large droplets were nonspherical. The objective of these experiments were to estimate the errors associated with assuming spherical drops. These experiments were conducted with the Berglund-Liu monodisperse droplet generator. Droplets of known volume but aspheric shape were produced with this device.

Calibration Procedure

A monodisperse string of droplets of 2.8 mm provided the required system calibration. These droplets were produced by allowing water to free fall through a syringe and a hypodermic needle. The size of these droplets was determined photographically to be 2.8 mm ± 5%. The light scattered by the moving droplets was focused onto the PMT of the receiving optics. A mask was placed in front of the collecting lens to adjust the collection F# and thus obtain a visibility appropriate for a

particular size range of interest. It should be pointed out that the visibility is not part of the size measurement but it provides the ac modulation required to make velocity measurements.

Finally, the gain to the PMT was adjusted manually to calibrate the size sensitivity. Figure 2 shows a representative size and velocity histogram obtained with the 2800 μm calibration drops.

Experimental Results

The results of the three kinds of experiments described above are presented now.

Characterization of Simulated Rain Spray

A rain spray produced by a single orifice of a BURR 2 nozzle was measured at an axial location of 2.65 m from the nozzle tip and two radial locations: r=0 and r=6 cm. The scattered light was collected at 90° and at 20°, at distances of 0.62 m and 4 m. Most of the measurements were conducted at 0.62 m but some measurements were made at 4 m to emulate the conditions expected in the wind tunnel. Nozzle pressures of 50, 60, and 70 psi were investigated.

Typical size and velocity histograms are shown on Figure 3 for a central radial position (r=0) and a pressure of 60 psi. Notice that the size range is only 10:1 which is a limitation imposed by the electronics. Broad size distributions were measured by splining several overlapping size ranges. Figure 4 shows the size distribution corresponding to the center of the spray obtained with three different size ranges. These measurements are plotted together to establish

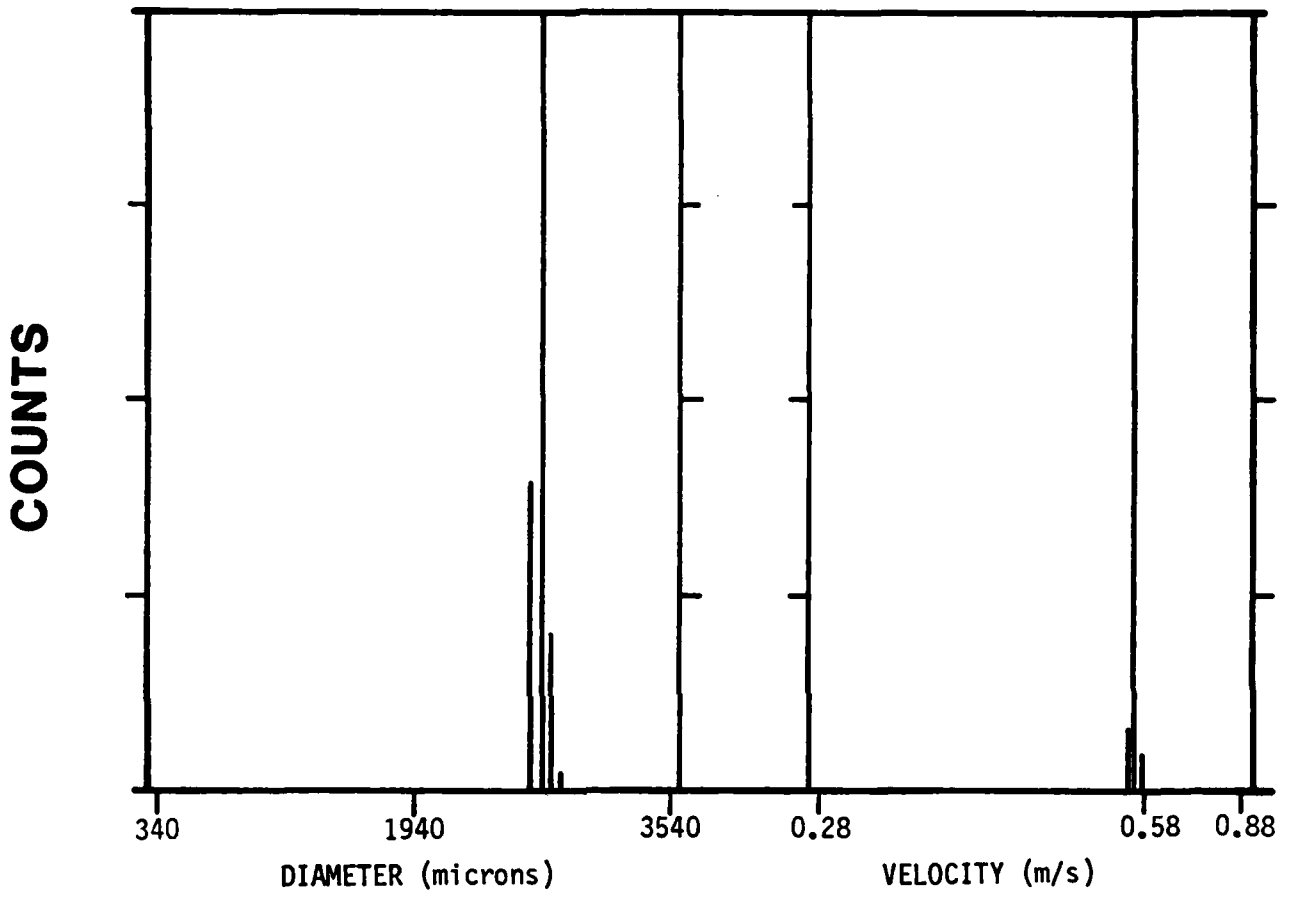

Figure 2. Size and velocity histograms of 2.8 mm diameter droplets produced by hypodermic needle.

discrepancies in the overlapping regions. The typical trend is that the number of counts is underestimated at the small size end of any range. To some extent this is due to the limited laser power available for this experiment (25 mW HeNe). Also plotted on the same figure is the size distribution corresponding to the edge of the spray. The size range of 100-1000 μm was calibrated with a 283 μm droplet produced by the Berglund-Liu. The measurement cross sectional area was smaller for this case: 0.6 x 2 mm, compared to 1.5 x 2 mm for the other ranges.

Figures 3 and 4 show that large droplets (up to about 8 mm) were produced by the nozzle. The number of droplets was inversely proportional to their volume down to a few hundred microns.

The measurements at the edge of the spray show a lower number density and smaller size distribution, therefore, yielding a smaller Sauter mean and linear mean diameters than those at the center position. This behavior depends on the nozzle geometry and it is quite common to experience the opposite trend (smaller drops in the center of the spray) in sprays produced by typical pressure nozzle.

The following table summarizes the results obtained at the center position (r=o) as a function of rain nozzle pressure.

Keep in mind that these are point measurements and will differ from integrated measurements taken at the same plane.

Spray Interference

To evaluate the effect of spray interference in the size measurement, monodisperse strings of droplets and polydisperse sprays were measured with and without the simulated rain spray interfering with the

SIZE AND VELOCITY HISTOGRAMS OF RAIN SPRAY

pressure=60 psi

radial position= 0

axial position= 2.65m

nozzle ID : BURR 2

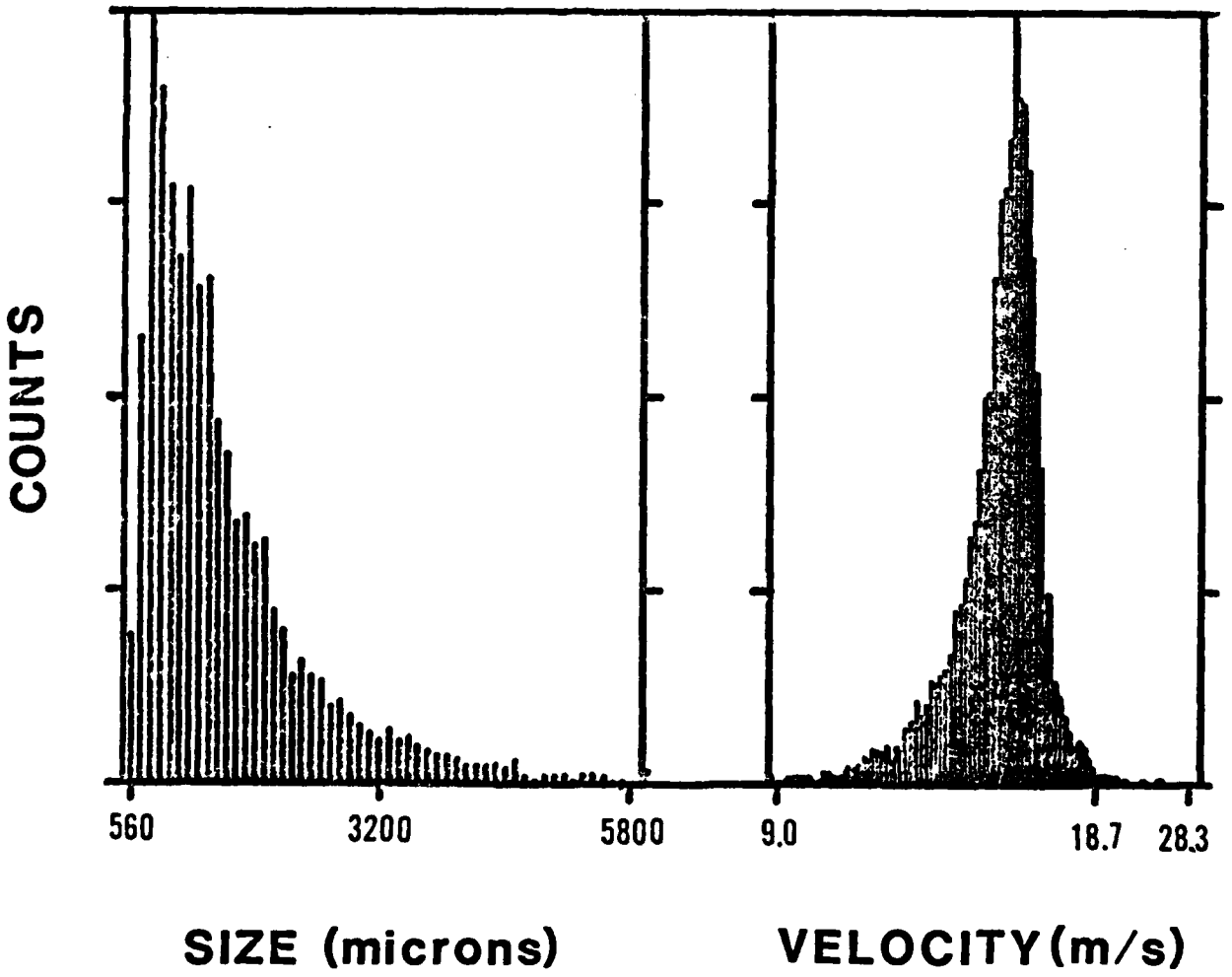

Figure 3.

85-61070
85-2424-1F/39

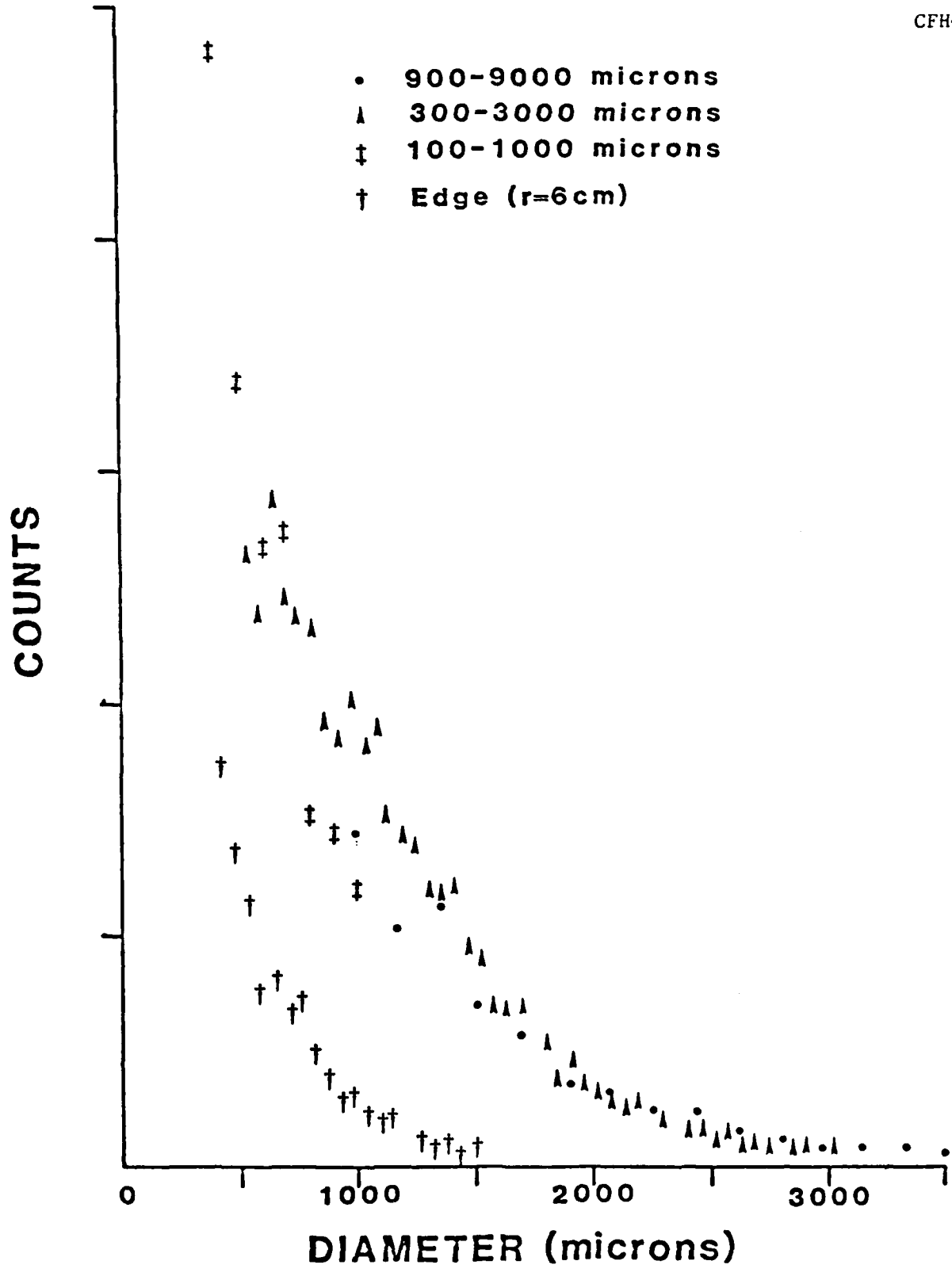

85-6107(

Figure 4. Size Distribution at the Center and Edge of Rain Spray at 60 psi.

beams before they crossed to form the probe volume. The results are shown below.

Monodisperse String of Droplets

To evaluate the effect of spray interference, droplets of a uniform size were measured with the laser beams traveling through a spray produced by the BURR 2 nozzle. These measurements were compared to those obtained without interference. Since the effect of the interference on the size can be a function of the signal level, different signal levels were obtained by masking the receiver to obtain an intensity and visibility corresponding to an appropriate size. Figures 5a and 5b, respectively, show the size histograms of a monodisperse string of drops with and without interference. Three effects were observed in these measurements: (1) the mode of the size distribution decreased (from 2739 μm to 2677 μm); (2) the distribution broadened; and (3) the data rate decreased and depended on the particle size. The first effect can be easily attributed to laser obscuration. In many practical situations this effect can be either ignored or compensated for by monitoring the transmitted beam. The second effect can be attributed to the random nature of the spray blockage. In the measurement of a polydisperse spray, this effect will go unnoticed since the broadening between bins will result in almost zero net exchange. The third effect can be more serious and difficult to correct. The trend was invariably the same; namely, the large drops are more susceptible to rejection than the small drops. This is illustrated on Figure 6 where the data rate (normalized to its value without interference) is shown for four

TABLE

NOZZLE PRESSURE (psi)	SMD (μm)	LMD (μm)	PEAK VELOCITY (m/s)
50	1649	1038	15
60	1575	956	16
70	1549	856	17

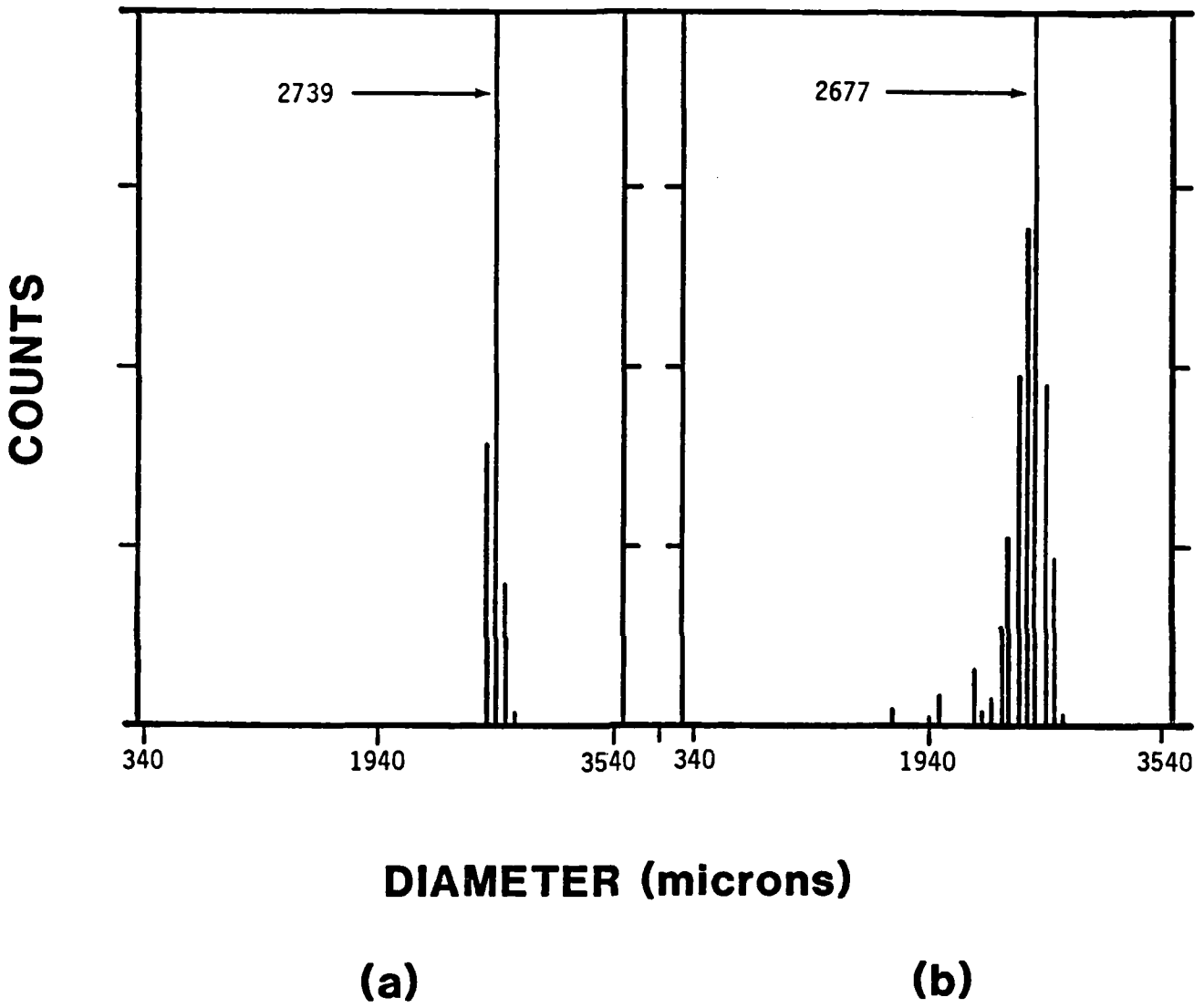

Figure 5. Size Histogram of Monidisperse Spherical Droplets Illuminated by (a) Undisturbed Laser Beams, (b) Laser Beams Traveling through Rain Spray.

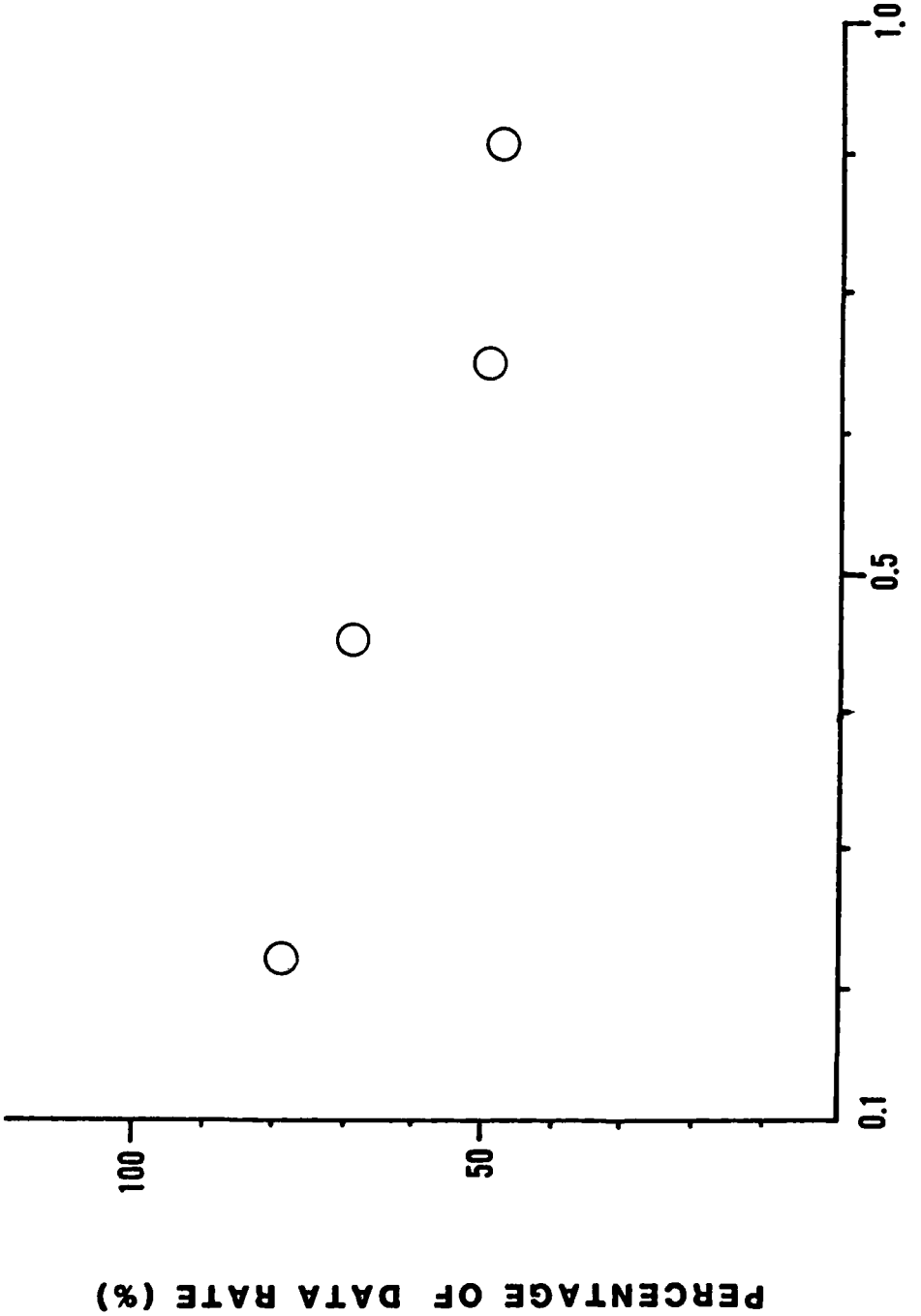

Figure 6. Effect of Spray Blockage on the Data Rate of Collection as a Function of Particle Size.

different drop sizes. This effect can be corrected, or at least minimized, with proper electronics. Analyses of the signals with a storage oscilloscope showed that the large drops, since they have a low visibility, are more subject to signal rejection. A low visibility results in a low ac signal level. Present LDV processors base their acceptance criterion on the number of equal time crossings. Spray interference will introduce random crossings which disturb the otherwise periodic function. This is illustrated in Figures 7a and 7b which are photographs from the storage oscilloscope. This disturbance is less important for high visibility signals. In the actual rain, or simulated rain experiments this effect will not be as pronounced since the LWC is typically two orders of magnitude smaller than the ones reported here. However, more sophisticated acceptance criteria will reduce considerably the errors due to the discrimination of the processor used in this work (VP1001).

Polydisperse Spray

A water spray produced by a pressure nozzle (Spray Systems Teejet TG10 at 4 psi) was measured with and without the additional interference introduced by the BURR 2. The results are shown on Figure 8. The most noticeable effect is the drop in data rate for the case with interference. As expected, the broadening is difficult to detect given that the measured distribution of sizes is broad to begin with.

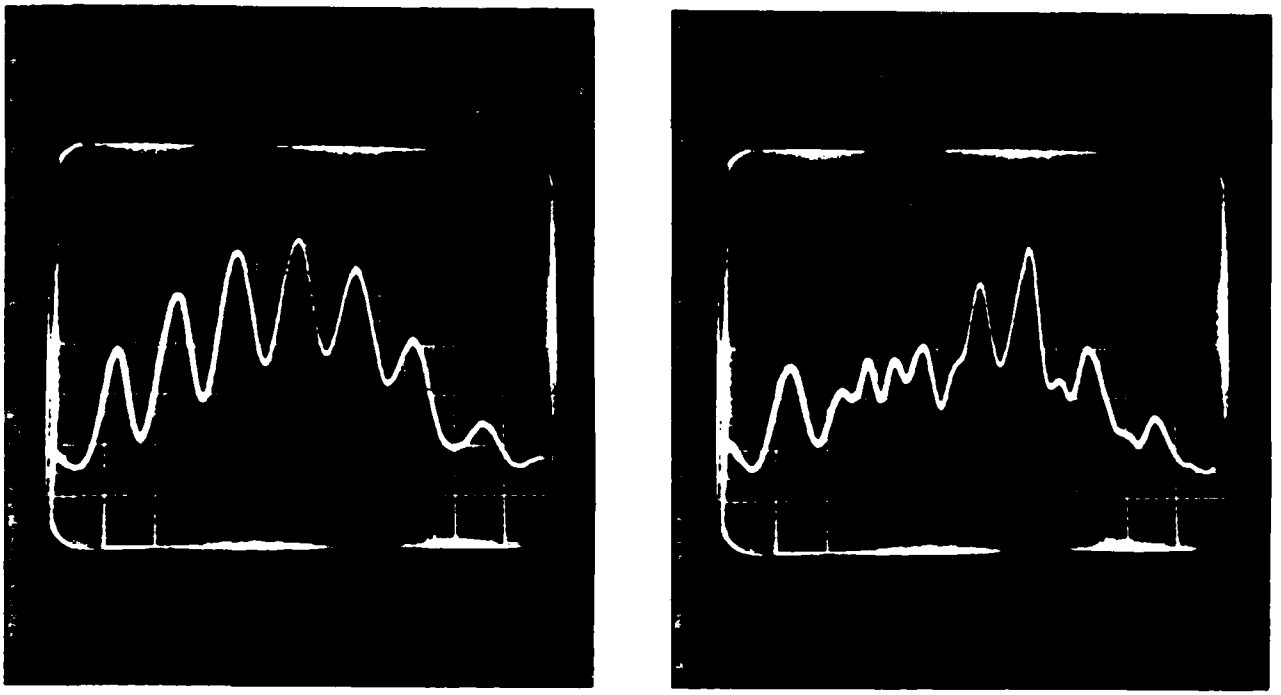

(a) (b)

Figure 7. Doppler Signal of Spherical Droplet Illuminated by (a) Undisturbed Laser Beams, (b) Laser Beams Traveling Rain Spray. Scale for both pictures 0.1 ms/div and 1v/div.

Figure 8.

85-61070

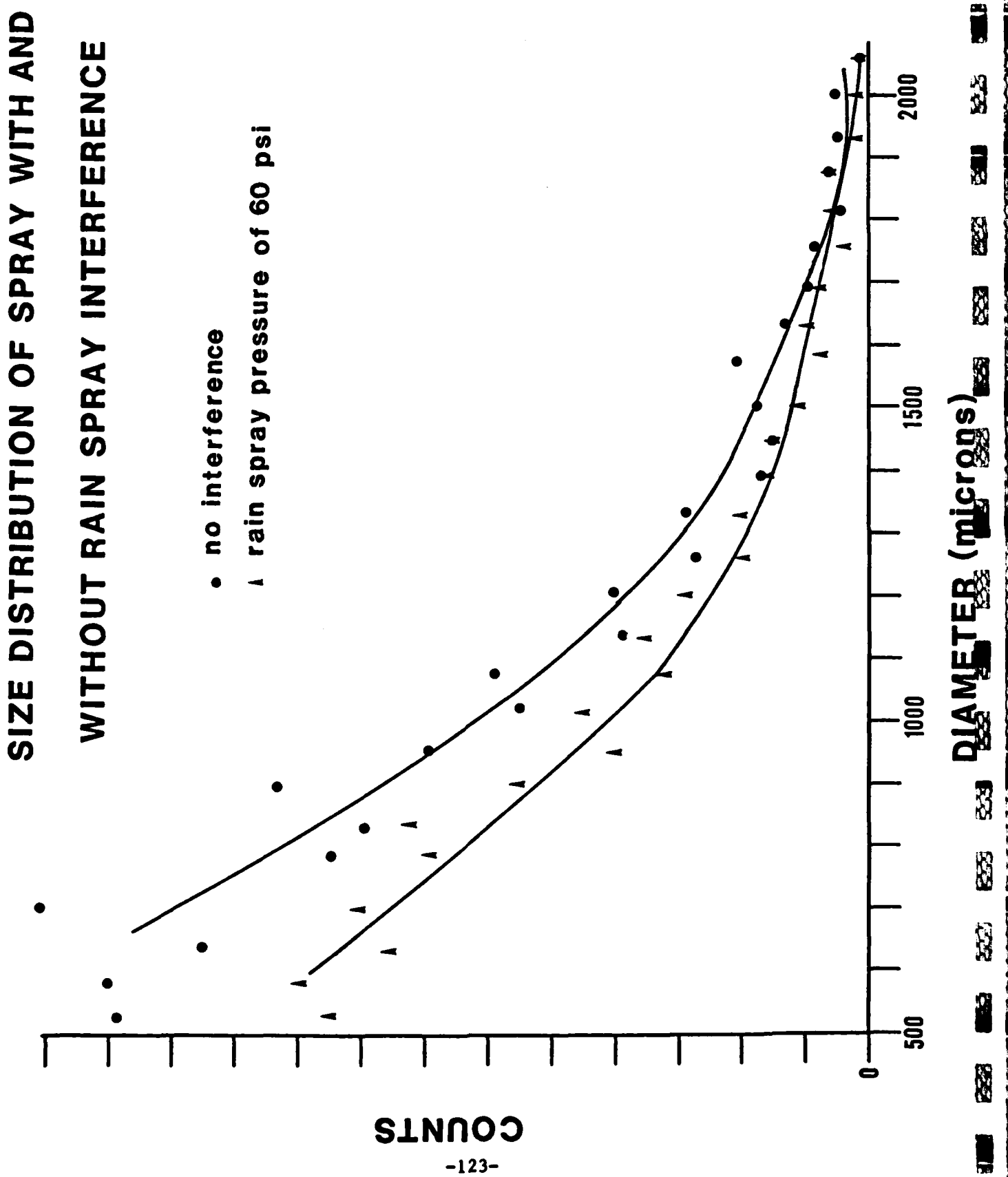

The Effect of Droplet Asphericity In The Scattering Signal

Slightly aspherical droplets were produced with the Berglund-Liu monodisperse generator. Droplets some distance from the vibrating orifice may be the result of the coalescence of two smaller droplets traveling at different speeds. These droplets will oscillate forming elongated spheroids. A strobe light triggered by a fraction of the frequency of the vibrating orifice permitted visual inspection of the droplets. The volume of the droplets is known since at any time the flow rate and number of droplets generated are known.

Receiving optics were positioned at 90° where the scattered light is primarily by reflection. Figure 9 shows the size histograms corresponding to spheroids of aspect ratios (a) 1.25, (b) 1, and (c) 0.83. These histograms contain in the order of 2000 samples. These aspect ratios were obtained from the strobe photographs shown on Figures 10a, b, c, respectively.

This trend, in which vertically elongated drops scatter more light than a spherical drop of equal volume, was also observed at a collection angle of 5°.

Numerical Model

In an effort to explain the effect of the droplet shape in the particle size, a very simple model was implemented. The model uses geometric scattering, therefore, dividing the scattered light into three components: reflection, refraction and diffraction. The model assumes that for a given angle of collection the scattered light due to either reflection or refraction is proportional to the illuminated area of the

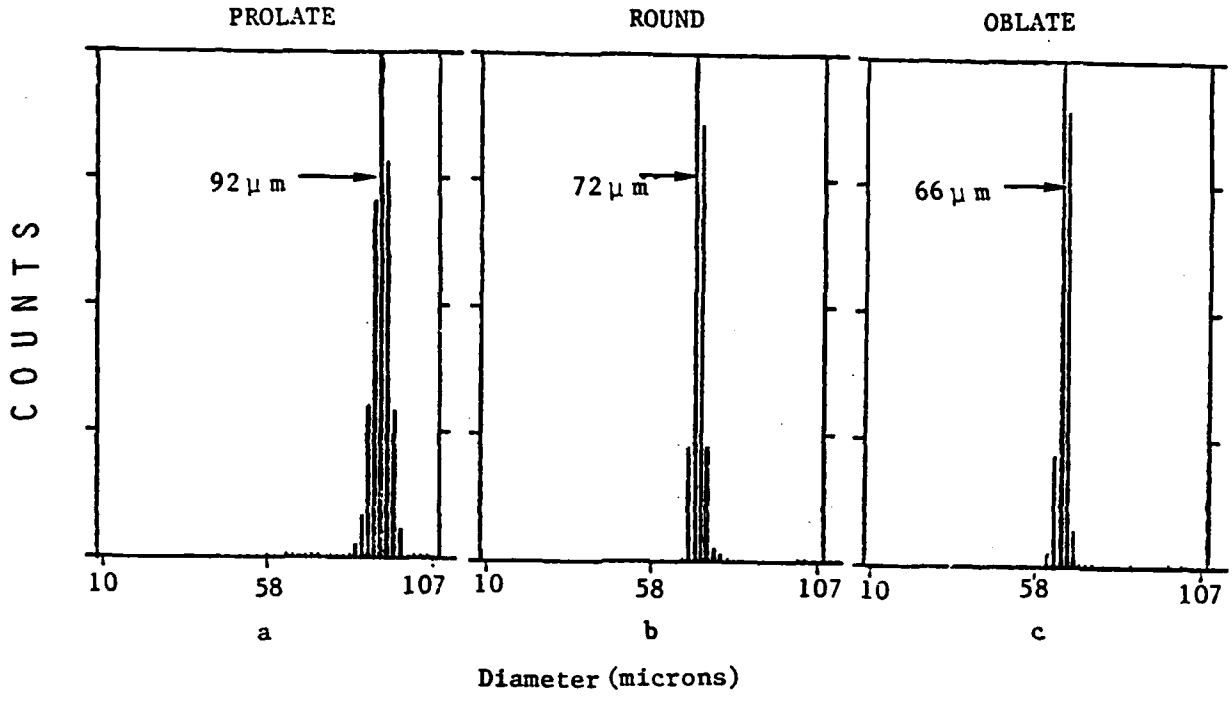

Figure 9. Size Histograms Obtained with Single Particle Counter at a Collection Angle of 90°.

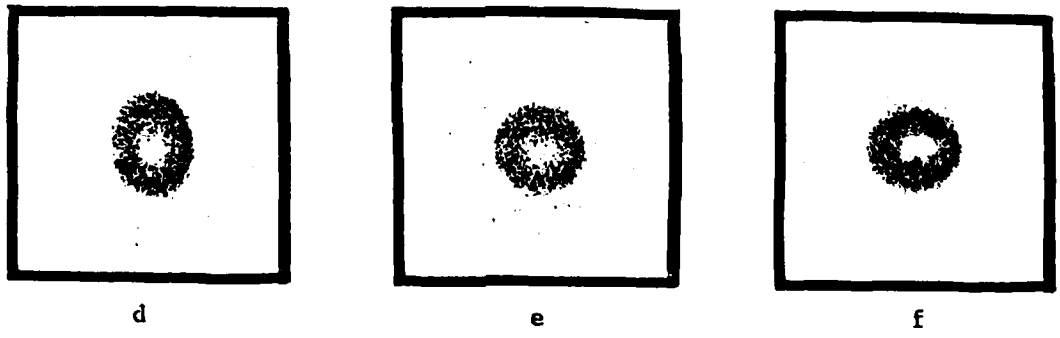

Figure 10. Photographs of Droplets Corresponding to Histograms in Figures 9a, b, c.

droplet. No regard is given to phase and interference since for the most part the light is collected over a finite solid angle. For angles of collection close to 90° the scattered light is primarily by reflection from the first surface of the droplet. Figure 11a shows that the laser beam travels along the y direction, and droplets of elliptical shape are moving down in the -z direction.

For an ellipsoid of revolution the cross section at the z = 0 plane is a circle of radius a. At the y = 0 plane the cross section is an ellipse with minor radius a and major radius b. If we place the receiving optics in the plane z = 0 and allow a finite solid angle of collection we get the following.

For the z = 0 plane it can be shown that

$$\left|\tan \frac{\theta}{2}\right| = \frac{\sqrt{a^2 - x^2}}{x} \quad (x > 0)$$

where θ is the angle of collection solving for x:

$$x = a \cos \frac{\theta}{2}, \; x > 0, \; \theta < \pi \quad .$$

Since the receiving lens sustains a finite angle ($\Delta\theta$), there will be a finite Δx along the equatorial plane of the droplet, where

$$\Delta x = \left| \frac{a}{2} \sin \frac{\theta}{2} \cdot \Delta\theta \right| \quad .$$

Similar calculations can be made along the ellipse described at y = 0. To simplify the mathematics the x and y axis are rotated by $-\tau$, such

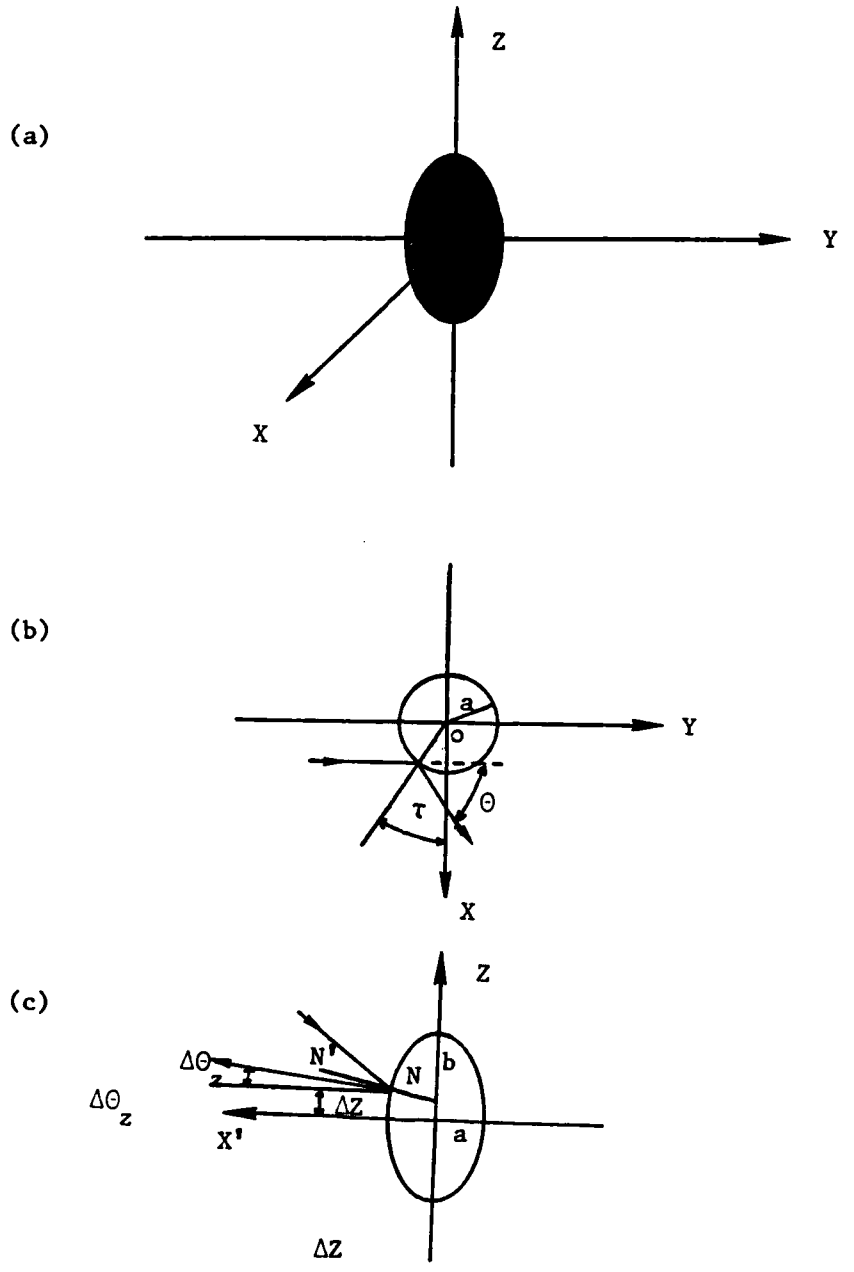

Figure 11. a) Coordinates of ellipsoid; b) Cross section of ellipsoid at z = o; c) Cross section of ellipsoid at y = o after converting to x' y' coordinates.

that the x axis is bisector of the incident and reflected beams. If we call this new coordinate x', the ellipse at y' = 0 is given by (Figure 11c)

$$\frac{x'^2}{a^2} + \frac{z^2}{b^2} = 1 \quad .$$

The collection angle in the x'z plane is $\Delta\theta_z$ which corresponds to half the angle sustained by the receiving optics around the equatorial plane. It can be shown that for small $\Delta\theta_z$

$$\Delta\theta_z \simeq 2 \sin \frac{\theta}{2} \frac{a}{b} \frac{\Delta z}{\sqrt{b^2-(\Delta z)^2}}$$

where Δz is the half width of the laser beam illuminating the ellipse on the x'z plane such that the edge of this beam after reflection sustains a $\Delta\theta_z$ angle with the x'y' plane. This yields at $\Delta z \ll b$

$$\Delta\theta_z \simeq 2 \sin \frac{\theta}{2} \frac{a}{b^2} \Delta z \quad ,$$

therefore,

$$\Delta z = \frac{1}{2 \sin \frac{\theta}{2}} \frac{b^2}{a} \Delta\theta_z \quad .$$

For the assumptions listed above, the scattered light is proportional to $\Delta x \cdot \Delta z$. For a sphere of radius c,

$$I_s \sim \left(\frac{c\Delta\theta}{2}\right)^2 R(\theta) \quad .$$

For the ellipsoid of radii a and b

$$I_s \sim \left(\frac{b\Delta\theta}{2}\right)^2 R(\theta)$$

where $R(\theta)$ is the reflectance of the droplet at a scattering angle θ.

It has been assumed that

$$\Delta\theta_z = \Delta\theta \text{ and } \cos(\Delta\theta_z) = 1.$$

Volume conservation establishes that

$$c^3 = a^2 b \quad .$$

Therefore, the ratio of the scattered light from a sphere to a prolate ellipsoid is:

$$\frac{I_{\text{sphere}}}{I_{\text{ell.}}} = \left(\frac{a}{b}\right)^{4/3} \quad .$$

A similar but more complicated analysis could be performed for the refracted light. Intuitively, we feel that the error due to shape changes will be smaller when collecting refracted light.

References

1. J. K. Luers, "Heavy Rain Effects on Aircraft," AIAA 21st Aerospace Sciences Meeting (1983).

2. V. Ramaswamy and P. Chylek, "Shape of Raindrops" in Light Scattering by Irregularly Shaped Particles, ed. by D. W. Schuerman, P.55, Plenum Press (1980).

3. van de Hulst, Light Scattering by Small Particles, Chapter 12, Dover Publications (1981).

4. W. J. Humphreys, "Physics of the Air," McGraw-Hill (1940).

4.0 PUBLICATIONS

1. Hess, C. F., "A Technique Combining the Visibility of a Doppler Signal with the Peak Intensity of the Pedestal to Measure the Size and Velocity of Droplets in a Spray," AIAA Paper Number 84-0203, presented at AIAA 22nd Aerospace Sciences Meeting, January 9-12, 1984, Reno, Nevada.

2. Hess, C. F. and Espinosa, V. E., "Spray Characterization with a Nonintrusive Technique Using Absolute Scattered Light," Optical Engineering, Vol. 23, No. 5 (1984).

3. Hess, C. F., "Nonintrusive Optical Single-Particle Counter for Measuring the Size and Velocity of Droplets in a Spray," Applied Optics, Vol. 23, No. 23 (1984).

4. Hess, C. F., "An Instrument to Measure the Size and Velocity of Particles in Particle Laden Flows," Paper No. AIAA-85-1443, presented at the AIAA/SAE/ASME 21st Joint Propulsion Conference, Monterey, CA, July 8-10, 1985.

5.0 PROFESSIONAL PERSONNEL

Cecil F. Hess, Ph.D.	Principal Investigator
Donn Silberman	Research Engineer
Victor Espinosa	Research Engineer

END

11-86

DTIC